MAGNETIC RELAXATION IN SOME PARAMAGNETIC AND ANTIFERROMAGNETIC SOLIDS STUDIED WITH NON-RESONANCE TECHNIQUES

J. SOETEMAN

MAGNETIC RELAXATION IN SOME PARAMAGNETIC AND ANTIFERROMAGNETIC SOLIDS STUDIED WITH NON-RESONANCE TECHNIQUES

PROEFSCHRIFT

TER VERKRIJGING VAN DE GRAAD VAN DOCTOR IN DE WISKUNDE EN NATUURWETENSCHAPPEN AAN DE RIJKSUNIVERSITEIT TE LEIDEN, OP GEZAG VAN DE RECTOR MAGNIFICUS DR. A.E. COHEN, HOOGLERAAR IN DE FACULTEIT DER LETTEREN, VOLGENS BESLUIT VAN HET COLLEGE VAN DEKANEN TE VERDEDIGEN OP WOENSDAG 20 FEBRUARI 1974 TE KLOKKE 14.15 UUR

door

Jan Soeteman
geboren te Rotterdam in 1943

Krips Repro - Meppel

PROMOTOR: *DR. C.J. GORTER*

DIT PROEFSCHRIFT IS TOT STAND GEKOMEN
ONDER LEIDING VAN *DR. A.J. VAN DUYNEVELDT*

Ter herinnering aan mijn vader
Aan mijn moeder

STELLINGEN

1) Bij de interpretatie van metingen van de differentiële susceptibiliteit bij magnetische faseovergangen, moet men er rekening mee houden, dat de resultaten sterk afhankelijk kunnen zijn van de frequentie en amplitude van het gebruikte wisselveld.

Dit proefschrift, hoofdstuk III.

2) Al'tshuler schrijft de resultaten van relaxatiemetingen verricht door Sitnikow aan $MnSO_4 \cdot 4H_2O$ bij kamertemperatuur, ten onrechte toe aan het directe spin-rooster relaxatieproces via het zogenoemde Waller-Al'tshuler mechanisme.

S.A. Al'tshuler, Izv. Akad. Nauk. (USSR) 20 (1956) 1207.

3) De methode van Inhaber om de parameter te bepalen van zijn fenomenologische beschrijving van de reversibele magnetisatiekromme in een type II supergeleider, is nodeloos ingewikkeld.

H. Inhaber, Physica 62 (1972) 427.

4) De drukbalans kan tegenwoordig ook in het gebied beneden 1000 torr worden gebruikt voor metingen met een nauwkeurigheid tot 1 op 10^6 en een precisie van 0,1 millitorr. De bruikbaarheid van het instrument zou nog aanzienlijk verhoogd worden, als een automatisch precisie-weeginstrument zou kunnen worden ingebouwd.

5) Op grond van beschouwingen van Klein kan men verwachten uit de druk-afhankelijkheid van de geluidsnelheid meer informatie te verkrijgen over de wisselwerking tussen paren edelgas moleculen, dan uit bepalingen van de tweede viriaal en Joule-Thomson coëfficiënt in hetzelfde temperatuurgebied boven de Boyle-temperatuur.

Max Klein, J. Res. N.B.S., 70a (1966) 259.

6) De wijze, waarop Fisher en Riehl kernspin relaxatieverschijnselen in HD-He gasmengsels bespreken, is onjuist.

C.J. Fisher en J.W. Riehl, Physica 66 (1973) 1.

7) Het verrichten van "colliding-beam" experimenten met gepolariseerde bundels electronen en positronen, levert een nieuwe toetsing voor de quantumelectrodynamica.

8) Niet alleen ten behoeve van de normalisatie der fysische eenheden, maar ook ter bevordering van de verkeersveiligheid is het gewenst de snelheid van motorvoertuigen aan te geven in meter per seconde.

9) Aldous Huxley kenschetste in 1932 de toekomstige maatschappij onder andere met het gezegde "ending is better than mending". In verband met de eindigheid van de aarde en haar grondstoffen, kan men deze uitdrukking beter omdraaien: "mending is better than ending".

A. Huxley, Brave New World, Penguin Books.

J. Soeteman

Leiden, 20 februari 1974

C O N T E N T S

INTRODUCTION

Magnetic relaxation can be defined as the response of a magnetic material to a disturbance of the equilibrium state. Such a disturbance is usually realised by a time dependent external magnetic field, e.g. a discrete change of this field. Magnetic relaxation phenomena can be divided into two groups: relaxation caused by energy exchange among the magnetic moments (spins), called spin-spin relaxation, and relaxation caused by energy exchange between the spins and the lattice vibrations, called spin-lattice relaxation.

In chapter I a survey will be given of the experimental techniques used and the related thermodynamic theory. Chapter II deals with microscopic spin-lattice relaxation theory and some experimental results in paramagnetic solids, while in chapter III relaxation phenomena at and near various magnetic phase transitions are described.

CHAPTER I

MEASURING TECHNIQUES

1.1 *Field-step method and dispersion-absorption method*

To study relaxation phenomena use has been made of two experimental techniques, which differ from each other mainly by the time dependence of the applied external magnetic field. One method is to apply a magnetic field whose time dependence can be described by a step function; this is called the field-step method. The other technique is to make use of a continuous sinusoidal time variation of the magnetic field and is named the dispersion-absorption method.

Using the field-step method one places the sample to be examined in an external field H, which is then changed instantaneously at time t_0 to a value $H + \Delta H$. In general the magnetization M, or any other quantity depending on the magnetic state, will need some time to reach a new equilibrium value. If the variation of this magnetic quantity as a function of time t is proportional to $\exp((t - t_0)/\tau)$, the characteristic time τ is called the relaxation time.

In practice most relaxation phenomena are studied with the dispersion-absorption method, which measures the response of the magnetic sample to the sinusoidal disturbance as a function of frequency. The sample is placed in a constant external magnetic field H_c on which a parallel oscillating field of amplitude h is superimposed, such that $H = H_c + h \sin\omega t$. Applying such a magnetic field one can observe the complex differential susceptibility parallel to H, defined by

$$\frac{dM}{dH} = \bar{\chi}(\omega) = \chi'(\omega) - i\chi''(\omega)$$

Casimir and Du Pré [1]) developed a thermodynamical theory which in many cases describes the frequency dependence of χ' and χ'' very well. They introduced the so-called spin system, i.e. that part of the magnetic material which consists of all magnetic properties. The spin system is supposed to be in internal thermal equilibrium characterized by the spin temperature T_s. The remaining part of the material containing the lattice and its vibrations is assumed to have a good heat contact internally and also with the cooling liquid, so the temperature of

the lattice T_l equals the temperature of the bath T_b. If the energy contact between the spin system and the lattice can be described by $dQ/dt = \alpha(T_s - T_l)$, where α represents the thermal conductivity coefficient between the spin system and the lattice, and all fluctuations due to the oscillating part of the external magnetic field are linear, we can derive for the real and imaginary component of the differential susceptibility the so-called Casimir-Du Pré relations:

$$\chi' = \chi_{ad} + (\chi_T - \chi_{ad})/(1 + \omega^2\tau^2) \qquad (1)$$

$$\chi'' = (\chi_T - \chi_{ad})\ \omega\tau/(1 + \omega^2\tau^2) \qquad (2)$$

The isotherm susceptibility χ_T is measured at low frequencies $\omega << \tau^{-1}$, and is equal to the static susceptibility $\chi_0 = M_c/H_c$ for paramagnetic substances unaffected by saturation effects. The susceptibility measured at high frequencies ($\omega >> \tau^{-1}$) approaches the adiabatic susceptibility χ_{ad}, which is equal to $(C_M/C_H)\chi_T$, C_M and C_H being the specific heats of the spin system at constant magnetization and constant external magnetic field respectively. In this theory the spin-lattice relaxation time τ is equal to C_H/α. To determine the relaxation time τ the absorption χ''/χ_0 is plotted against the dispersion χ'/χ_0 in a so-called Argand diagram [2,3]. If the differential susceptibility has a Debye-form [4], i.e. satisfies eq. (1) and (2) this plot yields a semicircle (fig. 1). The

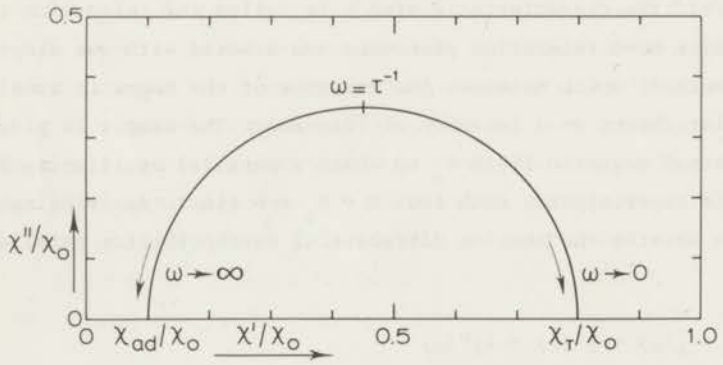

Fig. 1 *Argand diagram.*

relaxation time τ is related to the angular frequency ω corresponding to the top of this semicircle by $\tau = \omega^{-1}$.

Often the Argand diagram shows a flattened semicircle, indicating that the relaxation is proceeding with more than one time constant.

In this case an "averaged" value of a distribution of relaxation times can

be obtained from the top of the plot. Van den Broek [5]) introduced a deviation parameter d to describe such behaviour. It is defined by $d = 1 - 2h/F$, where h is the maximal absorption and F the difference between the values of the dispersion in the low frequency and the high frequency limit. The value of the parameter d is zero if the Argand diagram shows a semicircle, and differs more from zero as the curve becomes more flattened; the maximum value of 1 corresponds to a completely flat plot lying on the dispersion axis.

1.2 *Experimental equipment*

1.2.1 *Electronics.* Two electronic systems have been used to measure the complex differential susceptibility $\bar{\chi}(\omega)$. In the frequency range from 1 kHz to 1 MHz we used the apparatus built and described by De Vries [6]). It determines $\bar{\chi}(\omega)$ by detecting the variation of the self-inductance of a coil due to the presence inside it of a magnetic material. The self-inductance becomes $L = L_0(1 + 4\pi q\bar{\chi})$, where L_0 is the self-inductance without magnetic material and q is a filling factor. This variation of L, which is very small ($\delta L/L < 10^{-2}$), is measured by a kind of Wheatstone bridge consisting of four inductors. Two of them, belonging to different arms of the bridge, are placed in a cryostat, the other coils and additional compensating elements such as resistors and capacitors are placed in a metal box.

The coils in the cryostat are identical - but oppositely wound to reduce pick-up from disturbing signals - and are placed along the same quartz tube, so it is possible to move a magnetic specimen of about 1 gramme that is placed in a delrin sample holder from the centre of one coil to the centre of the other. This gives two different output voltages depending on the position of the sample. The difference between these output voltages depends only on the magnetic properties of the sample and is proportional to $\bar{\chi}$ of the sample if the bridge circuit was first balanced so that the variations in the impedance of the coils caused by the sample are small enough to ensure that the bridge circuit stays in the linear operation range.

In order to determine both components of the complex susceptibility the output voltage is led to two phase sensitive detectors, whose d.c. output voltages are proportional to the two quadrature components of the a.c. input voltage.

At frequencies between 0.1 Hz and about 10 kHz another type of measuring system is used which is based on the change of the mutual inductance between two coils caused by the presence of a magnetic sample. The measuring coils

consist of a primary coil of 1750 turns and two equivalent secondary coils wound around the primary coil next to each other. The secondary coils of 611 turns each, are wound in opposite direction not only to reduce the influence of disturbing signals but also to make certain that the voltages induced in the secondary coils due to a current flowing in the primary coil compensate each other. When a sample is moved from the centre of one secondary coil to the centre of the other, the difference in the output voltages from both secondary coils is due solely to the magnetic properties of the sample. This output voltage is led via a low noise transformer (Princeton Applied Research Corporation type TM 190) to a lock-in amplifier (P.A.R. model 124 L) with a two-phase accessory (P.A.R. model 127). The occasional occurrence of an "off-balance" signal (non-zero output not caused by the magnetic sample) can be cancelled by adjusting the offset voltages of the phase-sensitive detectors. This technique eliminates the need to use the Hartshorn bridge circuit [7]) with its extra coil system and transformer elements which become rather inefficient at the lowest frequencies.

1.2.2 *Cryostats and magnets.* The measurements described in this thesis were performed in a number of cryostats and magnets, each with its particular features. A survey of them will be given here.

1) Cryostat with water cooled magnet. The main characteristics of this solenoid which is about 40 years old are:

- maximum field: 4.2 kOe.
- the high stability of the magnetic field, fed from a 200 Amps stabilized rectifier (Standard Electric and Transforma).
- the measuring-coil system of both electronic systems can be used.
- the cryostat can be filled with all available cooling liquids to give a temperature range from 1.3 K to 300 K.
- only weak coupling between the magnet and the measuring coils.

2) Cryostat with superconducting magnet (measuring coils and magnet in the same bath. This magnet, wound from IMI Niomax S 25/40 wire was built in our laboratory [8]) to generate strong magnetic fields.

- maximum field 50 kOe at T = 4.2 K increasing to about 60 kOe at T = 1.3 K.
- efficiency factor H/i = 1.025 kOe/A.
- homogeneity: 0.4% over 4 cm (This is the distance over which the sample is moved).
- at the lower liquid helium temperatures "magnetic flux jumps" occur when the magnetic-field strength is varied. The flux jumps cause discrete

changes of the output voltage of the measuring system. At strong magnetic fields the current through the magnet and current leads dissipate enough Joule heat to change the temperature, especially at reduced pressures of liquid helium.

The magnet is energized by a Hewlett-Packard power supply type 6260 A (10 V - 100 A).

- the temperature range is restricted by the shared liquid helium bath to the interval 1.3 K - 4.2 K.
- the measuring-coil systems of both electronic systems can be applied.

3) Cryostat with magnet wound from superconducting multifilament wire and an inner-cryostat. In order to obtain more stable experimental conditions than possible with system 2), another system with an inner-cryostat which contains only the measuring coils and the sample under investigation was built; an outer-cryostat was especially made for the superconducting magnet and its liquid helium bath (fig. 2). Such a configuration eliminates the influence of the evaporation of the helium due to energizing the magnet (e.g. Joule heat in the current leads) on the temperature of the bath around the sample. Another advantage is the possibility of choosing the cooling liquid surrounding the sample independently of the helium required for the magnet. So the range of temperatures above 4.2 K is

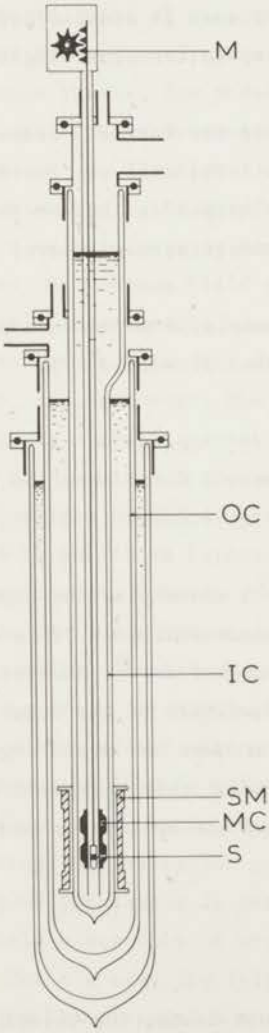

Fig. 2 *Cryostat with superconducting magnet and inner-cryostat (set-up 3). The inner-cryostat IC contains the measuring coils MC and the sample S, which can be moved by the motor M. The outer-cryostat OC contains the superconducting magnet SM.*

opened to experiments at strong magnetic field. When designing this apparatus the dimensions were chosen so that a liquid ^{3}He-cryostat could be incorporated if necessary. The solenoid magnet design was based on the method of minimal winding volume described by Girard and Sauzade [9]. The dimensions of the main coil are: inner diameter 54.0 mm, outer diameter 67.2 mm, length 142.0 mm. The correction coils, which are placed around the ends of the main coil, have an outer diameter of 75.8 mm and are each 19.0 mm long. To avoid "flux jumps" when varying the magnetic field, the magnet was wound from so-called "multifilament" wire, which is less prone to flux jumps [10]. This wire (IMI type Niomax-FM A 61/40) consists of a large number of thin superconductors separated from each other by a copper matrix. With this type of wire it is indeed possible to vary the magnetic field without observable flux jumps even at reduced helium pressures. The main coil and correction coils were wound from one single piece of wire of length 1228 m and diameter 0.425 mm.

Initially the superconducting magnet reached the "normal" state at 70% of the so-called short-sample value. To improve this the coil was impregnated with paraffin wax [10] and then the magnet went "normal" at 80% of the short-sample value. The main features of the superconducting magnet are:

- large clear bore: 51 mm.
- good homogeneity in the region where the sample is moved during the measuring procedure: 0.1% over 57 mm in axial direction [11].
- no detectable "flux jumps".
- efficiency factor: 0.462 kOe/A [11].
- maximum field strength nearly 30 kOe at T = 4.2 K and about 36 kOe at T = 2 K.

4) During the last experiments a new system [12] containing the superconducting magnet described in 2) and an inner-cryostat became available. This equipment is similar in construction to the apparatus described above. However, the clear bore of the magnet used here is smaller than that of the other superconducting magnet, therefore, the inner-cryostat is narrower and measuring coils of reduced size had to be constructed. The advantage of this equipment is the availability of magnetic fields up to 60 kOe, and the ability to use all available cryogenic liquids.

1.3 *Measuring procedures*

1.3.1 *Dispersion-absorption technique*. In most cases, the object is to

determine the dependence of the relaxation time on external magnetic field and temperature so it is necessary to measure the dispersion and absorption as a function of frequency for a number of values of magnetic field and temperature. The temperature of the cooling liquid surrounding the sample is controlled by controlling its vapour pressure. The vapour pressure can be reduced and stabilized at a desired value with an accuracy of about 0.1 mm Hg. The temperature of the cooling liquid is determined from the vapour-pressure tables. After the temperature is adjusted, measurements start by choosing the frequency of oscillation of the external magnetic field. If the high-frequency system is used, the bridge has to be balanced so that it operates in its linear range. Then the phase of the synchronous detectors is set, making use of the fact that at zero external magnetic field χ'' is zero for all frequencies as long as spin-spin relaxation can be neglected, an assumption which is justified in all cases described in this thesis. The phase sensitive detectors are adjusted in such a way that the signal due to movements of the sample at zero field can be seen only on one detector [6]). The signal on this detector is proportional to χ', while the other detector in the quadrature channel displays a signal proportional to χ''. Then a slowly increasing magnetic field is applied, while the sample is in one coil; at the maximum field the sample is moved into the other coil and the magnetic field is decreased slowly to zero. In the meantime, the output voltages of both synchronous detectors are plotted as a function of the magnetic field on an $X - Y_1 - Y_2$ recorder. The rate of change of the magnetic field has to be such that it is almost constant during a number of periods of the measuring frequency, and is slow in comparison with the relaxation time of the sample. To obtain complete Argand diagrams at each applied magnetic field, this measuring procedure has to be repeated for a range of frequencies.

At temperatures between the liquid helium and liquid hydrogen range and between hydrogen and nitrogen temperatures it is not possible to keep the temperature of the sample constant, so in these temperature ranges the "running method" [6]) is used. It starts with measuring a complete set of dispersion and absorption curves as a function of frequency while maintaining atmospheric pressure above the cooling liquid; then the liquid is boiled out. As the temperature of the assembly in the cryostat and the remaining gas increases slowly, the dispersion and absorption curves are measured at one fixed frequency. The temperature of the sample is determined from the dispersion signal at zero magnetic field since this is proportional to the static susceptibility and obeys e.g. Curie's law. The relaxation times at the different temperatures are obtained from the dispersion and absorption curves measured at these temperatures

and the Argand diagram at the constant temperature.

1.3.2 *Field-step techniques.* To investigate long relaxation times ($\tau > 0.5$ s), which occur at some magnetic phase transitions, the field-step method was used. This method requires an external magnetic field which changes from a value H to H + ΔH in a time short compared to the relaxation time to be measured. After this variation, the magnetic field H + ΔH has to be held constant during the full recovery of the magnetic sample. This response is detected by observing the behaviour of χ_{ad} as a function of time [6]. It is registered on a recorder simultaneously with the external magnetic field (fig. 3). Most

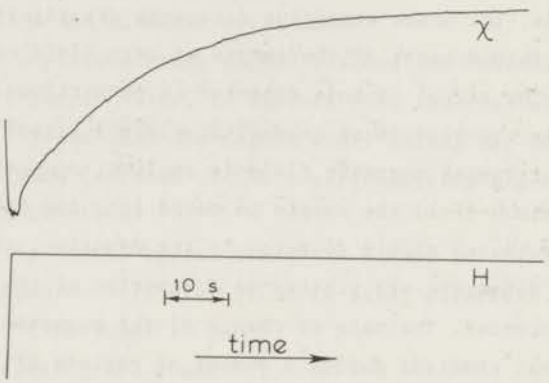

Fig. 3 *Time dependence of* χ *and H during a field-step measurement.*

magnetic phase transitions reported in this thesis occur at strong magnetic fields which can only be provided by superconducting magnets. The time constant of the superconducting magnets is about 15 s. This implies that without other equipment only very long relaxation times ($\tau > 50$ s) can be measured. To make it possible, however, to observe shorter times a fast varying magnetic field is necessary which keeps instantaneously constant at the value at which it is wished to observe the relaxation behaviour. This rapidly changing field is obtained by "misleading" the power supply of the magnet by having the magnetic field relax from a small initial value to a field much stronger than the desired final field. Just at the moment (or slightly before) when the magnetic field passes the desired final value on its way to the stronger field, the resistance which controls the output of the power supply is switched to precisely that

value which corresponds to the desired final magnetic field. Since it is important that the switching of the control resistance takes place at the right moment, an electronic switch has been built to do this. With this system it is possible to change the magnetic field at a rate of about 10 kOe/s and achieve the right constant field strength within 0.1 s.

This procedure decreases the lower limit of observable relaxation times to 0.5 s. The upper limit of 5000 s is determined by the long-term stability of the apparatus, especially the stability of the power supply of the magnet.

CHAPTER II

SPIN-LATTICE RELAXATION IN SOME PARAMAGNETIC SOLIDS

2.1 *Microscopic relaxation theory*

Most microscopic theories [13,14]) of paramagnetic spin-lattice relaxation are based on a model of isolated magnetic ions with two low-lying energy levels E_a and E_b separated by an energy δ, while the next level has an energy $\Delta >> \delta$. Relaxation of the spin system may take place as a result of spin flips between the two low-lying levels and simultaneous energy exchange with the lattice vibrations (phonons) to ensure conservation of energy. The interaction mechanism between phonons and spins is rather complicated. The most successful idea proved to be a suggestion of Kronig and Van Vleck [15]). It starts with the concept that the phonons modulate the crystal electric field at the sites of the magnetic ions. The orbital motion of the ions is directly coupled to this crystal field. The spin-orbit coupling in the ion completes the energy contact between the phonons and the spins. Quantum mechanical time-dependent perturbation theory yields for the transition probability from a state $|\alpha>$ to a state $|\beta>$ of the combined system of spins and lattice [14]):

$$w_{\alpha\beta} = \left(\frac{2\pi}{\hbar}\right)\left|<\alpha|V'(\vec{r}_1 \ldots \vec{r}_n)|\beta>\right|^2 \rho(E) +$$

$$\left(\frac{2\pi}{\hbar}\right)\left\{\left|<\alpha|V''(\vec{r}_1 \ldots \vec{r}_n)|\beta>\right|^2 + \right. \tag{3}$$

$$\left.\left|\sum_\gamma \frac{<\alpha|V'(\vec{r}_1 \ldots \vec{r}_n)|\gamma><\gamma|V'(\vec{r}_1 \ldots \vec{r}_n)|\beta>}{E_\alpha - E_\gamma}\right|^2\right\}\rho(E_1)\rho(E_2) \ .$$

The first and second order perturbing potentials $V'(\vec{r}_1 \ldots \vec{r}_n)$ and $V''(\vec{r}_1 \ldots \vec{r}_n)$ originate from the series expansion of the electrostatic potential at the sites $\vec{r}_1 \ldots \vec{r}_n$ of the magnetic ions due to their displacements from the equilibrium positions $\vec{r}^{\,o}_1 \ldots \vec{r}^{\,o}_n$. So the first term of eq. (3) has its origin in first order perturbation theory while the other terms both originate from second order theory. State $|\gamma>$ denotes an intermediate state, which may be real or virtual; the energy density of the final state is represented by the terms $\rho(E)$. The

assumption is made that the interaction between the phonons and ions is weak, so that it is possible to write the state function of the whole system as the product of the state functions of the phonons and the ions considered separately. The phonon states are usually assumed to have a Debye distribution

$$\rho(\omega) = \hbar\rho(E) = \frac{1}{2\pi^2}\left(\frac{2}{v_t^3} + \frac{1}{v_l^3}\right)\omega^2 V \qquad (4)$$

where V is the volume and v_t and v_l are the transverse and longitudinal velocities of sound in the material respectively, usually considered to be equal. The distribution has a maximum frequency ω_m, to which the Debye temperature Θ_D is related by the expression $\hbar\omega_m = k\Theta_D$.

In the two-level model the spin-lattice relaxation time is related to the transition probabilities $w_{\alpha\beta}$ and $w_{\beta\alpha}$ by [16]: $\tau^{-1} = w_{\alpha\beta} + w_{\beta\alpha}$. For temperatures higher than δ/k these two transition probabilities are equal to each other. Now consider the contributions of the different terms of eq. (3) to the inverse relaxation time. The first term represents a spin-flip accompanied by the simultaneous creation or annihilation of one single phonon with angular frequency $\omega = \delta/\hbar$ in order to fulfil the requirement of energy conservation. Further calculations [13] for this first order process, called the direct process, yield:

$$\tau^{-1} = A_1\delta^3\coth(\delta/2kT) \qquad (5)$$

The coefficient A_1 contains only terms independent of temperature and external magnetic field. The dependence of τ^{-1} on temperature originates from the phonon system. If there is no crystal field splitting, $\delta = g\mu_B H$, and if this splitting is much smaller than kT, eq. (5) transforms to the well-known expression:

$$\tau^{-1} = AH^2T \qquad (6)$$

This simple relation reflects the fact that the direct process involves only phonons with energy $\hbar\omega = \delta$. This process becomes faster at increasing temperature and external magnetic field since then the number of phonons in contact with the spins increases.

The two-phonon processes are represented by the second and third term of eq. (3). When the energy of the next higher lying level is larger than $k\Theta_D$, the third term of eq. (3) represents a spin-flip to a virtual intermediate state $|\gamma>$, accompanied by the creation or annihilation of a phonon ω_1 followed by a

reverse spin-flip from the state $|\gamma>$ to the final state accompanied by the annihilation or creation of a phonon ω_2. The frequencies of both phonons are related to each other by the requirement for the conservation of energy, i.e. $|\hbar\omega_1 - \hbar\omega_2| = \delta$. This two-phonon process, called the Raman relaxation process, is independent of the external magnetic field if the spins are isolated from each other. The relaxation time for the Raman process is related to the temperature by [13]):

$$\tau^{-1} = BT^7 J_6(\Theta_D/T) \quad , \tag{7}$$

$J_6(\Theta_D/T)$ is one of the family of integrals [17])

$$J_n(\Theta_D/T) = \int_0^{\Theta_D/T} \frac{x^n e^n}{(e^x - 1)^2}\, dx \quad ,$$

n being a positive integer. These integrals are constants for temperatures much lower than the Debye temperature and proportional to T^{2-n} above the Debye temperature. B is called the coefficient of the Raman process. For temperatures much larger than the Debye temperature eq. (7) gives a T^{-2}-dependence for the relaxation time and for temperatures much smaller than the Debye temperature a T^{-7}-dependence. The same results would be obtained starting from the second term of eq. (3).

When the next higher spin level lies within the phonon spectrum ($\Delta < k\Theta_D$) a two-phonon relaxation process with a real intermediate state is possible. Then energy is conserved at both stages of the process, so it can be considered as two direct-process transitions after each other. If the temperature is much smaller than Δ/k, it can be shown that this process, called the Orbach-relaxation process, depends mainly on the availability of phonons capable of inducing transitions from the intermediate state to the final state. The relaxation time of the Orbach process may be characterized by [13]):

$$\tau^{-1} = Ce^{-\Delta/kT} \tag{8}$$

It has been tacitly assumed in this discussion that the magnetic ions are not Kramers ions [Kramers ions [18]) are ions with an odd number of electrons whose energy levels occur in doublets and which cannot have the degeneracy lifted by an operator which is invariant under time reversal, as is the electrical field]. This implies that the matrix elements of the crystal field between the

levels of a Kramers doublet are zero. The magnetic field, however, which is not invariant under time reversal can lift the degeneracy. So it is necessary to consider admixtures of higher lying levels into the ground doublet by the external magnetic field to obtain non-zero matrix elements. These matrix elements are, in first order, proportional to the external field, so they contribute an extra H^2-dependence to the inverse relaxation time, when compared with non-Kramers salts. Now one obtains for the direct process (cf. eq. (5)):

$$\tau^{-1} = A_1 H^5 \coth\left(\frac{g\beta H}{2kT}\right) . \tag{9}$$

In the case $g\beta H \ll kT$, eq. (9) transforms into:

$$\tau^{-1} = AH^4 T . \tag{10}$$

Applying in Kramers salts the arguments just mentioned above to the second term of eq. (3), one derives from eq. (7) for the Raman process an extra H^2-dependence in comparison with non-Kramers salts, that is [13]):

$$\tau^{-1} = B_1 H^2 T^7 J_6(\Theta_D/T). \tag{11}$$

This dependency is rarely observed [19]).

Starting from the third term of eq. (3), calculations are more complicated since it is necessary to consider admixtures of higher lying levels which are themselves also Kramers doublets, into the ground doublet. Two terms contributing to $w_{\alpha\beta}$ are obtained. If the energy Δ is larger than $k\Theta_D$, calculations lead to the expression:

$$\tau^{-1} = B_2 T^9 J_8(\Theta_D/T) \tag{12}$$

and, if the energy Δ is small compared with kT, to [20]):

$$\tau^{-1} = B_3 T^5 J_4(\Theta_D/T). \tag{13}$$

If the energy is conserved at both stages before and after the spins reaching a real intermediate state - only possible if Δ is smaller than $k\Theta_D$ but larger than kT - one observes an Orbach process with a similar temperature dependence to that of non-Kramers salts (eq. (8)).

Sometimes the Raman relaxation process shows a small dependence on the

magnetic field, caused by interactions between the magnetic ions. This dependence may often be described by the Brons-Van Vleck relation [21]:

$$\tau(H) = \tau(0)\,\frac{1 + H^2/(b/C)}{1 + pH^2/(b/C)} \qquad (14)$$

where C is Curie's constant, b originates from the expression for the specific heat at constant magnetization $C_M = b/T^2$ and p is a constant with value about 0.5 [22]. The expression $(b/C)^{\frac{1}{2}}$ represents an internal magnetic field due to the interactions between the magnetic ions.

For both Kramers and non-Kramers salts, the coefficients A, B, and C are such that the direct process is the fastest below a temperature of about 4 K, while the Raman and Orbach process dominate at higher temperatures and magnetic fields of about 4 kOe and less, which are typical of the fields developed by the old water-cooled magnet. Since superconducting magnets are available (section 1.2.2) magnetic fields up to 60 kOe can be realized. At these strong fields it is possible to observe the direct process at liquid hydrogen temperatures when it becomes faster than the other processes due to its considerable field dependence.

Summarizing these results, one can expect Kramers salts with one low lying doublet (the case considered in this chapter) to have a spin-lattice relaxation time according to

$$\tau^{-1} = AH^4T + BT^9J_8(\Theta_D/T)\ . \qquad (15)$$

2.2 *Phonon bottleneck*

At liquid helium temperatures the relaxation behaviour as described in section 2.1 is sometimes obscured. This is due to the fact that the assumption that the occupation numbers of the phonon modes are not affected by the energy exchange between the spin system and the phonons "on speaking terms" (o.s.t.) with the spins, is no longer fulfilled. This happens when the energy exchange between the phonons o.s.t. with the spin system on one side, and the other phonons and the bath on the other side, is not capable of maintaining the surplus (or shortage) of phonons o.s.t. negligibly small. Then the thermal equilibrium among the phonons of both the lattice and the bath is disturbed. To describe this situation, one may introduce a thermodynamical model that divides the magnetic substance into two parts: the spin system already mentioned in section 1.1 and the lattice system consisting of the phonons o.s.t. with the spin system.

The third system to be taken into consideration is the bath of supposedly infinite heat capacity, to which all other phonons in the lattice are linked. A temperature is defined for each system. Energy transfers are only possible between the spin system and the lattice system, and between the lattice system and the bath; the transfer of energy is assumed to depend linearly on the temperature difference between the systems involved. The energy transfer between the spin system and the lattice system is characterised by the spin-lattice relaxation time τ (cf. section 1.1); the energy exchange between the lattice system and the bath is characterised by the lattice-bath relaxation time τ_{LB}. If these two relaxation times are of the same magnitude, the spin-bath relaxation time, τ_{obs}, which one actually measures, will differ notably from the spin-lattice relaxation time. Making the assumptions that $\delta << kT << \Delta$ and that the specific heat of the lattice system C_L is small compared to the specific heat of the spin system C_M, Stoneham [23]) has shown τ_{obs} to be:

$$\tau_{obs} = \tau + \frac{C_M}{C_L} \tau_{LB} \quad . \tag{16}$$

These phonon bottleneck effects mainly influence measurements of the direct relaxation process since in that case the lattice system consists of a small band of phonons o.s.t., and the specific heat of this system is small. This makes the last term of eq. (16) have a great influence on the observed relaxation time. The surplus (or shortage) of the phonons o.s.t. tends to disappear at the crystal surface or by inelastic phonon scattering. Therefore, the spatial density of the phonons o.s.t. will depend on the position in the crystal. This causes the spin-bath relaxation times of the different ions to depend on their positions. Thus one observes a relaxation behaviour that cannot be described by one relaxation time but must be described by a range of times [24]).

Since the distance between the magnetic ions and the crystal surface influences the magnitude of τ_{LB}, one may expect that phonon-bottleneck effects will depend on the size of the crystals of the sample. This dependence has been confirmed in many experiments [25,26]). In order to minimize these phonon-bottleneck effects, measurements are often performed on powdered samples with an averaged grain diameter of 0.1 mm. Another possibility to decrease the influence of the phonon bottleneck is to reduce the concentration of the magnetic ions. Then the specific heat of the spin system C_M will be smaller, which brings about that the contribution of the last term of eq. (16) to τ_{obs} decreases. Experimental verification of this effect can be found in [26,27]).

2.3 *Introduction to spin-lattice relaxation in copper Tutton salts*

The work reported in the sections 2.4 and 2.5 was carried out in order to investigate the direct and the Raman relaxation processes in magnetically concentrated copper Tutton salts. These copper Tutton salts have the general formula $CuX_2(SO_4)_2 \cdot 6H_2O$, where X denotes a monovalent non-magnetic cation. The crystal structure is monoclinic [28]. The Cu^{2+} ions are each surrounded by a distorted octahedron of six water molecules. By the combined effect of the crystal field and the spin-orbit coupling the ground state is a Kramers doublet, which is some thousands of degrees below the first excited level [29]. The direct relaxation process is observable with the present equipment because it enables us to work with strong external magnetic fields, where the direct process dominates at both liquid-helium and liquid-hydrogen temperatures. The field-independent relaxation observed by Cox, Gill and Wharmby [30] in copper caesium Tutton salt at a temperature of 1.4 K between 2 and 4 kOe and ascribed by these authors to isotropic exchange interactions was also investigated. Since the direct relaxation process is known to behave analogously in a series of copper Tutton salts with different non-magnetic cations [31], it was only studied on copper caesium Tutton salt.

The Raman relaxation process, however, was observed in a series of copper Tutton salts with the intention of determining the Debye temperatures of these salts and possibly explaining the different results reported by various authors [32,33,34].

2.4 *Direct spin-lattice relaxation in copper caesium Tutton salt*

2.4.1 *Experimental methods*. One of the reasons for the present research was the verification of the rather long relaxation times at fields up to 10 kOe as reported by Cox et al. [30]. At the beginning of the experiments described in this thesis the dispersion-absorption technique could not be used to examine relaxation times longer than 1 s. Therefore part of the experiments described in this section was carried out at the Natuurkundig Laboratorium in Amsterdam. At this laboratory we used a solenoid magnet that can produce fields from 2.5 up to 400 kOe with adjustable pulse shape and length [35]. During these experiments the sample was exposed to a pulsed field of 60 kOe for 0.1 s followed by a relatively weak constant field H for 2.0 s. The tail of the stainless-steel cryostat which contains the sample in a cylindrical holder made of teflon, is placed inside the magnet. The sample holder, which has an inner-diameter of 3.5

mm is perforated to ensure a good heat contact between the sample and the cooling liquid. The temperature is controlled by a pump and manostat. The sample of maximum length 20 mm is inserted in a properly designed pick-up coil [36]). The signal induced in this coil is led to an integrator in order to measure the magnetization. During a measurement both magnetic field and magnetization are registered as a function of time on a Honeywell visicorder. The relaxation behaviour is studied by analysing the recovery of the magnetization to its equilibrium value at the weak field H.

The range of relaxation times that can be measured with this technique is restricted by the fall-off time of the strong pulse field, yielding a lower limit of 10^{-2} s and by the maximum length of the field H, giving rise to an upper limit of about 10 s.

In Leiden the relaxation behaviour is examined with the dispersion-absorption technique using the low-frequency equipment, described in chapter I, at external magnetic fields up to 34 kOe at both liquid-helium and liquid-hydrogen temperatures.

2.4.2 *Experimental results.* Using the pulsed-field method, measurements on three different samples were performed at T = 1.4 K. This temperature has been chosen to compare our results with those obtained by Cox et al. [30]).

Sample a: small crystals of $CuCs_2(SO_4)_2 \cdot 6H_2O$, average diameter about 1 mm. Relaxation times of copper Tutton salts are easily influenced by (non-)magnetic impurities [37]). For this reason measurements were performed on a sample provided by Gill to make sure that our measurements were carried out on the same type of "impure" material.

Sample b: a powder ground from the same material as sample a; average grain diameter 0.1 mm.

Sample c: a powder of $CuCs_2(SO_4)_2 \cdot 6H_2O$ prepared from spectroscopically pure chemicals, obtained from De Vroomen; average grain diameter 0.1 mm.

It was not possible to describe the observed decay of the magnetization in any sample with one single time constant. The deviation from a pure exponential is greatest at magnetic fields below about 10 kOe. The relaxation times shown in fig. 4a, are obtained from the tail of the magnetization since there the recovery approaches a single exponential function. The results thus obtained may be considered to be near the upper limit of a distribution of relaxation times.

At strong fields all samples show a field dependence given by $\tau \propto H^{-2.8}$, though the relaxation of sample a, which consists of small crystals, is about a

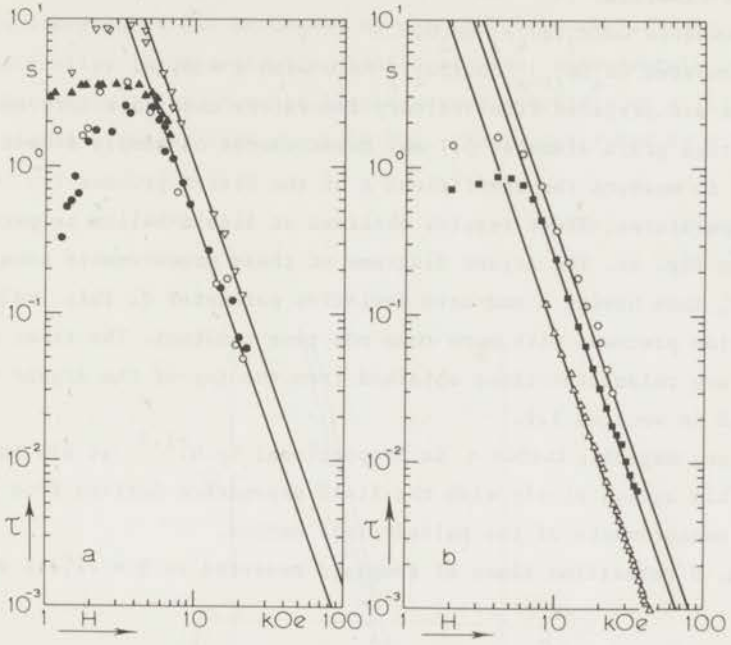

Fig. 4 *The spin-lattice relaxation time of $CuCs_2(SO_4)_2 \cdot 6H_2O$ as a function of the external magnetic field. a) Measurements with the pulsed-field method at T = 1.4 K. ▽ sample a; ○ sample b; ● sample c; ▲ Cox et al.; —— $\tau \propto H^{-2.8}$. b) Measurements with the dispersion-absorption method on sample d. ○ T = 1.43 K; ■ T = 2.10 K; △ T = 4.25 K; —— $\tau \propto H^{-2.9}$.*

factor two slower than the relaxation of the powdered samples b and c. Within the experimental accuracy, the relaxation times measured on the spectroscopically pure sample are identical to those of sample b.

The results obtained at magnetic fields below 4 kOe are less reliable since during the time the field decreases from its initial large value to its final constant value H, the region of maximum relaxation time is passed (fig. 4). One expects that these long relaxation times would lengthen the relaxation times observed at fields below 4 kOe. However, it is remarkable to see how fast the relaxation is at magnetic fields nearing 1 kOe. For comparison the results by Cox et al. [30]) are also displayed in fig. 4a.

The short relaxation times which could not be detected with the pulsed-field method were measured using the dispersion-absorption technique. Two samples were examined:

sample d: powdered $CuCs_2(SO_4)_2 \cdot 6H_2O$,

sample e: powdered $Cu_xZn_{(1-x)}Cs_2(SO_4)_2 \cdot 6H_2O$ with x = 0.14.

Both samples are prepared from ordinary laboratory chemicals (pro analysi, Merck), average grain diameter 0.1 mm. Measurements on sample d have been carried out to measure the coefficient A of the direct process ($\tau^{-1} = AH^4T$) at various temperatures. These results obtained at liquid-helium temperatures are displayed in fig. 4b. The Argand diagrams of these measurements show flattened semicircles, thus having a non-zero deviation parameter d. This indicates that the relaxation proceeds with more than one time constant. The times plotted in fig. 4b are relaxation times obtained from the top of the Argand diagram as described in section 1.1.

At strong magnetic fields τ is proportional to $H^{-2.9}$ at all temperatures measured. This agrees nicely with the field dependence derived from the magnetization measurements of the pulsed-field method.

In fig. 5 relaxation times of sample d measured at T = 14.1 K are given.

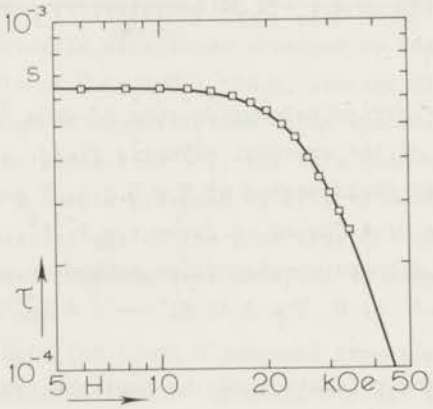

Fig. 5 *The spin-lattice relaxation time of sample d as a function of the external magnetic field at T = 14.1 K.* $\tau^{-1} = AH^4T + B$.

At this temperature no deviation from the Debye form is found. At weak magnetic fields an almost field-independent relaxation due to Raman processes is observed. At strong fields the relaxation becomes faster because of the influence of the direct process. The relaxation time exhibits an $H^{-2.0}$ dependency at external fields stronger than 30 kOe.

The observed $H^{-2.9}$ dependence of the relaxation time (fig. 4b) at liquid-helium temperatures and strong fields differs notably from the field dependence expected for the relaxation time of the direct process ($\tau_{dir}^{-1} = AH^4T$, see eq. (10)). This discrepancy can be caused by phonon-bottleneck effects. Since these effects are smaller in magnetically diluted samples, measurements have been performed on sample e. It shows at liquid-helium temperatures a field dependence which, at fields stronger than about 10 kOe, can be described by $\tau \propto H^{-4}$ (fig. 6).

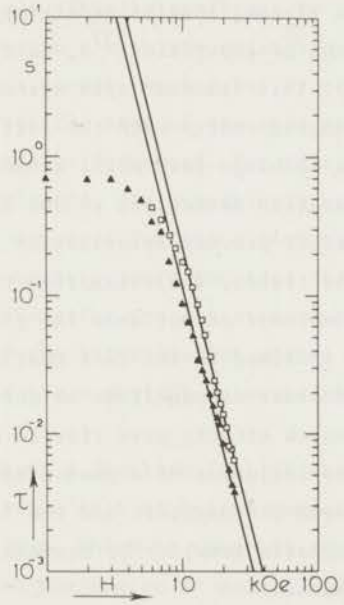

Fig. 6 *The spin-lattice relaxation time of sample e ($Cu_{0.14}Zn_{0.86}Cs_2(SO_4)_2 \cdot 6H_2O$) as a function of the external magnetic field.* □ *T = 2.10 K;* ▲ *T = 4.25 K;*——— $\tau \propto H^{-4}$.

These measurements are less accurate than those on the non-diluted sample d, simply because of the magnetic dilution. In particular, the dispersion measurements are less reliable. Therefore the relaxation times in fig. 6 are determined only from absorption measurements.

2.4.3 *Discussion.* The relaxation times of the powdered sample, obtained by the pulsed-field method (fig. 4a), are significantly longer than those measured with the dispersion-absorption technique (symbol o in fig. 4b), especially at weak magnetic fields. Such a difference is expected for a distribution of relaxation times. With the pulsed-field method, one measures - as stated above - the long relaxation times of a distribution, whereas the dispersion-absorption method yields an average time constant. However, both measuring techniques do not show the field-independent relaxation reported by Cox et al. [30]) that is also displayed in fig. 4a.

The fact that the complex susceptibility does not have a Debye form at weak magnetic fields and liquid-helium temperatures can be ascribed to the existence of a "second" spin system, consisting of copper ions with short relaxation times due to the presence of impurities [37]), lattice imperfections [38]), or exchange interactions [30,39]). This "second" spin system offers the (first) spin system an extra way of exchanging energy with the lattice and the helium bath. At weak magnetic fields this exchange path might be more effective than that of the direct spin-lattice relaxation mechanism; so one observes an average time which is shorter than the direct process spin-lattice relaxation time.

Also, at strong magnetic fields, the relaxation times of the undiluted samples as measured by both methods do not show the field dependence of the direct process. This may be ascribed to the fact that the lattice-bath relaxation time τ_{LB} is of the same order of magnitude as the spin-lattice relaxation time τ_{SL}. Such phonon-bottleneck effects give rise to a non-Debye relaxation [24]). As stated in section 2.2, the influence of a phonon bottleneck can be reduced by decreasing the ratio between the magnetic and the lattice specific heat (smaller concentration of magnetic ions) or by decreasing the lattice-bath relaxation time (smaller crystals).

The observed field dependences at strong magnetic fields, $\tau \propto H^{-2.8}$ in fig. 4a and $\tau \propto H^{-2.9}$ in fig. 4b, might be ascribed to a direct relaxation process slowed down by phonon-bottleneck effects. Similar field dependences for τ have been observed in powdered cobalt fluosilicate [26]) and cobalt Tutton salts [38]). Assuming that both the lattice specific heat and the lattice-bath relaxation time τ_{LB} of identical grains of cobalt and copper Tutton salt do not differ much, one can expect that the exponents of the field dependences of the relaxation times only differ from each other because of the different values of the specific heat of the spin systems involved. The exponents for cobalt Tutton salt, -2.3 for the magnetically undiluted salt and -3.2 for a sample with a magnetic concentration of 7.7 %, are plotted as a function of the logarithm of the specific

heat of the spin system. For convenience the spin-specific heat of the 100 % cobalt Tutton salt at a certain field is taken as unity. Since the spin-specific heat of 100 % copper Tutton salt at that field is about 4 times smaller than that of cobalt Tutton, the value 0.25 on the abscissa of this plot will correspond to the 100 % copper Tutton salt. Following this idea, the exponent of the field dependence of τ in this salt is expected to be -2.8, a value close to the experimentally observed results (-2.8 and -2.9). This consistency suggests the existence of a relation between the specific heat of a magnetic spin system and the deviation from $\tau \propto H^{-4}$. A closer analysis of this effect may be of some help in predicting possible influences of phonon-bottleneck effects in other cases.

The influence of the phonon bottleneck is stronger if the measurements are performed on large crystals. This is confirmed by comparing the relaxation times of the powdered samples b and c with the relaxation times of sample a (small crystals) which are over a factor two longer. By replacing copper ions by non-magnetic ions, the specific heat of the spin system, and thus the influence of a phonon bottleneck, can be decreased. For this reason, sample e (14 % magnetic ions) was investigated. The resulting field dependence of τ is close to the H^{-4} dependence as expected for the direct relaxation process (fig. 6).

The above given arguments support the idea that phonon-bottleneck effects influence the observed relaxation process at strong external magnetic fields. It seems obvious to apply the interpolation method as introduced by Roest et al. [26]) in order to determine the numerical value of the coefficient A of the direct relaxation process.

The deviation parameter d (section 1.1) of the complex susceptibility measurements on the undiluted salt at helium temperatures has as a function of the magnetic field a minimum, which is (nearly) zero, see fig. 7. This occurs at magnetic fields between the region at weak fields, where d is larger due to the second spin system, yielding a relaxation time $< \tau_{SL}$, and the strong-field region where the measurements show a relaxation time $> \tau_{SL}$ due to phonon-bottleneck effects. According to the phenomenological interpolation method proposed by Roest et al. [26]), the "true" spin-lattice relaxation time, unaffected by the second spin system or the phonon bottleneck, is equal or close to the relaxation time observed at that field where the deviation parameter d is minimal. By substitution of that value of the magnetic field - 24 kOe at 4.25 K, 19 kOe at 2.10 K, and 12 kOe at 1.43 K, see fig. 7 - and the corresponding relaxation time in the equation governing the direct process ($\tau^{-1} = AH^4T$), the coefficient A is obtained (table I).

At 14.1 K, influence of phonon bottleneck is not observed. The results of

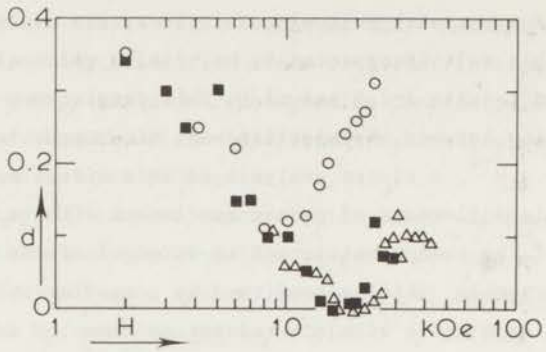

Fig. 7 *The d-parameter of sample d as a function of the external magnetic field.* ○ *T = 1.43 K;* ■ *T = 2.10 K;* Δ *T = 4.25 K.*

Table I

Coefficient A of the direct process
($\tau^{-1} = AH^4T$) in $CuCs_2(SO_4)_2 \cdot 6H_2O$

T(K)	$A(s^{-1}kOe^{-4}K^{-1})$
1.43	$(1.5 \pm 0.2) \times 10^{-4}$
2.10	$(1.1 \pm 0.2) \times 10^{-4}$
4.25	$(1.3 \pm 0.2) \times 10^{-4}$
14.1	$(1.3 \pm 0.1) \times 10^{-4}$

fig. 5 are described very well by a least-square computer fit according to $\tau^{-1} = A \times 14.1 \times H^4 + B$, where B represents the field-independent Raman process dominant at weak magnetic fields. The value for A obtained from the computer fit is also given in table I, and is in good agreement with the results from the measurements at liquid-helium temperatures.

If one assumes a proper H^{-4} dependence of τ for the diluted sample (fig. 6),—

the value of A at 2.10 K and 4.25 K is $(2.1 \pm 0.3) \times 10^{-4}$ and $(1.9 \pm 0.3) \times 10^{-4} s^{-1} kOe^{-4} K^{-1}$, respectively. These values are somewhat larger than those of the undiluted salt.

Using E.S.R. techniques, Gill [32]) measured the spin-lattice relaxation times in highly diluted copper potassium Tutton salts (single crystals); his results, obtained at approximately 3 kOe, can be expressed as $\tau^{-1} = 3.4 \times 10^{-4} H^4 T\ s^{-1}$ (H in kOe). De Vroomen et al. [33]), also using E.S.R. techniques, give for A in single crystals of copper ammonium Tutton salt a series of values depending mainly on the magnetic concentration. These results, also at external fields of about 3 kOe, range from $A = 10 \times 10^{-4} s^{-1} kOe^{-4} K^{-1}$ for the undiluted salt to $A = 0.6 \times 10^{-4} s^{-1} kOe^{-4} K^{-1}$ for a salt with 0.2 % copper ions. It is remarkable that this concentration dependence of τ, observed for the copper ammonium Tutton salt at weak magnetic fields, is opposite to the concentration dependence at strong fields for the copper caesium Tutton salt resulting from the present work. Recently De Vroomen et al. [39]) reported measurements of the spin-lattice relaxation times in concentrated $CuCs_2(SO_4)_2 \cdot 6H_2O$. From the temperature dependence of τ at about 3 kOe they find $A = 7.0 \times 10^{-4} s^{-1} kOe^{-4} K^{-1}$. However, from their measurements of the relaxation times at 1.28 K in magnetic fields up to 8 kOe, one can derive $A = 1.9 \times 10^{-4} s^{-1} kOe^{-4} K^{-1}$.

Stoneham [29]) calculated direct spin-lattice relaxation times of Cu^{2+} ions in potassium zinc Tutton salt, with the external magnetic field along the three principal axes of the electrical crystal field. The difference between the so-obtained relaxation times does not exceed 50 %. If one assumes the angular dependence of τ to be smooth, an estimate for A in powdered copper potassium Tutton salt will be the average value from the calculations in [29]): $A = 1.2 \times 10^{-4} s^{-1} kOe^{-4} K^{-1}$. This result is strongly dependent on the poorly known values for the velocity of sound and the electrical crystal field splitting.

As to the differences between the direct process relaxation times in the series of copper Tutton salts with different monovalent cations, it may be noted that the variations of for example the crystal field splitting and g-value among these salts, have less influence on the value of τ than some uncertain factors in the theoretical calculations. Also the differences between the experimental results are larger than those due to the choice of the salt.

Summarizing, one may conclude that the best agreement between the experimentally determined values for A in copper Tutton salts is obtained from the strong-field measurements. These mutually agreeing experimental results are confirmed by the value for A as derived from Stoneham's calculations.

2.4.4 *Conclusion.* The observed relaxation behaviour in $CuCs_2(SO_4)_2 \cdot 6H_2O$ at weak magnetic fields is dependent on the measuring method. The direct relaxation process, as derived from the measurements at strong magnetic fields, is in good agreement - both in form and numerically - with earlier experiments and with the theoretical prediction.

2.5 *Raman spin-lattice relaxation and related Debye temperatures for various copper Tutton salts*

2.5.1 *Survey of earlier results.* Many experiments performed on copper Tutton salts by resonant as well as by non-resonant techniques gave evidence for the existence of the Raman relaxation process in weak magnetic fields. From the temperature dependence of the Raman relaxation times one can obtain the Debye temperature Θ_D according to eq. (12). However, these Debye temperatures as derived by various authors do differ much from each other. Gill [32]) deducts from E.S.R. measurements on copper potassium Tutton salt a Θ_D of 113 K; Lijphart [31]), also using resonant techniques, reported Θ_D to be between 60 and 130 K for five different copper Tutton salts. Up till now, measurements obtained by non-resonance techniques yielded other Debye temperatures. De Vries [34]) reported values of 160 and 180 K for copper caesium and ammonium Tutton salt respectively. A whole series of experiments of various copper Tutton salts as performed by Van Duyneveldt et al. [37]) have been reanalysed and the Debye temperatures are found to lie between 170 and 180 K. The difference from the values for Θ_D from resonance experiments is the more striking if one realizes that the numerical values for the relaxation time τ, as obtained by both techniques, are in mutual agreement (see e.g. fig. 8).

As stated above, a reasonable agreement with the $T^9 J_8$ dependence of eq. (12) can be obtained for the earlier experiments of reference [37]). However, these experiments were performed for the study of the effect of non-magnetic impurities on the relaxation behaviour, and the authors did not execute detailed and accurate measurements in the temperature range above 14 K. The measurements reported in this section are meant to add some information to the results of reference [37]).

2.5.2 *Results and discussion.* All investigated samples consisted of small crystallites of $CuX_2(SO_4)_2 \cdot 6H_2O$ where X is the monovalent ion: Cs, Rb, K, NH_4, or Tl. The crystallites were grown from the aqueous solutions. No special precautions for extreme chemical purity have been taken, as earlier experiments

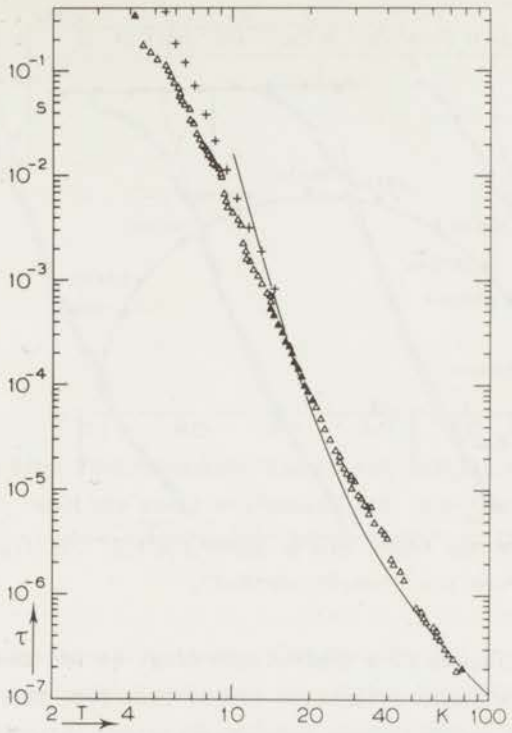

Fig. 8 *Relaxation time versus temperature for small crystallites of copper caesium Tutton salt at an external magnetic field of 1 kOe. The times indicated with closed symbols have been obtained from the Argand diagrams, the open symbols are from measurements at one frequency (running method). The crosses are from* [33] *(single crystal, H//K_1 axis, H = 3 kOe).*

never showed anomalies in the Raman relaxation if the samples were grown from Analar Chemicals supplied by Merck [34,37]).

The resulting relaxation times for copper caesium Tutton salt in the temperature range between 4 and 78 K at an external magnetic field of 1 kOe, are given in fig. 8. The times obtained from the complete Argand diagram (fig. 9) are indicated by the closed symbols. Performing such a set of measurements takes some time and can be done only when the sample is kept at constant temperature. The open symbols refer to χ', χ'' measurements at one frequency, performed during the warming up of the cryostat assembly after evaporation of the cooling liquid (running method [6])). If the relaxation proceeds by the Raman

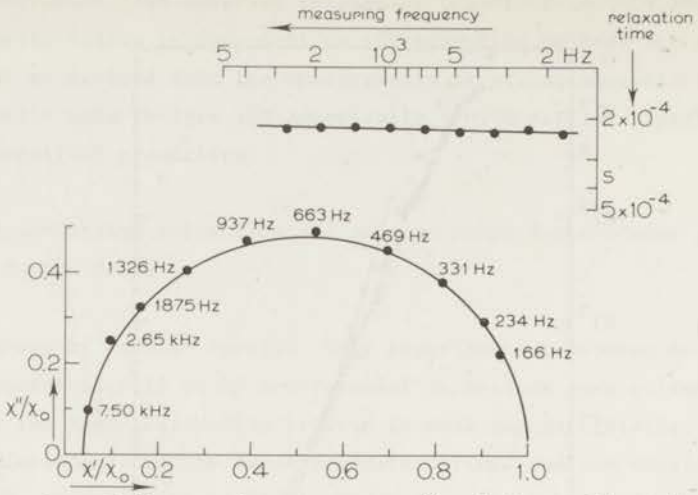

Fig. 9 *Argand diagram for copper caesium Tutton salt at T = 16.46 K and H = 1 kOe. The relaxation times obtained from this Argand diagram are shown in the upper part of the figure; the result justifies the "running method".*

process, the Argand diagram is a semi-circle (fig. 9) and the one-frequency measurements reveal reliable relaxation times. Therefore the results of the running method can be trusted above approximately 8 K, although one cannot expect the same accuracy as from measurements at fixed temperatures. It is known that, at liquid-helium temperatures and weak external fields, the relaxation process can not be characterized by one single relaxation time because of the influence of impurities, Temperley processes, etc. [37,39,40]). In such cases the Argand diagram is flattened and the running method does not lead to the average relaxation time. As a result the τ vs T graph shows a discontinuity at 4.2 K. For the present investigation this effect is of minor importance as the Raman process is our main part of interest. However, using relaxation times of fig. 8 below 8 K one must be careful.

The comments for copper caesium Tutton salt also refer to the copper rubidium, potassium, ammonium and thallium Tutton salt. For completeness, the relaxation times at 1 kOe in these four samples have been given in fig. 10, curves a to d.

From the figs. 8 and 10 one can see that the agreement between the observed relaxation times and the curve $T^9 J_8$ (drawn lines) is rather poor. The lines in the figures are matched to the measurements in such a way that the relaxation times at liquid-hydrogen and liquid-nitrogen temperatures have major

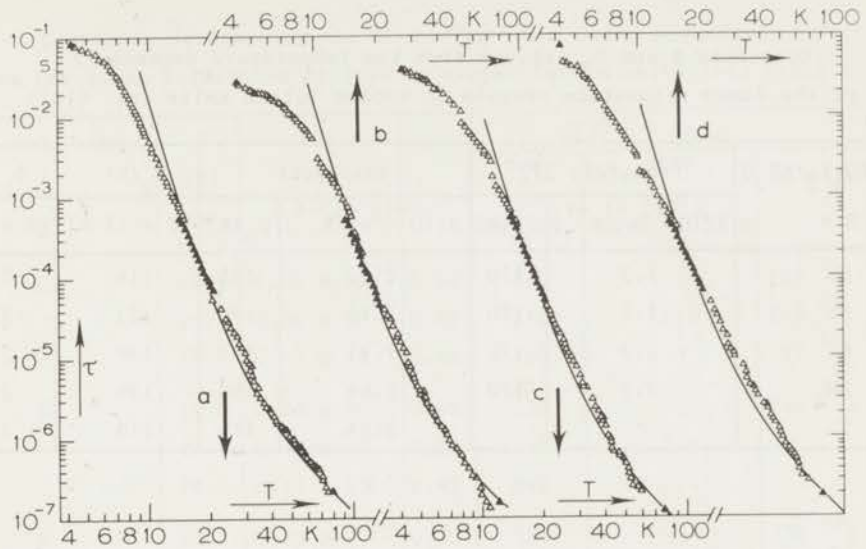

Fig. 10 *Relaxation time versus temperature for small crystallites of copper rubidium (curve a), copper potassium (curve b), copper ammonium (curve c) and copper thallium (curve d) Tutton salt at an external magnetic field of 1 kOe. The times indicated with closed symbols have been obtained from the Argand diagrams, the open symbols are from measurements at one frequency. The arrows point to the temperature scales of the various curves. The drawn lines represent* $\tau^{-1} \propto T^9 J_8(\Theta_D/T)$.

importance. In fact this is what has been done with the measurements of [37]) and, as can be seen in table II, our present results are in reasonable agreement with the data obtained from [37]).

As a check whether τ can be ascribed to a Raman process one must examine also the field dependence of the relaxation times. In the strong field approximation the Raman relaxation times are field independent. At weak external magnetic fields one has to consider the internal field $(b/C)^{\frac{1}{2}}$, yielding the so-called Brons-Van Vleck relation for the relaxation time (eq. (14)). Within the experimental accuracy all τ vs H curves could indeed be fitted to eq. (14). An example is shown in fig. 11 where the relaxation times of copper thallium Tutton salt at 14, 20 and 78 K are given as a function of the external magnetic

Table II

Constants B and Θ_D derived from the temperature dependence of the Raman relaxation process in copper Tutton salts (eq. (12))

$CuX_2(SO_4)_2 \cdot 6H_2O$ X =	from ref. 37)		this work		Θ_D(K)	Θ_D(K)
	$B(10^{-12} s^{-1} K^{-1})$	Θ_D(K)	$B(10^{-12} s^{-1} K^{-1})$	Θ_D(K)	(T = 17 K)	(T = 60 K)
Cs	1.5	170	2.12	165	114	250
Rb	1.5	170	1.73	170	122	250
K	3.0	170	1.93	175	139	240
NH_4	3.0	170	1.66	190	139	240
Tl	-	-	1.63	175	110	250

field. The drawn lines agree with eq. (14). Similar pictures have been obtained for the copper caesium, rubidium, potassium and ammonium Tutton salts. Instead of showing all results in figures we summarized our data in table III by giving the values of the constant $\tau(0)$, the internal field $(b/C)^{\frac{1}{2}}$ and the parameter p. The parameter p and the internal field values of this analysis are not particularly accurate (appr. 10 %). The internal fields can also be calculated from the adiabatic susceptibility [6]) at 4.2 K; for comparison the so-obtained $(b/C)^{\frac{1}{2}}$ values (acc. 3 %) are given in table III also, together with some results from earlier experiments on powdered samples.

The field dependences of τ described above justify the description of the relaxation processes as Raman processes. On the other hand the poor agreement between the measuring points and the drawn lines in the figs. 8 and 11 shows that the description with a curve $\tau^{-1} \propto T^9 J_8$ using a Debye temperature of approximately 180 K can not be applied over the whole temperature range. The deviations from $\tau^{-1} \propto T^9 J_8$ are more or less identical for the five copper Tutton salts that were examined. Above 20 K the actual relaxation times are longer than expected from the curves; below 14 K the reverse situation exists.

To study the deviations a close analysis of the slope of the log τ - log T curves may be of interest. The term $T^9 J_8$ in eq. (12) causes the log τ - log T curves (figs. 8 and 10) to vary from -9 towards -2 with increasing temperature. In fact -9 can only be measured if $T < 0.1\ \Theta_D$ and -2 is reached if $T > \Theta_D$. Our measurements have been performed in the intermediate temperature

Table III

Constants determining the Brons-Van Vleck field dependence of the Raman relaxation process in copper Tutton salts (eq. (14))

$CuX_2(SO_4)_2 \cdot 6H_2O$ X =	T (K)	$\tau(0)$ (s)	p	$\sqrt{b/C}$ (Oe) from Br.-Vl.	from χ_{ad} at T = 4.2 K	others
Cs	14.1	0.24×10^{-3}	0.40	210		208 [34]
	20.4	0.34×10^{-4}	0.45	210	213	215 [49]
	78	0.57×10^{-7}	0.50	195		215 [50]
Rb	14.0	0.28×10^{-3}	0.45	235		244 [49]
	20.6	0.40×10^{-4}	0.50	210	239	
	78	0.67×10^{-7}	0.45	240		
K	14.1	0.29×10^{-3}	0.45	330		324 [49]
	20.4	0.22×10^{-4}	0.40	330	322	
	78	0.70×10^{-7}	0.40	310		
NH_4	14.1	0.28×10^{-3}	0.40	400		392 [34]
	20.4	0.31×10^{-4}	0.50	375	395	389 [51]
	78	0.67×10^{-7}	0.50	390		387 [49]
Tl	14.1	0.21×10^{-3}	0.30	400		
	20.4	0.37×10^{-4}	0.40	380	373	
	78	1.0×10^{-7}	0.50	330		

range and therefore will show a slope α: $-9 < \alpha < -2$. From eq. (12) one sees that α is a function of the quotient Θ_D/T. We performed a computer calculation to define this function. The result showed a severe change in α if $0.05 < T/\Theta_D < 0.3$. To get an idea of the variations in α some numbers are quoted in table IV.

The relaxation times between 14 and 21 K were obtained from detailed and accurate susceptibility measurements. If one considers this small temperature range in the double logarithmic plot the measurements can be represented by a straight line. As an example fig. 12 shows such a plot, this time for the copper rubidium sample. The line in fig. 12 corresponds to $\alpha = -5.8$. If this value of α is taken to be representative for the slope of the log τ - log T curve at

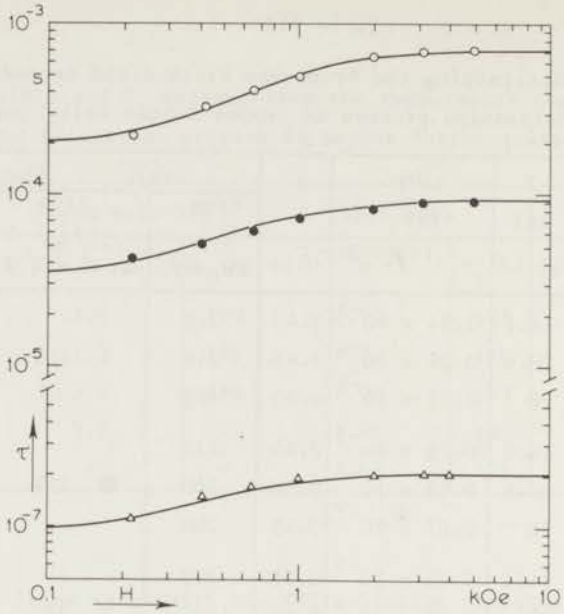

Fig. 11 *Relaxation time versus external magnetic field for copper thallium Tutton salt at 14.1 (O), 20.4 (●) and 78 K (Δ). The drawn lines are the Brons-Van Vleck field dependences (constants in table III).*

Table IV

Various values for α (= d log τ/d log T)
calculated from $\tau^{-1} = T^9 J_8(\Theta_D/T)$

$-\alpha$	Θ_D/T	$-\alpha$	Θ_D/T
2.1	0.88	5.8	7.2
2.5	2.0	6.3	8.0
3.0	3.0	6.9	9.1
3.6	3.9	7.4	10.2
4.3	5.0	8.3	12.8
5.0	6.0	8.8	16.0

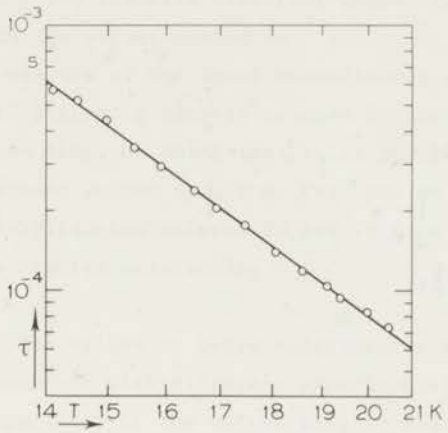

Fig. 12 *Relaxation time versus temperature for copper rubidium Tutton salt (H = 1 kOe). The drawn line shows* $\tau \propto T^{-5.8}$ *leading to* $\Theta_D = 122$ *K.*

17 K, then table IV shows the corresponding Θ_D-value to be 122 K. A similar approach to the relaxation times of the other copper Tutton salts at these temperatures leads to the Θ_D-values given in the fifth column of table II. All values are definitely lower than 170 K and become close to the results obtained from resonance experiments.

One may conclude that the value of the Debye temperature is directly related to the temperature interval where the measurements are done. In fact this result implies that the phonon spectrum can not be described by the Debye model. This is, of course, not a new conclusion as many other experiments did show similar effects (e.g. ref 41). However, usually the Raman relaxation processes can be described by expressions similar to eq. (12) or (13) (e.g. references 8, 26 and 42), which suggests that the Debye model is applicable to the relaxation phenomena.

The approach to the relaxation times at liquid-hydrogen temperatures and the consequent Debye temperatures suggest an extension of this analysis over the whole temperature range. This has been done by calculating the slope of the smooth curve through the measurements of figs. 8 and 10. As a result one derives

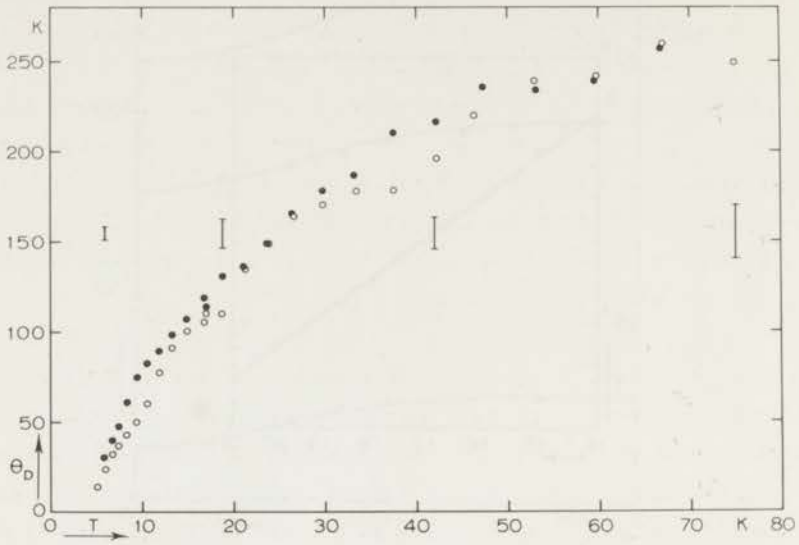

Fig. 13 *Debye temperatures derived from the slope of the log τ - log T curves of copper caesium (closed circles) and copper thallium Tutton salt (open circles). The vertical bars indicate the accuracy of the determination in the various temperature ranges.*

a whole series of Debye temperatures. An example is given in fig. 13 where the Θ_D-values of copper caesium and copper thallium Tutton salt obtained in this way are plotted against the temperature where the slope of the log τ - log T curve has been determined. Below 10 K the resulting Debye temperatures are extremely low, but these values are not to be considered seriously as the influence of other relaxation processes becomes important. This conclusion can be made not only because of the flattened Argand diagram, but also from the fact that the Brons-Van Vleck field dependence of τ is not fulfilled below 10 K. The Debye temperatures in fig. 13 seem to reach a limiting value of 250 K at about T = 60 K. The resulting Debye temperatures for the other copper Tutton salts showed a behaviour similar to that in fig. 13. For copper potassium and copper ammonium Tutton Θ_D reached 240 K; the copper rubidium salt showed maximally Θ_D = 250 K. Although these limiting values are not too accurate (10 %) we have included them in table II, last column.

Graphs like fig. 13 explain the discrepancies between the Debye temperatures

obtained by resonance and non-resonance techniques. E.S.R. experiments to determine τ are usually not extended above 14 K so the Θ_D-values will correspond to the left hand part of fig. 13. In fact our measurements at 10 K show Θ_D to lie between 60 and 90 K for the five different copper Tutton salts, which is in perfect agreement with the values quoted in [31]).

Considering the results of the above measurements and the fact that the phonon frequency distribution is closely related to the temperature dependence of the Raman relaxation time, we think that it is possible to obtain more information about the actual phonon spectrum. For such an analysis it is necessary that a temperature stabilization between 20 and 78 K is obtained, so that the Argand diagram can be studied accurately.

2.5.3 *Conclusion.* The values of Debye temperatures obtained from Raman relaxation time measurements with different experimental techniques must be treated carefully, especially if the values rely on measurements over a limited temperature interval. The reported difference between Θ_D-values from resonance and non-resonance techniques in the case of copper Tutton salts could be explained by a close study of the Raman processes between 14 and 78 K. More accurate measurements may in fact give information about the phonon spectrum.

2.6 *Spin-lattice relaxation in ytterbium chloride hexahydrate*

2.6.1 *Introduction.* Kramers salts, which have an anisotropic Zeeman energy splitting of the ground doublet, such as many crystals containing rare-earth ions, show a direct relaxation process that depends not only on the temperature and magnetic field value but also strongly on the orientation of the crystal with respect to the external magnetic field [13]). If the electrical crystal field has axial symmetry at the site of the magnetic ion, the splitting of the ground doublet can be described by an anisotropic g-value [43]),

$$g(\theta) = (g_{//}^2 \cos^2\theta + g_{\perp}^2 \sin^2\theta)^{\frac{1}{2}} \qquad (17)$$

where $g_{//}$ and $g_{\perp}$ are the g-values measured parallel and perpendicular to the symmetry axis. The angle between this axis and the magnetic field is denoted by θ.

Brom [44]) applied Orbach's relaxation theory [13]) to the case of ytterbium chloride hexahydrate. Starting from hexagonal crystal field symmetry at the site of the magnetic ion [45]) and from the fact that the value of $g_{\perp}$ is 0.08,

which is negligibly small compared to the $g_{//}$-value of 5.6, he derived for the direct process electron spin-lattice relaxation time in the high temperature approximation:

$$\tau_{dir}^{-1} = 0.7 \times 10^{-2} H^4 T \sin^2\theta\cos^2\theta \; s^{-1} \quad (H \text{ in kOe, } T \text{ in K}) \; . \qquad (18)$$

The proton spin-lattice relaxation measurements of Brom verified the angular dependence of eq. (18), while a reasonable numerical agreement was achieved also [44].

Earlier non-resonance experiments on the relaxation phenomena in powdered $YbCl_3 \cdot 6H_2O$ [52] did agree with eq. (18) if one allows for a random orientation distribution of the small crystals in the powder. The measurements reported in this section confirm these preliminary results. In addition to this direct relaxation process studied at 4.2 K, the relaxation occurring at weak external magnetic fields has also been investigated at temperatures between 1.8 and 21 K. We shall discuss in 2.6.3 that these results are described by the Raman spin-lattice relaxation process and not by an Orbach mechanism via the next excited doublet of 197 K as suggested by Kalvius et al. [46].

2.6.2 *Experimental results.* The relaxation behaviour has been studied by applying the dispersion-absorption technique. In order to avoid interference with other relaxation processes, the measurements of the direct relaxation process have to be performed at strong external magnetic fields. However, at these field values, phonon-bottleneck effects are likely to occur (cf. $CuCs_2(SO_4)_2 \cdot 6H_2O$ section 2.4). To minimize the influence of phonon bottleneck, the experiments were started on a powdered sample of $YbCl_3 \cdot 6H_2O$ with average grain diameter 0.1 mm. To see whether some influence of the angular dependence of the direct relaxation time can be found, we also carried out measurements on a single crystal of size about 10 x 9 x 2 mm.

The paramagnetic spin-lattice relaxation times of the powdered sample were measured up to 24 kOe at a temperature of 4.2 K (fig. 14). At magnetic fields below 2 kOe, the field dependence of τ can be described by the Brons-Van Vleck formula (eq. (14)) valid for the Raman relaxation process:

$$\tau(H) = 3.0 \times 10^{-3} \times [1 + H^2/(9 \times 10^4)]/[1 + 0.2\, H^2/(9 \times 10^4)] \; s \qquad (19)$$

At magnetic fields stronger than 6 kOe the direct process starts to dominate, causing a sharp decrease of the relaxation time with increasing magnetic field.

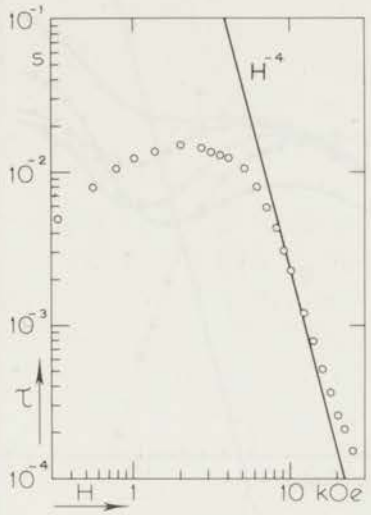

Fig. 14 *Relaxation time τ versus external magnetic field H for a powdered sample of $YbCl_3 \cdot 6H_2O$ at 4.2 K.*
——— $\tau \propto H^{-4}$.

At fields stronger than 8 kOe the relaxation time is proportional to $H^{-3.0}$.

The relaxation times obtained on the single crystal, also at the temperature of 4.2 K, are displayed in fig. 15 as a function of the magnetic field at various orientation angles θ. The accuracy of the determination of θ is about 5^{o}.

At weak magnetic fields, H < 3 kOe, the relaxation times do not vary much when changing the orientation angle θ. The field dependence of τ, determined at fixed crystal orientations, can be described by Brons-Van Vleck relations. A numerical determination of the parameters p and b/C has not been performed.

At magnetic fields above 5 kOe the slope of the τ vs H curve becomes dependent on crystal orientation. The observed relaxation times do not show an H^{-4} dependence as expected from eq. (18). This is not surprising since the results on the powdered specimen exhibit, instead of the H^{-4} dependence of

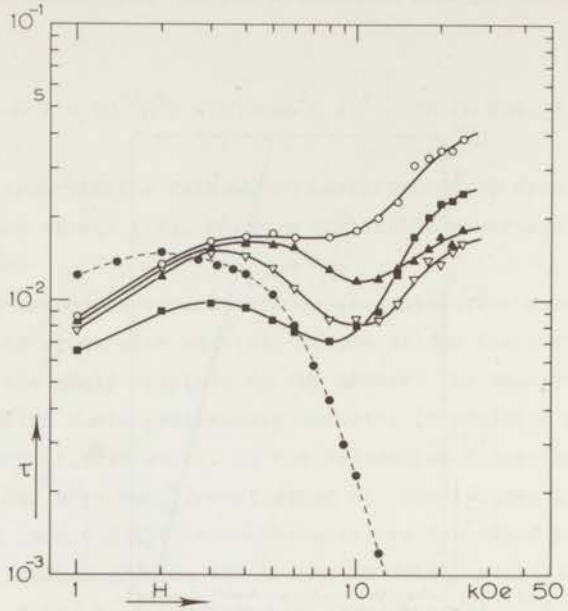

Fig. 15 *Relaxation time τ of $YbCl_3 \cdot 6H_2O$ (single crystal) versus external magnetic field H for various orientation angles θ at 4.2 K.*
○ : θ = 0° ; ▲ : θ = 5° ; ▽ : θ = 20° ; ■ : θ = 30° ;
● : *powdered sample.*
Drawn lines are for visual aid only.

τ, a $H^{-3.0}$ dependence due to the influence of phonon-bottleneck effects (see discussion). So one may expect a severe phonon bottleneck to be present at the direct process in a large single crystal of this salt. The increase of the relaxation time at the strongest magnetic fields may also be due to this phonon bottleneck.

As mentioned above, the relaxation at weak external magnetic fields can be described by Brons-Van Vleck relations. This means that the above-mentioned experiments already suggest the existence of a Raman relaxation process. This Raman process has been investigated by observing its most obvious property: the strong temperature dependence of the relaxation time. Fig. 16 shows this dependence for the powdered specimen at an external magnetic field of 1 kOe. From 4 K up to liquid-hydrogen temperatures the relaxation time is proportional

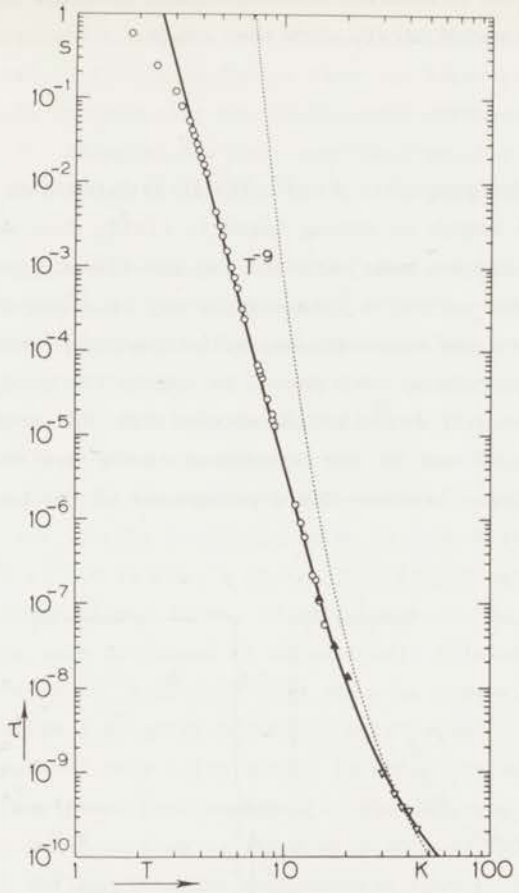

Fig. 16 *Relaxation time versus temperature for a powdered sample of* $YbCl_3 \cdot 6H_2O$ *in an external magnetic field of 1 kOe.*
○ : present work; ▲ : Hillaert [47]*; ▽ : Kalvius et al.* [46]*).*
——— : $\tau^{-1} = 0.47 \times 10^{-8}\ T^9 J_8\ (180/T)\ s^{-1}$.
- - - : $\tau^{-1} = 4.8 \times 10^{11}\ exp(-197/T)\ s^{-1}$.

to T^{-9} as expected for the Raman relaxation process in this salt. The results between the liquid-helium and the liquid-hydrogen temperatures were obtained using the "running method" [6]. Since at temperatures above about 15 K the relaxation times become too short to be measured by our equipment, Hillaert [47] performed some dispersion and absorption measurements in this temperature region, using a double T-bridge [48]. His results are denoted by the symbol Δ in fig. 16. The very short times between 10^{-9} and 10^{-10} s indicated by the

symbol ▽ in the same figure were obtained from Mössbauer measurements by Kalvius et al. [46]). The relaxation times obtained by these three different measuring techniques match nicely with each other.

2.6.3 *Discussion*

a) *Relaxation at strong magnetic fields.* The field dependence of the relaxation time of the powdered sample at strong magnetic fields does not show the H^{-4} dependence which would have been expected for the direct process (fig. 14). The deviation from the theoretical H^{-4} dependence may be ascribed to phonon-bottleneck effects, which become more serious as the magnetic field increases [26]). Such behaviour is observed in many cases, it occurs for example in the undiluted copper caesium Tutton salt described in section 2.4. The existence of a phonon bottleneck is also confirmed by the dependence of the deviation parameter d on magnetic field. Fig. 17a shows the d-parameters of the powdered sample. At

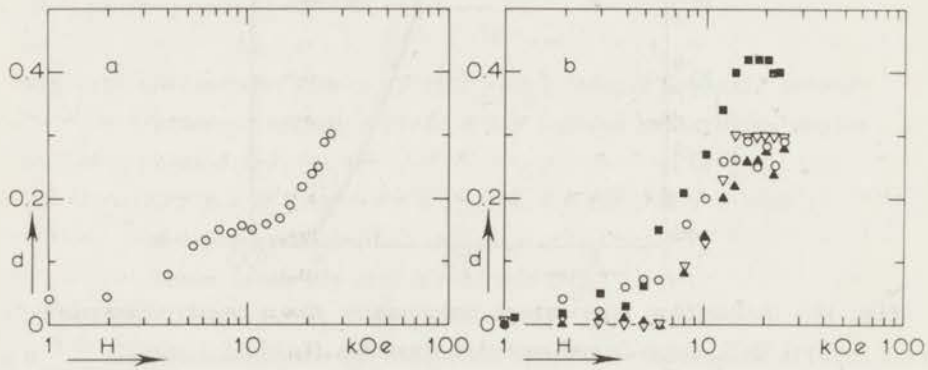

Fig. 17 *Deviation parameter d versus external magnetic field H for* $YbCl_3 \cdot 6H_2O$ *at 4.2 K.*
a. powdered sample.
b. single crystal, symbols as in fig. 15.

weak fields these values are very small; at moderate field strengths from 7 kOe up to 11 kOe this value is about 0.15. At stronger magnetic fields, however, the deviation parameter d increases considerably due to the influence of phonon-bottleneck effects. To determine the coefficient A of the direct

relaxation process ($\tau^{-1} = AH^4T$) in the powdered sample according to the interpolating method [26]), one uses the relaxation time at 11 kOe, the field value where the phonon-bottleneck effects are minimal. At this magnetic field the direct process is only a factor 10 faster than the Raman process, so the Raman process gives a small contribution to the observed inverse relaxation time according to eq. (15). Allowing for this contribution, the interpolation method yields a value of $(1.0 \pm 0.1) \times 10^{-2} kOe^{-4} K^{-1} s^{-1}$ for the coefficient A of the direct process.

Brom [44]), using the Bloembergen relation, derived the expression $\tau^{-1} = 6.9 \times 10^{-2} H^4 T \sin^2\theta \cos^2\theta$ from proton spin-lattice relaxation measurements for the Yb^{3+} electron spin-lattice relaxation time. Starting from this result one can calculate a value for the coefficient A expected for the averaged relaxation process in a powder with a random distribution of the orientations of the crystallites. At the same time a weight factor has to be introduced due to the anisotropic susceptibility. Taking these effects into account one derives an averaged value for the inverse relaxation time in a powdered sample: $\tau^{-1} = 1.1 \times 10^{-2} H^4 T\ s^{-1}$ (H in kOe, T in K). This result agrees nicely with the experimental results mentioned above, in particular if one realizes that the measurements of Brom were performed on magnetically diluted samples. In an earlier paper Brom et al. [52]) derived from the same measurements on proton spin-lattice relaxation a slightly different expression: $\tau^{-1} = 0.9 \times 10^{-2} H^4 T$ (H in kOe, T in K), based on a calculation, in which the anisotropy of the susceptibility was not taken into account. In the same way, the theoretical expression eq. (18) leads to a value for A of $0.10 \times 10^{-2} kOe^{-4} K^{-1} s^{-1}$ for a powder, a factor 10 smaller than the experimental result. Taking into consideration the order of magnitude character of the theoretical calculation, this discrepancy is not large.

The constant value of the deviation parameter d between 7 and 11 kOe, as may be seen in fig. 17a, is quite large at these field strengths in comparison to the corresponding values of the d-parameter in other salts (cf. section 2.4). This large d-parameter may be inherent to the anisotropic character of the direct spin-lattice relaxation process. Starting from the same premises, as used in the calculation of the average coefficient A, one can calculate the complex susceptibility for a powder. The Argand diagram so-obtained can be characterized by a d-parameter of 0.13. This is in good agreement with the experimental results between 7 and 11 kOe, considered their absolute accuracy of about 0.05. The accuracy of the relative changes of the d-parameter as a function of field, which are really important for the interpolation method is

much better (e.g. 0.01).

To demonstrate the strong angular dependence of the direct relaxation process, the measurements on the single crystal (fig. 15) were performed; although one cannot expect to obtain results according to eq. (18) because of the usually large phonon-bottleneck effects in single crystals [26]). In fig. 18

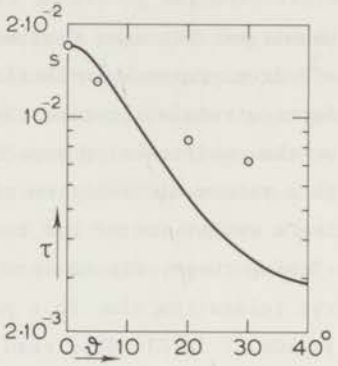

Fig. 18 *Relaxation time τ of $YbCl_3 \cdot 6H_2O$ (single crystal) versus orientation angle θ in an external field of 8 kOe at 4.2 K. ——: $\tau^{-1}_{observed} = \tau^{-1}_{dir} + \tau^{-1}_{Ram}$ (excluding phonon-bottleneck effects).*

the relaxation time observed is plotted as a function of the orientation angle θ at an external magnetic field of 8 kOe. This field value was chosen since the orientation dependence is most pronounced while the phonon-bottleneck effects are not yet very severe. The variation of the relaxation time as a function of the angle θ is less than the $\sin^{-2}\theta\cos^{-2}\theta$-dependence predicted by theory (eq. (18)) and determined by proton spin-lattice relaxation measurements [44]). The experimentally determined relaxation time is always a sum of the direct and the Raman relaxation process according to eq. (15). Since in this salt the Raman process yields a relaxation time of 17×10^{-3}s at 8 kOe and 4.2 K (fig. 15), one will not notice the direct process if its relaxation time becomes much larger than 17×10^{-3}s. The drawn line in fig. 18 represents the observed relaxation time, if the anisotropic direct and the Raman process operate parallel to each other. The fact that the observed relaxation times exceed

the drawn line is not surprising as phonon-bottleneck effects, which lengthen the relaxation time, were not considered in determining the drawn line. These phonon-bottleneck effects are so large in this single crystal that at stronger external fields the τ vs H curves increase again (fig. 15).

The picture as discussed above, agrees with the behaviour of the d-parameter as a function of the external magnetic field (fig. 17b). This d-value starts to differ from zero at fields of about 5 kOe and increases gradually to the larger values of 0.3 and even 0.4 at the strongest fields. In fig. 15 it is seen that the phonon bottleneck occurring at the strongest magnetic fields has more influence on the observed relaxation time at the orientation $\theta = 30^{o}$ than at the other directions. This is in agreement with the fact that the largest d-value (0.4) is observed at $\theta = 30^{o}$.

Finally, let us compare on the one side the present results and on the other side the results from the proton spin-lattice relaxation measurements, which are related via the Bloembergen relation to the electron-spin relaxation. Then we conclude that the dispersion-absorption measurements confirm the existence of the direct electron-spin relaxation process as deduced from the proton-spin relaxation measurements.

b) *Relaxation in weak magnetic fields*. The graph of the deviation parameter d of the powdered sample as a function of the magnetic field, fig. 17a, shows this parameter to be almost zero at fields below 2 kOe. This indicates that the observed relaxation process is not affected seriously by typical weak-field complications caused by, for example, physical or chemical impurities (cf. $CuCs_2(SO_4)_2 \cdot 6H_2O$, section 2.4).

As fig. 16 shows, the experimental results obtained by the three different measuring methods give an excellent fit to eq. (12) for the Raman process with a Debye temperature Θ_D of 180 K:

$$\tau^{-1} = 0.47 \times 10^{-8}\, T^9 J_8(\Theta_D/T)\ s^{-1} .$$

This good agreement between the theoretical and experimental results for the Raman relaxation indicates that the phonon frequency spectrum is described fairly well by the Debye model. This is not true for all salts, as was seen in section 2.5. Measurements of the specific heat [53]) yield a value of 200 K for the Debye temperature, which is close to the value derived from the Raman relaxation times.

The difference between the experimental results and the drawn curve in

fig. 16 at the lower liquid-helium temperatures may be due to a small influence of fast relaxing weak-field mechanisms. The description of the field dependence of the relaxation time by the Brons-Van Vleck formula yields a rather small p-value (0.2 in eq. (19)). This effect may be caused by typical weak-field mechanisms, as these mechanisms give rise to a more pronounced field dependence (cf. section 2.5). However, these "impurity relaxations" at weak fields always influence the susceptibility to deviate from the Debye form, causing a non-zero d-parameter. As stated above, this effect is not seen in $YbCl_3 \cdot 6H_2O$, so we conclude that "impurity relaxations" are not very effective in this salt.

The small dependence of the relaxation time of the single crystal on the orientation at magnetic fields below 3 kOe (fig. 15), can be attributed to the internal field $(b/C)^{\frac{1}{2}}$, which is proportional to $\cos^{-1}\theta$, as Curie's constant C is proportional to $\cos^2\theta$ and b, which is equal to the asymptotic value of $C_M T^2$, does not depend on θ. The $(b/C)^{\frac{1}{2}}$-value influences the Raman relaxation time according to the Brons-Van Vleck relation (eq. (14)), while also small temperature differences affect the relaxation time of the Raman process ($\tau \propto T^{-9}$) easily.

From Mössbauer experiments at temperatures above 30 K, Kalvius et al. [46]) suggest for the paramagnetic spin-lattice relaxation time in $YbCl_3 \cdot 6H_2O$: $\tau^{-1} = 4.8 \times 10^{11} \exp(-197/T)\ s^{-1}$. This Orbach process would lead to a slope of the log τ - log T curve that exceeds -9 and to relaxation times that are considerably longer than our present results as is illustrated by the dotted line in fig. 16. In the same figure one may notice that the extrapolation of the Raman relaxation process down to 50 K gives to the experimental results of Kalvius a closer agreement than obtained with the Orbach process. The conclusion must be that the Orbach mechanism is not involved in the relaxation processes observed in $YbCl_3 \cdot 6H_2O$.

2.6.4 *Conclusion.* The dispersion-absorption measurements have clearly demonstrated the existence of the direct relaxation process at strong external magnetic fields and the Raman relaxation process at weak fields. Also the orientation dependency of the direct process has been confirmed. Summarizing one can describe the spin-lattice relaxation time in powdered $YbCl_3 \cdot 6H_2O$ by (H in kOe, T in K):

$$\tau^{-1} = (1.0 \pm 0.1) \times 10^{-2} H^4 T + 0.47 \times 10^{-8} T^9 J_8\ (180/T)\ s^{-1}.$$

CHAPTER III

RELAXATION PHENOMENA AT AND NEAR MAGNETIC PHASE TRANSITIONS

3.1 *Survey*

Magnetic phase transitions have been the subject of many experimental and theoretical studies. Most of this work concerns mainly the static properties of a magnetic material; for example, to find out which magnetic state prevails under certain conditions of temperature and externally applied magnetic field. The question how much time it takes to reach an equilibrium situation near a phase transition, is usually kept without consideration. Some publications refer indirectly to these relaxation phenomena by mentioning that one had to wait some time to obtain a stationary situation after a change of the external conditions. In 1958 Lasheen et al. [54]) reported measurements on such time dependent behaviour in a magnetically ordered state. Since that time only a few investigations have been carried out [55,56]).

The work described in this chapter extends the experimental knowledge on relaxation phenomena near several types of magnetic phase transitions. In the first part relaxation phenomena near the phase transition between the paramagnetic and antiferromagnetic region of $MnCl_2 \cdot 4H_2O$ and $MnBr_2 \cdot 4H_2O$ are presented. Also relaxation times in the paramagnetic state are reported. Next some results on the antiferromagnetic - spin flop transition of $CsMnCl_3 \cdot 2H_2O$ are given. The last section deals with the complicated relaxation behaviour at the antiferromagnetic-ferrimagnetic and ferrimagnetic-ferromagnetic phase transitions in $CoCl_2 \cdot 2H_2O$.

3.2 *Relaxation phenomena near the magnetic phase transition of manganese chloride and manganese bromide tetrahydrate*

3.2.1 *Introduction and survey of previous results.* Crystals of $MnCl_2 \cdot 4H_2O$ (the α form*) and $MnBr_2 \cdot 4H_2O$ are isomorphous, having both a monoclinic crystal

---

* It should be noted that Groth referred to this modification of manganese chloride, which is stable at room temperature, as the β form in disagreement with the generally used nomenclature [58]).

structure [57]). An X-ray diffraction study of $MnCl_2 \cdot 4H_2O$ by Zalkin et al. [58]) showed that each manganese ion is the centre of a distorted octahedron consisting of four water molecules and two chlorine atoms adjacent to each other. The antiferromagnetism of these salts is detected from specific heat measurements on the manganese chloride by Friedberg and Wasscher [59]) and magnetization measurements on the chloride and the bromide salt by Henry [60]). The temperature below which antiferromagnetism occurs, the Néel temperature T_N, as determined from this early work is 1.62 K for the chloride [59]) and 2.2 K for the bromide [60]). Recent high resolution specific heat measurements yield T_N = 1.6257 K for $MnCl_2 \cdot 4H_2O$ [61]) and T_N = 2.120 K for $MnBr_2 \cdot 4H_2O$ [62]). The magnetic phase diagrams of both salts are known from measurements of the magnetization and resonance experiments by Gijsman, Poulis and Van den Handel [63]) on single crystals orientated along various directions with respect to the externally applied magnetic field. Their results, which proved to be in qualitative agreement with calculations of Gorter and Tineke van Peski-Tinbergen [64]) based on Néel's molecular field model, gave evidence for the existence of two magnetic sublattices with the crystallographic c axis as the preferred direction of the sublattice magnetizations (easy axis). Below about 1.25 K, in external fields stronger than 8 kOe, a spin-flop phase is detected in $MnCl_2 \cdot 4H_2O$, which means that the directions of the two sublattice magnetizations are nearly perpendicular to the preferred axis and opposite to each other [63]). The antiferromagnetic spin arrangement has been investigated by Spence and Nagarajan [65]) using proton and chlorine N.M.R. Their work suggests that the two magnetic sublattices are formed by alternating sheets of Mn^{2+} spins parallel to the bc crystallographic plane.

The study of magnetic relaxation times by means of the dispersion-absorption method on $MnCl_2 \cdot 4H_2O$ samples has been commenced by Lasheen, Van den Broek and Gorter [54]). Using a single crystal of $MnCl_2 \cdot 4H_2O$, with the external magnetic field parallel to the crystal c axis, these authors could not detect any relaxation process in the antiferromagnetic state. However, measurements on a powdered sample could be carried out successfully at temperatures lower than T_N. The relaxation times at an external field of 4.5 kOe are of the order of 10^{-2} s and can be given as $\tau \propto T^{-2.4}$, with an indication of a local maximum at the transition temperature. Another interesting result of this early work is the existence of a second relaxation process below T_N with relaxation times that are about a factor 100 smaller.

Encouraged by these interesting investigations the study of the relaxation behaviour of manganese chloride and bromide was resumed in 1969 [55]). Since the relaxation times involved are rather long, we were obliged at that time to

analyze the recovery of the adiabatic susceptibility as a function of time after a step change of the external magnetic field (field step method, section 1.1). The sensitivity of this method is determined by the quantity $(\partial\chi_{ad}/\partial T)_H$. This quantity is largest in single crystals with the preferred axis parallel to the external magnetic field. The results in this case for $MnCl_2 \cdot 4H_2O$ showed the occurrence of a maximum value of the relaxation time at the phase-transition temperature. In the antiferromagnetic region the relaxation behaviour could not be described with a single time constant. This measuring procedure did not reveal time constants for a powdered specimen as the derivative $(\partial\chi_{ad}/\partial T)_H$ is very small in this case.

The extension of the measuring facilities to very low frequencies (section 1.2.1) made it possible for us to reexamine the above-mentioned features of the manganese chloride and bromide single crystals, by means of the dispersion-absorption technique.

3.2.2 *Qualitative behaviour of the measurements.* As described in chapter I the dispersion-absorption method enables us to record the real and imaginary component of the susceptibility (χ' and χ'') as a function of a quasistatic varying external magnetic field. The plots registered in this way for paramagnetic substances generally show a decreasing χ' accompanied by an increasing χ'' as a function of the applied magnetic field; examples for this case are given by De Vries [66]. For an antiferromagnetic material a more complicated plot is obtained. Fig. 19 shows such a dispersion-absorption measurement determined by the measuring procedure described in chapter I. In this figure the quasistatic field passes the phase boundary between the antiferromagnetic and paramagnetic region at the transition field H_t. The measuring frequency is of the order of magnitude of τ^{-1}. χ' increases in the antiferromagnetic region towards a maximum at H_t. In the following paramagnetic region χ' decreases. These pictures are analogous for all measuring frequencies; however, it is noticeable that the dispersion χ'/χ_0 observed at H_t is largest for the lowest frequencies. χ'' is only observed over a limited range of frequencies: $10^{-1} < \omega\tau < 10$. χ'' also increases as a function of the external field until a maximum is reached at H_t. At the start of the following paramagnetic region χ'' decreases rapidly to zero, after which it increases at stronger external magnetic fields.

As is known from measurements of the static magnetization [60,67,68,69] the isothermal susceptibility $\chi_T = (\partial M/\partial H)_T$ plotted as a function of external magnetic field shows a maximum near the phase boundary. This susceptibility χ_T corresponds to the dispersion measured at frequencies which are small compared

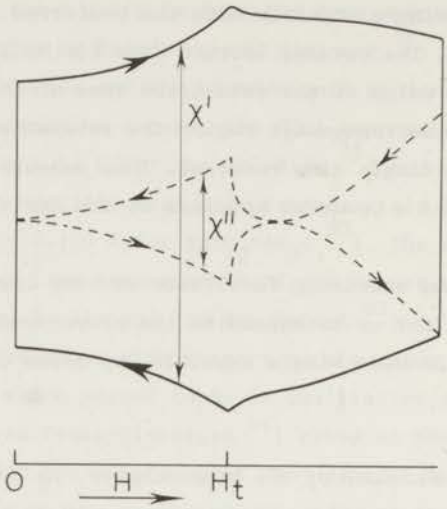

Fig. 19 *Absorption χ'' and dispersion χ' as a function of the external magnetic field for $MnCl_2 \cdot 4H_2O$ (H//c axis). For clarity χ'' has been enlarged by a factor 5; H_t is the transition field.*

to τ^{-1} (eq. (1)). According to the Casimir-Du Pré formula one expects at higher frequencies a dispersion decreasing from χ_T to the high frequency limit χ_{ad}. At intermediate frequencies χ'' differs from zero, and is maximally $\frac{1}{2}(\chi_T - \chi_{ad})$. The above-mentioned susceptibilities are related to each other by:

$$\frac{\chi_T - \chi_{ad}}{\chi_T} = \frac{C_H - C_M}{C_H} = 2\,\frac{\chi''_{max}}{\chi_T} \quad . \tag{20}$$

The following thermodynamic expression [70]) relates the specific heats of the spin system at constant field and magnetization, C_H and C_M to each other:

$$C_H = C_M + T\left(\frac{\partial M}{\partial T}\right)^2_H \Big/ \left(\frac{\partial M}{\partial H}\right)_T \quad . \tag{21}$$

Since $(\partial M/\partial H)_T$ is χ_T, eq. (20) yields:

$$\chi_T = \chi_{ad} + \frac{T}{C_H}\left(\frac{\partial M}{\partial T}\right)^2_H \qquad (22)$$

and

$$\chi''_{max} = \frac{T}{2\,C_H}\left(\frac{\partial M}{\partial T}\right)^2_H \quad . \qquad (23)$$

The term $(T/C_H)(\partial M/\partial T)^2_H$ in these equations expresses the part of the susceptibility that participates in the relaxation process. By means of eqs. (22) and (23) it is now possible to sketch the behaviour of χ' and χ'' as a function of the external field near the phase transition, if the magnetization M and the specific heat C_H are known as functions of the external field H and the temperature T. The restriction must be made that the relaxation time τ does not vary too drastically in the field region concerned. At zero magnetic field M is zero for all temperatures, so the derivative $(\partial M/\partial T)_H$ is zero, which brings about that then $\chi' = \chi_T$ and $\chi'' = 0$. From the measurements of the magnetization and the specific heat [68]) the behaviour of $(\partial M/\partial T)_H$ and C_H as functions of temperature at H = 4 kOe, is obtained, as displayed in fig. 20. The intervals

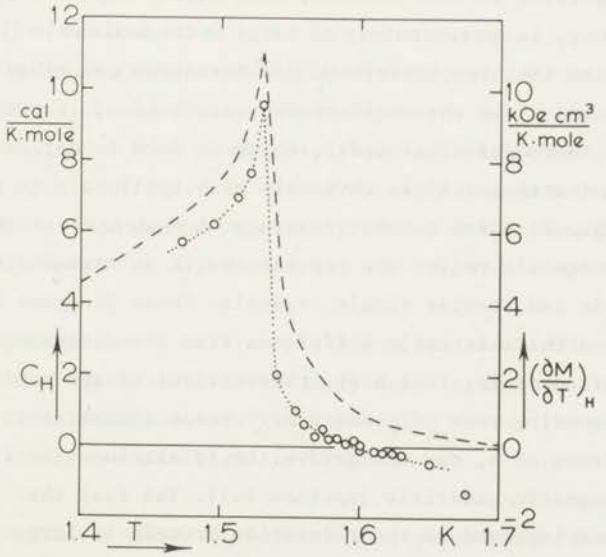

Fig. 20 *C_H(- - -) and $(\frac{\partial M}{\partial T})_H$ (...) as a function of temperature for $MnCl_2 \cdot 4H_2O$. (H = 4 kOe; H//c axis; measurements from [68]).*

of the magnetic field at which these measurements are performed are too large to derive the corresponding plots of $(\partial M/\partial T)_H$ and C_H versus H at constant temperature. Since the temperature dependence of both $(\partial M/\partial T)_H$ and C_H will not change drastically by varying the external field, one can expect that the behaviour of both $(\partial M/\partial T)_H$ and C_H as function of T and as function of H will be at least qualitatively similar. So one can expect that at increasing magnetic field both C_H and $(\partial M/\partial T)_H$ increase until the transition field is reached. The increase of the quadratic derivative $(\partial M/\partial T)_H^2$ will dominate the term $(T/C_H) \times (\partial M/\partial T)_H^2$. In the following paramagnetic region $(\partial M/\partial T)_H$ will decrease as a function of H and even become negative. The specific heat C_H will decrease also but stays positive. As a result $(T/C_H)\ (\partial M/\partial T)_H^2$ will decrease rapidly to zero in the beginning of the paramagnetic region, while it increases slowly at higher external magnetic fields. The signal proportional to χ'' in fig. 19 shows a field dependence which corresponds qualitatively to the behaviour just described for the expression (23). For all applied field values, χ' in fig. 19 will have a value between χ_T and χ_{ad} as given by eq. (22). One can derive from magnetization measurements (e.g. [68])) that χ_T shows when plotted as a function of the magnetic field at constant temperature a rather sharp maximum near the phase boundary. Measurements of χ' and χ'' versus H, carried out at frequencies $\omega >> \tau^{-1}$, which will be described later in this section, show hardly any anomaly, indicating that the maximum in χ_T is approximately as large as the maximum in $(T/C_H)\ (\partial M/\partial T)_H^2$.

The assumption that the Casimir-Du Pré formalism describes the frequency dependence of χ' and χ'' in the antiferromagnetic region, is confirmed by our experiments. The thermodynamical model, which is used to derive the Casimir-Du Pré formalism (section 1.1) is obviously also applicable to antiferromagnetic materials. In figs. 21 a and c some frequency dependences of the susceptibility in the antiferromagnetic region are represented in an Argand diagram for both manganese chloride and bromide single crystals. These diagrams also yield semicircles, but a characteristic difference from the diagrams obtained for paramagnetic substances is, that both intersections of the semicircle with the abscissa, corresponding to χ_{ad}/χ_0 and χ_T/χ_0 exceed the value 1. From this frequency dependence of $\bar{\chi}$, one can derive the relaxation time in just the same way as for paramagnetic materials (section 1.1). The fact that the part of the susceptibility not involved in the relaxation process is large in the antiferromagnetic state $(\chi_{ad}/\chi_0 > 1)$, makes it necessary to measure $\bar{\chi}$ with a higher accuracy than for paramagnetic substances, in order to study the relaxation mechanism with the same accuracy. Actually this explains most of the experimental difficulties in earlier experiments. As the absorption does not have –

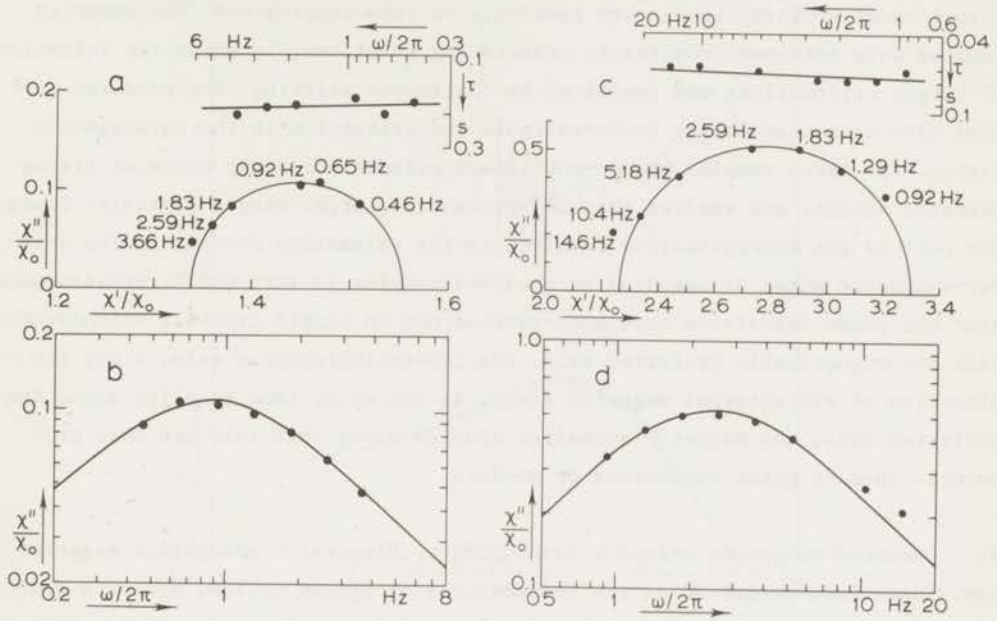

Fig. 21 *Argand diagrams (a and c) and absorption versus frequency curves (b and d). a) and b) represent measurements on* $MnCl_2 \cdot 4H_2O$ *with a magnetic field of 4 kOe parallel to the c axis at T = 1.3 K. c) and d) represent measurements on* $MnBr_2 \cdot 4H_2O$ *with a magnetic field of 8 kOe parallel to the c axis at T = 1.3 K.*

a frequency independent part, this complication has less influence on the absorption than on the dispersion. Accordingly most relaxation times presented in this chapter have been obtained from absorption versus frequency curves obeying eq. (2) as is shown in figs. 21 b and d.

3.2.3 *Experimental results.* Dispersion-absorption measurements have been performed on four samples:

a) a powdered sample of $MnCl_2 \cdot 4H_2O$; average grain diameter: 0.1 mm;

b) a single crystal of $MnCl_2 \cdot 4H_2O$ with the external magnetic field H parallel to the crystal c axis; average diameter: 7 mm.

c) a powdered sample of $MnBr_2 \cdot 4H_2O$; average grain diameter: 0.1 mm;

d) a single crystal of $MnBr_2 \cdot 4H_2O$ with H // c axis; average diameter: 7 mm.

The single crystals were grown from slowly evaporating saturated aqueous solutions of ordinary laboratory chemicals at room temperature. The powdered samples were obtained from faster evaporating solutions, in which the formation of larger crystallites was inhibited by continuous stirring. The powdered samples have been used mainly to investigate the relaxation in the paramagnetic region. For these samples phonon-bottleneck effects which may occur at strong magnetic fields, are smaller than in the case of larger single crystals. Since the part of the susceptibility involved in the relaxation process in the antiferromagnetic phase as measured on powdered samples is very small, measurements near the phase transition have been carried out on single crystals orientated with the magnetically preferred axis, the crystallographic c axis, along the direction of the external magnetic field. As the spins tend to align along the preferred axis, the magnetic anomalies studied along this axis are more pronounced than at other directions or powders.

a) *Powdered manganese chloride tetrahydrate.* Dispersion-absorption measurements have been performed at the temperatures of liquid helium, hydrogen and nitrogen. At a temperature of 1.38 K $MnCl_2 \cdot 4H_2O$ is antiferromagnetic at weak fields and paramagnetic above approximately 8 kOe. The dispersion and absorption as registered in the measuring plots, showed a pattern similar to, but more smoothed than that sketched in fig. 19. The part of the susceptibility participating in the relaxation process is rather small: χ''_{max}/χ_0 does not exceed 0.04 for any field value in the antiferromagnetic state. In the paramagnetic region just above 8 kOe the intensity χ''_{max}/χ_0 decreases, but does not vanish completely. At magnetic fields above 15 kOe larger intensities have been observed. The relaxation times at this temperature as displayed in fig. 22 are all obtained from plots of the absorption against frequency. Due to the small values of the absorptions, the accuracy of these relaxation times is not particularly good, especially around 8 kOe as is indicated by the error bars in the figure. However, a clear maximum of τ is observed at the transition field. In the following paramagnetic region, up to about 20 kOe, the relaxation time has an almost constant value, a factor 3 smaller than the maximum value; at stronger fields the relaxation time decreases again.

At a temperature of 4.2 K the salt is paramagnetic at all field values. The relaxation time observed at that temperature, also displayed in fig. 22, increases slowly as a function of the external field up to about 30 kOe,

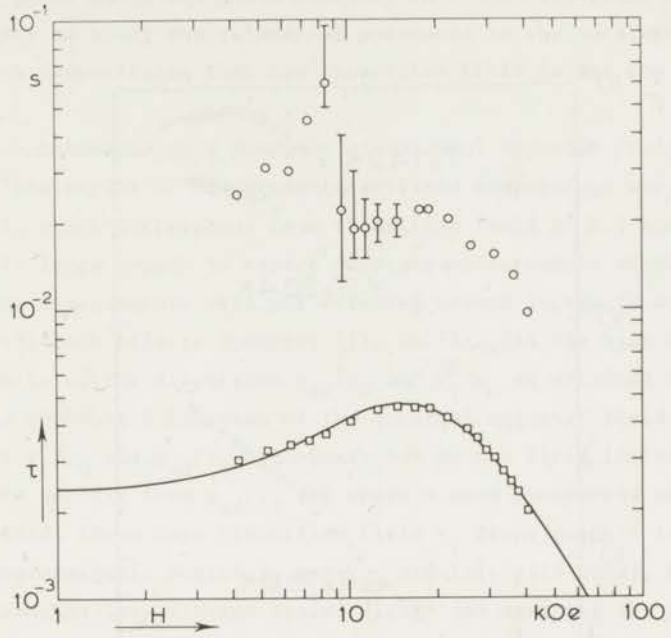

Fig. 22 *Spin-lattice relaxation time of powdered* $MnCl_2 \cdot 4H_2O$ *as a function of external magnetic field.* ○ *T = 1.38 K;* □ *T = 4.2 K;* —— *computer fit according to eq. (26).*

whereas at the strongest fields the relaxation time becomes noticeably shorter and exhibits a $\tau \propto H^{-1.6}$ relationship.

Fig. 23 shows the field dependences of the relaxation time at 14.2 K, 20.4 K and 78 K. At the liquid-hydrogen temperatures the relaxation time depends positively on the external field up to about 30 kOe; this increase is maximally $\tau \propto H^{+1.0}$. At the strongest fields the increase diminishes, in fact, at 14.2 K a decrease of the τ vs H curve is observed. At 78 K one observes about the same maximum slope of the field dependence, but at this temperature the increase of τ continues up to the strongest fields.

b) *Manganese chloride tetrahydrate, single crystal H//c axis.* This sample was studied to investigate the relaxation behaviour near the magnetic phase transition. In order to do so, this phase transition is passed along two different

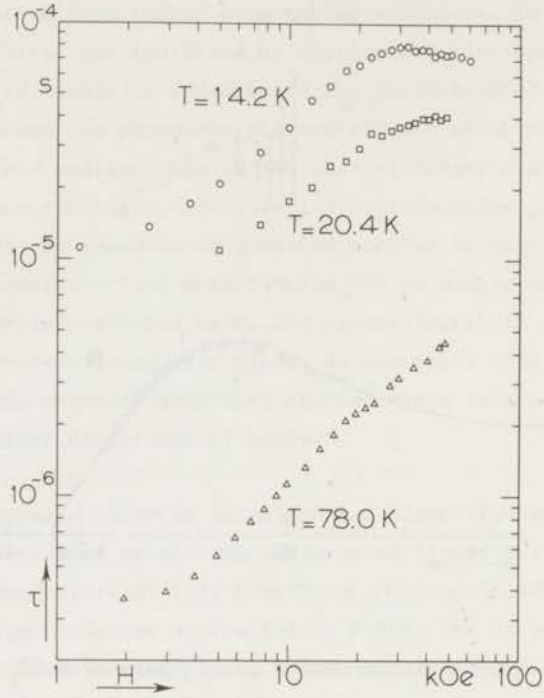

Fig. 23 *Spin-lattice relaxation time of powdered $MnCl_2 \cdot 4H_2O$ as a function of external magnetic field at various temperatures.*

directions in the H-T plane. One set of measurements has been done at fixed temperature with the external magnetic field as running parameter and another set has been performed at fixed external field with temperature as the variable. Within experimental accuracy, the frequency dependence of the complex susceptibility, both in the antiferromagnetic and in the paramagnetic region, can be described by the Casimir-Du Pré relations. An example of this dependence in the antiferromagnetic region is given in the Argand diagram and the corresponding absorption vs frequency curve of fig. 21, corresponding to measurements at 1.3 K and 4.0 kOe. As mentioned in section 3.2.2, the relaxation times are

generally determined from the absorption plots. The part of the susceptibility involved in the relaxation process at the phase transition diminishes, approaching the Néel point along the phase boundary in the H-T diagram. For this reason it is necessary to study the relaxation phenomena in the antiferromagnetic region at such temperatures that the transition field is not too small.

The relaxation behaviour as a function of external magnetic field at constant temperature. The series of measurements at fixed temperature were carried out at T = 1.44 K, which corresponds to a transition field of 5.5 kOe [68]. This field value is large enough to expect accurate measurements of the relaxation phenomena. The measurements were not extended beyond 10 kOe to avoid influences of phonon-bottleneck effects (chapter II). In fig. 24a the high and low frequency limits of the dispersion χ_{ad}/χ_0 and χ_T/χ_0 as obtained from Argand diagrams, are shown as a function of the external magnetic field. At weak external fields χ_T/χ_0 and χ_{ad}/χ_0 are equal, but as the field increases, χ_T/χ_0 increases more rapidly than χ_{ad}/χ_0 and shows a more pronounced maximum at the transition field. Above this transition field χ_T drops quickly to the value χ_{ad}. In the paramagnetic region χ_T and χ_{ad} are initially equal, but at increasing field strengths they diverge again. Figure 24b exhibits the field dependence of the maximal absorption χ''_{max}/χ_0. This curve indicates that χ''_{max}/χ_0 is zero at zero external field, but has non-zero values in the antiferromagnetic region at increasing field values. At the transition field a sharp maximum is reached. Just above the transition field the intensity of the relaxation decreases to zero in a small field region, followed by an increase at stronger magnetic fields. Since the measured susceptibilities fulfil the Casimir-Du Pré relations the curves of figs. 24a and 24b are related to each other by $(\chi_T - \chi_{ad})/\chi_0 = 2\chi''_{max}/\chi_0$. It has to be noticed that the measuring points in the Argand diagram corresponding to the susceptibilities at H_t = 5.5 kOe did not lie on a semicircle very well, due to irregularities of the dispersion. This may be caused by small differences of the field strength between measurements at various frequencies. This difficulty in determining χ_T at 5.5 kOe can be overcome. At this field value χ_{ad}/χ_0 can be found accurately from measurements of χ_{ad}/χ_0 at neighbouring field values since this susceptibility varies smoothly in that field region. The value of χ''_{max}/χ_0 can be obtained with good accuracy from a plot of the absorption vs frequency fulfilling eq. (2). Now the isothermal susceptibility χ_T/χ_0 can be calculated by means of eq. (1). The so-obtained result is inserted in fig. 24a (symbol ●) and agrees nicely with the other exposed measurements.

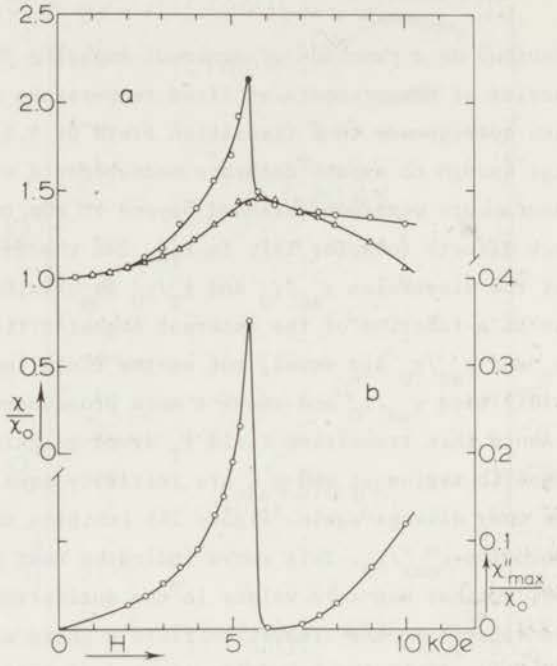

Fig. 24 *Relative susceptibilities as a function of external field for a single crystal of* $MnCl_2 \cdot 4H_2O$ *(H//c axis) at T = 1.44 K.*
a) ○ χ_T/χ_0; △ χ_{ad}/χ_0; ● *see text.*
b) ○ χ''_{max}/χ_0.
Drawn lines for visual aid only.

The relaxation times, as obtained from plots of the absorption against frequency, are given in fig. 25. In the antiferromagnetic region, the relaxation

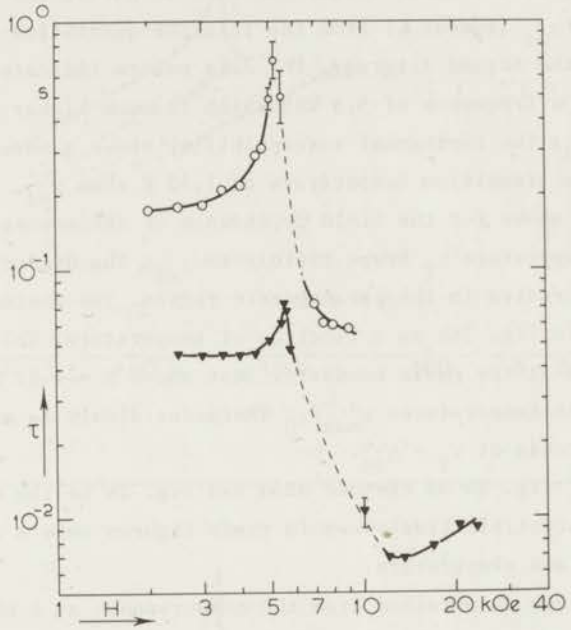

Fig. 25 *Spin-lattice relaxation times against external magnetic field (H//c axis).* ○ $MnCl_2 \cdot 4H_2O$, *T = 1.44 K;* ▼ $MnBr_2 \cdot 4H_2O$, *T = 1.98 K. Drawn lines for visual aid only.*

time increases if the magnetic field reaches the critical value. In the subsequent paramagnetic phase the relaxation time cannot be determined below 7 kOe, since the absorptions are too small. At stronger fields, where the absorptions increase again, relaxation times are observed, which are almost constant, but about a decade shorter than the time measured near the transition field.

Relaxation behaviour as a function of temperature at fixed external magnetic field. A series of dispersion-absorption measurements was performed at a constant external magnetic field of 4.0 kOe using the water-cooled solenoid (section 2.3). This choice was made because this magnet can produce discrete field values with high stability. The measurements do not show any systematic deviation from the

Casimir-Du Pré relations. The susceptibilities χ_T and χ_{ad} (in arbitrary units) are displayed in fig. 26a as a function of temperature. In the same figure, measurements of the zero-field susceptibility χ_0 are plotted (symbol ■) in the same arbitrary units. These values are used to derive the absolute values χ_T (symbol ▼) and χ_{ad} (symbol ▲) from the relative quantities χ_T/χ_0 and χ_{ad}/χ_0 as obtained from the Argand diagrams. The data points indicated by the symbol ○ are measured at a frequency of 5.3 kHz which is much higher than τ^{-1}, so they also represent χ_{ad}. The isothermal susceptibility shows a more pronounced maximum near the phase transition temperature of 1.52 K than χ_{ad}, a behaviour similar to that described above for the field dependence of the susceptibility. Above the transition temperature χ_T drops rapidly to χ_{ad}. The difference between χ_T and χ_{ad} slowly increases in the paramagnetic region. The maximum absorption χ''_{max}/χ_0 is given in fig. 26b as a function of temperature. This curve also exhibits a maximum at the phase boundary. Just above T = 1.52 K the absorptions are zero; at higher temperatures χ''_{max}/χ_0 increases slowly as expected from the corresponding increase of $\chi_T - \chi_{ad}$.

Inspection of fig. 24 on the one hand and fig. 26 on the other hand makes clear that the susceptibilities shown in these figures show a similar dependence on magnetic field and temperature.

Relaxation times as obtained from the measurements at 4 kOe are displayed as a function of temperature in fig. 27. These times increase in the antiferromagnetic region towards a maximum near the transition temperature. At temperatures between 1.53 K and 1.65 K the absorption is too small to determine relaxation times. At higher temperatures τ is about a decade shorter than at the phase transition and decreases further as the temperature rises.

c) *Powdered manganese bromide tetrahydrate.* This powdered sample has been examined in order to study the paramagnetic relaxation effects. At liquid-helium temperatures measurements of the complex susceptibility are performed in external fields up to 24 kOe. The observed relaxation behaviour at temperatures both above and below the Néel temperature of 2.1 K cannot be described by a single time constant. The absorptions χ''/χ_0 are only a few percent but extended over a wide range of frequencies, indicating that a distribution of relaxation times is present. In this distribution two bands of times are more pronounced; one band around 10^{-3} s, which is observed only in the paramagnetic region and the other band around 10^{-4} s, present in the paramagnetic and antiferromagnetic states as well. The smoothed character of these results makes it difficult to determine field or temperature dependences accurately.

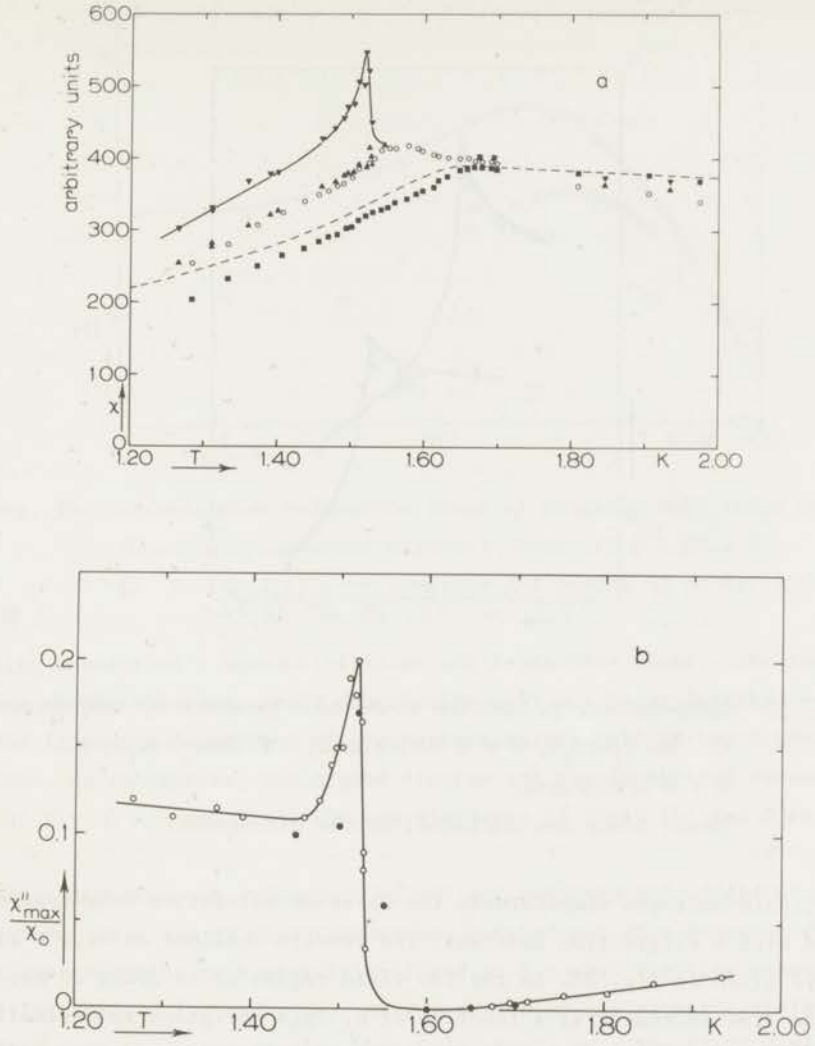

Fig. 26 *a) Susceptibilities as a function of temperature for $MnCl_2 \cdot 4H_2O$ (H//c axis),* ■ χ_0; ○ χ_{ad} *(4 kOe) from measurements at 5.3 kHz;* ▲ χ_{ad} *(4 kOe), determined from Argand diagrams;* ▼ χ_T *(4 kOe) determined from Argand diagrams;* - - - χ_0 *from Lasheen et al.*[54]*). Drawn lines for visual aid only.*

b) χ''_{max}/χ_0 *as a function of temperature for* $MnCl_2 \cdot 4H_2O$ *(H = 4 kOe//c axis)* ○ *from* χ''/χ_0 *versus frequency;* ● *calculated according to eq. (27).*

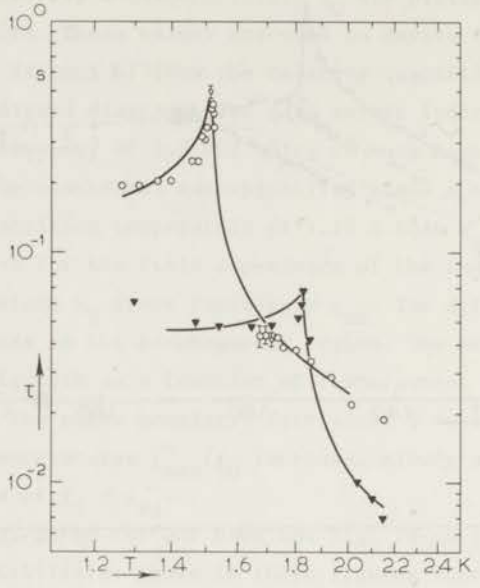

Fig. 27 *Spin-lattice relaxation times as a function of temperature.* ○ $MnCl_2 \cdot 4H_2O$, *H = 4 kOe//c axis;* ▼ $MnBr_2 \cdot 4H_2O$, *H = 8 kOe//c axis.* *Drawn lines are explained in the discussion.*

At liquid-hydrogen temperatures the observed relaxation behaviour can be described with a single time constant. The results obtained at 14.2 K and 20.5 K are given in fig. 28. In the low field region up to about 20 kOe the relaxation time increases as a function of H. This variation is maximally $\tau \propto H^{+0.5}$. At the strongest fields one observes a decrease of the relaxation time, which is more pronounced than in the corresponding chloride sample. The measurements at 14.2 K, which are extended up to 60 kOe, exhibit at these strong fields a relaxation time proportional to $H^{-1.6}$.

d) *Manganese bromide tetrahydrate, single crystal H//c axis.* This sample is used to study the relaxation behaviour near the magnetic phase transition. Two sets of measurements have been carried out: one series as a function of external magnetic field and one as a function of temperature in the same way as was performed on the single crystal of the chloride. Since the features of the

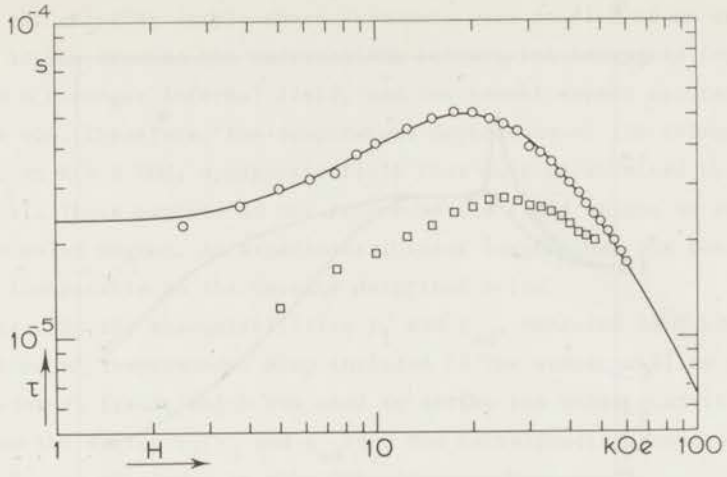

Fig. 28 *Spin-lattice relaxation times of powdered* $MnBr_2 \cdot 4H_2O$ *as a function of external magnetic field.* ○ *T = 14.2 K;* □ *T = 20.5 K;* —— *computer fit according to eq. (26).*

resulting quantities - susceptibilities and relaxation times - are analogous to these of the chloride, their description will not be so lengthy.

The frequency dependence of the susceptibility fulfils the Casimir-Du Pré relations. As an example, the Argand diagram and the absorption versus frequency curve at T = 1.3 K and H = 8 kOe are displayed in figs. 21c and d respectively.

Relaxation behaviour as a function of the external magnetic field at fixed temperature. This set of measurements was carried out at a temperature of 1.98 K corresponding to a transition field of 5.6 kOe. Fig. 29a shows the susceptibilities χ_T/χ_0 and χ_{ad}/χ_0 as a function of the magnetic field, while fig. 29b shows the corresponding behaviour of χ''_{max}/χ_0. The field dependences of these quantities are similar to these encountered at the corresponding chloride sample. Because the experiments were extended up to an external field of 24 kOe, the effect of paramagnetic saturation, causing the decrease of χ_T above 10 kOe, becomes noticeable. The field dependence of the relaxation time as derived from the absorption versus frequency curves, is given in fig. 25. Although the maximum of the relaxation time near the transition field is less pronounced than for the chloride sample, a similarity between the results on both crystals cannot be denied.

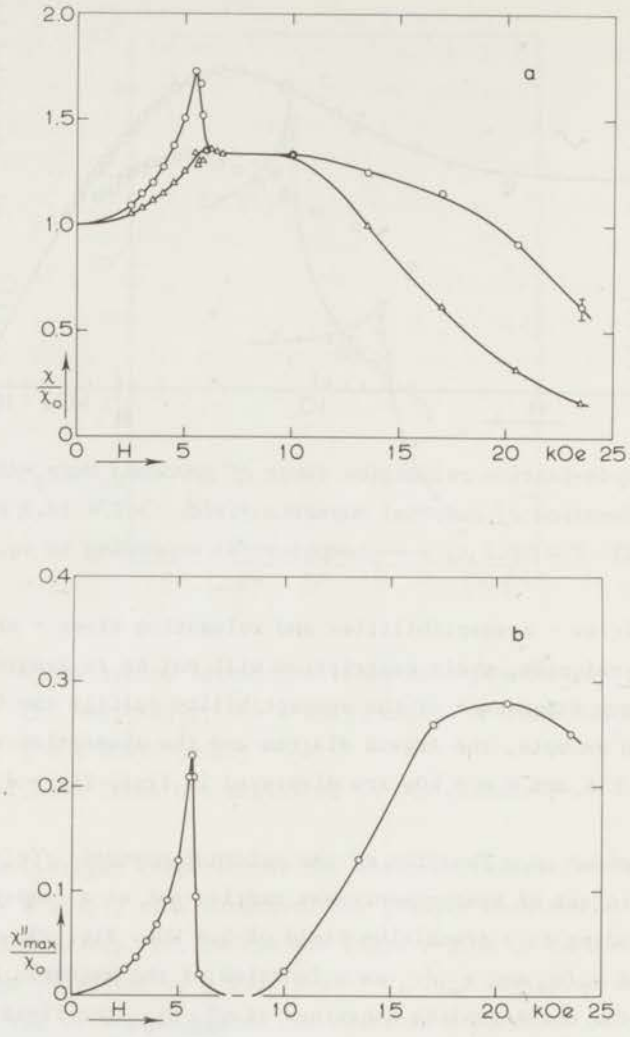

Fig. 29 *Relative susceptibilities as a function of external field for a single crystal of* $MnBr_2 \cdot 4H_2O$ *(H//c axis) at T = 1.98 K.*

a) ○ χ_T/χ_0; △ χ_{ad}/χ_0;

b) ○ χ''_{max}/χ_0.

Drawn lines for visual aid only.

Relaxation behaviour as a function of temperature at constant external magnetic field. On the chloride sample these phenomena were studied at an external field of 4 kOe. In the bromide the interactions between the manganese ions are larger, leading to a stronger internal field, and one cannot expect accurate measurements at 4 kOe. Therefore, the temperature dependence of the relaxation behaviour is studied at H = 8 kOe, a magnetic field that must be obtained by a superconducting coil. These magnets do not reproduce the field values as accurately as the water-cooled magnet. An experimental error larger than for the chloride sample is insuperable in the results described below.

In fig. 30a the susceptibilities χ_T and χ_{ad}, measured at 8 kOe are shown as a function of temperature. Also included is the susceptibility χ_0 measured at zero external field, which was used to derive the other quantities in this figure from the ratios χ_T/χ_0 and χ_{ad}/χ_0. The corresponding temperature dependence of χ''_{max} is displayed in fig. 30b.

The relaxation times as obtained from plots of the absorption against frequency, are given in fig. 27. The relaxation times obtained above the lambda point of the surrounding liquid-helium bath are seriously affected by phonon-bottleneck effects and have been omitted in fig. 27.

3.2.4 *Discussion.* Since the results on both of the manganese salts investigated are quite similar, they will be discussed together. In the first part of this discussion the paramagnetic relaxation behaviour will be treated, the second part deals with the results obtained near the magnetic phase transition.

a) *Paramagnetic relaxation.* As was demonstrated in chapter II, the spin-lattice relaxation behaviour of isolated paramagnetic ions can be characterized by a Raman process, dominant at weak external magnetic fields, and a direct process, which prevails at strong fields due to its striking field dependence.

Manganese ions have zero orbital angular momentum. The doublets of the resulting S = 5/2 multiplet have zero-field splittings which are small compared to kT [71]). In such cases the paramagnetic relaxation rate can be given as (section 2.1):

$$\tau^{-1} = ATH^2 + BT^5 J_4(\Theta_D/T) \quad . \qquad (24)$$

This expression exhibits the simplified high field approximation; most manganese samples show relaxation times that obey relation (24). Both manganese chloride and bromide tetrahydrate have large internal field values due to the strong exchange interactions between the magnetic ions, and the applied external

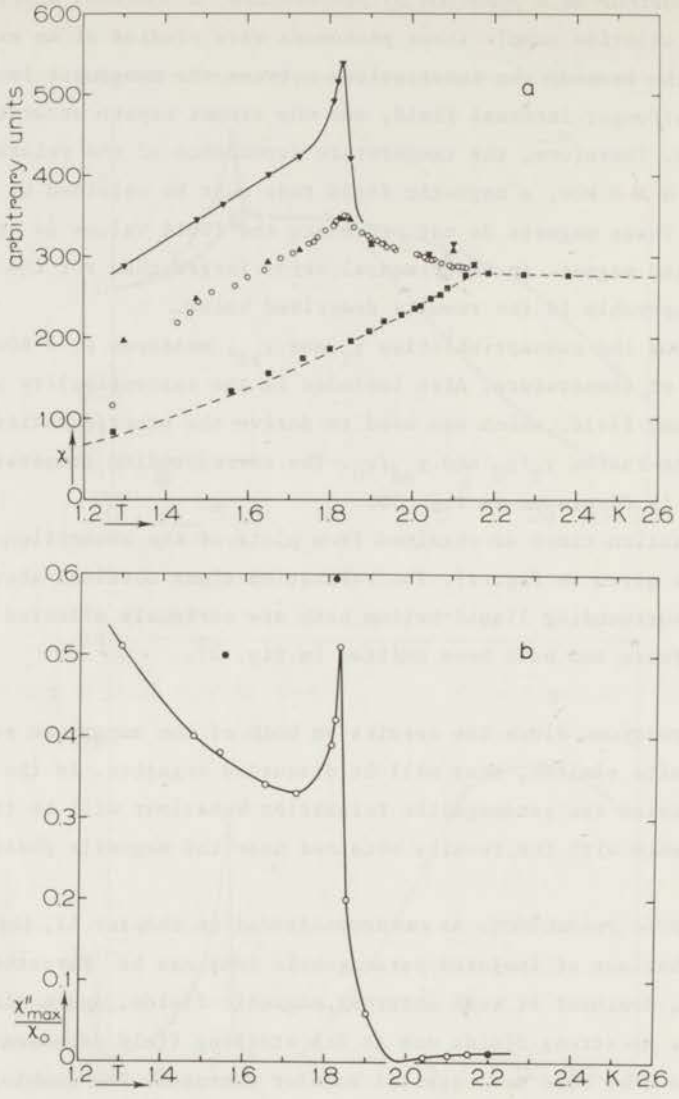

Fig. 30 *a) Susceptibilities as a function of temperature for $MnBr_2 \cdot 4H_2O$ (H//c axis). ■ χ_0; - - - χ_0 from [75]; ○ χ_{ad}(8 kOe) from measurements at 5.3 kHz; ▲ χ_{ad}(8 kOe) determined from Argand diagrams; ▼ χ_T(8 kOe) determined from Argand diagram. The drawn line for visual aid only.*

b) χ''_{max}/χ_0 versus T for $MnBr_2 \cdot 4H_2O$ (H = 8 kOe//c axis) ○ from χ''/χ_0 versus frequency; ● calculated according to eq. (27). The drawn line for visual aid only.

magnetic fields are insufficient to fulfil the high field approximation. There is no applicable theoretical expression for the direct relaxation process in relatively weak external magnetic fields but it seems reasonable to insert into the first term of eq. (24) the sum of the internal and external fields, thus:

$$\tau_{dir}^{-1} = AT(b/C + H^2) \quad . \tag{25}$$

The expected influence of the internal fields on the Raman relaxation can be accounted for by a Brons-Van Vleck relation (eq. (14)).

The observed relaxation times of the powdered $MnCl_2 \cdot 4H_2O$ at T = 4.2 K (fig. 22) indeed show a Brons-Van Vleck-like character at weak external magnetic fields and a decrease due to the direct process at the strongest fields. The values of the deviation parameter d, associated with the measurements at 4.2 K, are small at all applied magnetic fields. This suggests that the influence of phonon-bottleneck effects on the direct process in the powdered sample may be neglected, so there is no reason to apply the interpolation method as for the measurements in chapter II. Measurements on other salts that obey eq. (24) support this simplification [72,73]. Because of the absence of the phonon bottleneck, the measurements at 4.2 K can be analyzed using a least-square computer fit in which both processes of eq. (24) are considered, each with their appropriate field dependence:

$$\tau^{-1} = AT((b/C) + H^2) + B \frac{1 + pH^2/(b/C)}{1 + H^2/(b/C)} \quad . \tag{26}$$

The b/C value, inserted in this expression, is 54 kOe^2 as was given in [55]. The best fit was obtained for A = 0.052 $s^{-1}kOe^{-2}K^{-1}$ and B = 410 s^{-1} with the parameter p equal to 0.23. This result gives a reasonable description of the measurements at 4.2 K as can be seen in fig. 22 (drawn line). The value of p is smaller than the predicted value of 0.5 [22], usually obtained for manganese samples [42]. At the higher temperatures the applied external magnetic fields are not sufficient to reach the region of direct relaxation (fig. 23). The relaxation times at weak fields showed field dependences similar to that observed at 4.2 K. The increase in τ is even larger, resulting in smaller p values. At 14.2 K and 20.4 K p is about 0.1 while at 78 K p is even smaller. The measurements on the bromide sample at 14.2 and 20.5 K (fig. 28) also show p values of about 0.1.

The fact that these p values are rather small and that they depend on the temperature suggests that relaxation mechanisms, different from the above-

mentioned T^{-5} Raman process, participate in the spin-lattice relaxation at weak external magnetic fields.

More information about the weak field relaxation behaviour can be obtained from the temperature dependence of τ [74]). However, our experimental equipment restricts the measurements in fields above 4 kOe to liquid helium, hydrogen or nitrogen temperatures. The running method (section 1.2.1) can not be used in strong fields. Another complication is the fact that the second term of eq. (24) describes the temperature dependence of the Raman relaxation time in the strong field limit ($H >> (b/C)^{\frac{1}{2}}$). For $MnCl_2 \cdot 4H_2O$ we have measurements at four temperatures from which one can calculate τ_{Raman} ($H = \infty$) assuming the above-mentioned p values to be correct. The relaxation times obtained in this way can be described rather poorly by the second term of eq. (24) leading to a Debye temperature of 45 K. Specific heat measurements on $MnCl_2 \cdot 4H_2O$ [59]) yield a value of about 240 K for Θ_D. This large discrepancy together with the unusual p values, support the suggestion that the Raman process of eq. (24) is not observed in these salts.

The results from the manganese bromide sample are not compared with the temperature dependence of the Raman process, as only two reliable series of weak-field relaxation measurements are available (fig. 28). Another point of interest is the fact that for $MnBr_2 \cdot 4H_2O$ at 4.2 K the relaxation times could not be determined properly. The character of the dispersion and absorption curves indicates a strong influence of "impurity relaxation" (section 2.4). Probably the influence of these impurities is important at all temperatures, even in the chloride sample, thus suppressing the Raman relaxation process.

During the description of the computer fitting of the results on the manganese chloride at 4.2 K, it was mentioned that the strong-field behaviour could be ascribed to the direct process with a coefficient $A = 0.052\ s^{-1}kOe^{-2}K^{-1}$. The relaxation times obtained at T = 1.38 K at fields stronger than 30 kOe, where τ decreases as a function of H, are well-described by the expression for the direct process eq. (25), in which the value just derived for A is substituted. At higher temperatures the influence of the direct process shifts towards stronger external magnetic fields. Therefore the measurements at 14.2 K cannot be analyzed using this computer programme. However, if one extrapolates the Brons-Van Vleck type of field dependence towards fields of about 60 kOe, and one subtracts this relaxation rate from the observed inverse relaxation time, one obtaines for the coefficient of the direct process: $A = 0.06 \pm 0.01\ s^{-1}kOe^{-2}K^{-1}$. This value should only be regarded as an estimate, but it confirms the result obtained from the measurements at 4.2 K.

The strong behaviour of the τ vs H curves obtained for powdered manganese bromide is different. The field dependence at 14.2 K shows a clear decrease for the relaxation time at strong fields. This dependence allows the use of the computer analysis. The result (drawn line) gives A = 0.95 $s^{-1}kOe^{-2}K^{-1}$, a value which is about 20 times larger than that for the chloride sample. This large difference is quite unexpected since the manganese bromide and chloride tetrahydrate are crystallographically isomorphous. Most other manganese salts show $\tau_{dir}^{-1} = ATH^2$ with A of the order of 0.2 $s^{-1}kOe^{-2}K^{-1}$ [73]). Both values given above do not agree with this result. Possibly the large exchange interactions, present in these samples, have their influence on the observed direct relaxation time, although it is surprising that this influence is of different character in both salts. At present we are not able to perform a detailed theoretical calculation of the relaxation processes in these salts as is necessary to explain the values of A given above.

Summarizing the paramagnetic relaxation behaviour in $MnCl_2 \cdot 4H_2O$ and $MnBr_2 \cdot 4H_2O$ we conclude that the Raman process is obscured in these salts, while the direct process can be given as $\tau_{dir}^{-1} = ATH^2$ with A being 0.05 and 0.95 $s^{-1}kOe^{-2}K^{-1}$ for the chloride and bromide salt respectively.

b) *Relaxation behaviour near the phase transition*

Susceptibilities. According to eq. (20) it is possible to express the part of the susceptibility involved in the relaxation process $\chi_T - \chi_{ad} = 2\chi''_{max}$ as a function of the static quantities C_H and $(\partial M/\partial T)_H$. Since the specific heat C_H and the magnetization M of both $MnCl_2 \cdot 4H_2O$ and $MnBr_2 \cdot 4H_2O$ are known at various values of the external field and the temperature, it is possible to compare the values of χ''_{max} resulting from our experiments, with those calculated from direct C_H and M measurements. As our measurements yield only relative susceptibilities eq. (20) is rewritten in the form:

$$\frac{\chi_T - \chi_{ad}}{2\chi_0} = \frac{\chi''_{max}}{\chi_0} = \frac{T}{2C_H\chi_0}\left(\frac{\partial M}{\partial T}\right)^2_H \quad . \tag{27}$$

This relation will be verified first for the results on $MnCl_2 \cdot 4H_2O$ as displayed in fig. 26b. Giauque et al. [68]) performed accurate measurements of the magnetization of $MnCl_2 \cdot 4H_2O$ as a function of the temperature at various constant external magnetic fields and published their results in detailed tables, which are very suitable to calculate the derivative $(\partial M/\partial T)_H$ at H = 4 kOe. Measurements of the specific heat at 4 kOe are reported by the same authors [68]). From these

results given in fig. 20 the points in the χ''_{max}/χ_0 vs T graph indicated by the symbol ● are calculated. It must be noted that during this calculation the absolute value of the susceptibility was also needed, we used the result of Gijsman [63]: χ_0 (T = 1.66 K) = 58.6×10^{-5} c.g.s units per gram. For $MnBr_2 \cdot 4H_2O$ detailed measurements of the magnetization are not known. It is possible to make an estimate of some χ''_{max} values from specific heat measurements by Schelleng and Friedberg [75]) and magnetization measurements of Schmidt and Friedberg [69]). Using Gijsman's absolute value for the susceptibility (χ_0 (T = 2.14 K) = 33.8×10^{-4} c.g.s. units per gram), we calculated χ''_{max}/χ_0 for three temperatures near T_N (symbol ● in fig. 30b). In general the agreement between the calculations and our measurements is reasonable, demonstrating the applicability of the thermodynamic relation (27) to the relaxation phenomena in manganese chloride and bromide tetrahydrate.

The study of relaxation phenomena includes more or less automatically measurements of the static zero-field susceptibility χ_0. In fig. 26 some earlier measurements of Lasheen et al [54]) have been inserted (- - - line). One may notice a small difference between both series of measurements in the antiferromagnetic region. We suggest a slightly different crystal orientation to be the cause of this discrepancy. The smoothly varying χ_0 vs T curve shows a maximum gradient at the Néel temperature T_N and a rather flat maximum at a slightly higher temperature. T_N is taken as the temperature at which the specific heat diverges. The similar temperature dependence of the static zero field susceptibility for $MnBr_2 \cdot 4H_2O$ is given in fig. 30 along with the results obtained by Berger mentioned in ref. 75. Both sets of measurements are in perfect agreement.

Fisher and Sykes [76]) compared the critical behaviour of χ_0 of $MnCl_2 \cdot 4H_2O$ to their calculations for cubic Ising lattices based on exact series expansions. Their calculations yield a smoothly varying χ_0 vs T curve with an infinite gradient $(\partial\chi_0/\partial T)$ at T_N and a maximal susceptibility at $T(\chi_{max}) = 1.098\ T_N$ for the simple cubic lattice and $T(\chi_{max}) = 1.065\ T_N$ for the body-centered cubic lattice respectively. In table V these characteristic temperatures obtained from our measurements are given for manganese chloride and bromide tetrahydrate.

The agreement between T_N and $T((\partial\chi_0/\partial T)_{max})$ is satisfactory; for both salts the ratios $T(\chi_{0\ max})/T((\partial\chi_0/\partial T)_{max})$ are somewhat smaller than derived for the body-centered cubic lattice. As remarked by Fisher and Sykes [76]) the effective lattice of $MnCl_2 \cdot 4H_2O$ appears to be more "closely packed" than the b.c.c. lattice. The same remark holds for $MnBr_2 \cdot 4H_2O$. In table V results obtained by Turrell and Yue [77]) are given also. These authors derived the quantity $(\partial\chi_0/\partial T)$

Table V

	T_N (from C_H measurements)	$T((\frac{\partial \chi_0}{\partial T})_{max})$	$T(\chi_{0\ max})$	$\frac{T(\chi_{0\ max})}{T((\frac{\partial \chi_0}{\partial T})_{max})}$
$MnCl_2 \cdot 4H_2O$ H//c axis	1.62 [68] 1.6257 [61]	1.62 ± 0.005 1.611 [77]	1.67 ± 0.01 1.638 [77]	1.03 1.017 [77]
$MnBr_2 \cdot 4H_2O$ H//c axis	2.13 [75] 2.120 [62]	2.10 ± 0.02 2.11 [75]	2.19 ± 0.02	1.04 ± 0.02
$MnBr_2 \cdot 4H_2O$ polycrystalline		2.117 [77]	2.149 [77]	1.02 [77]

from the shift of a radio-frequency oscillator due to temperature-dependent variations of the susceptibility of a sample placed in a coil in the oscillator circuit. Their results from measurements of $MnCl_2 \cdot 4H_2O$ single crystals and polycrystalline $MnBr_2 \cdot 4H_2O$ yield smaller values of the ratio $T(\chi_{0\ max})/T((\partial\chi_0/\partial T)_{max})$ than our measurements. Recently Cerdonio and Paroli [78] performed magnetization measurements at very weak constant external magnetic fields ($H < 10$ Oe), which suggest that the ratio $T(\chi_{0\ max})/T((\partial\chi_0/\partial T)_{max})$ goes to unity if H goes to zero. This result suggests the applicability of the molecular field theory to the behaviour of χ_0 of $MnCl_2 \cdot 4H_2O$. The amplitude of the oscillating field during our measurements of χ_0 is about 5 Oe. Measurements performed with reduced amplitude of the oscillating field, did not show a different temperature dependence, but since the accuracy of these measurements was also reduced, they were not very conclusive. The fact that a different behaviour of χ_0 is observed under different experimental conditions, indicates that one must be careful with the interpretation of these measurements in the limit of zero external magnetic field.

As a function of temperature, the adiabatic susceptibility (observed in non-zero field) behaves similarly to χ_0, but there is a shift to lower temperatures. This shift is due to the fact that the transition temperature in an external magnetic field T_t is lower than T_N. The isothermal susceptibility χ_T exhibits an extra peak at T_t which is superimposed on the curve of χ_{ad} vs T. As far as we know, no theoretical calculations have been performed for the susceptibility of three-dimensional antiferromagnetic lattices in non-zero external magnetic fields. For a two-dimensional "decorated" super exchange

Ising antiferromagnet Fisher [79]) derived rigorously the partition function in non-zero fields from the corresponding partition function of the basic lattice. The "decoration" of the basic lattice consists of placing a "non-magnetic" spin on each bond between the magnetic spins. These calculations give rise to an extra term contributing to χ_T which is proportional to the magnetic specific heat [80]).

The transition temperature of $MnCl_2 \cdot 4H_2O$ at H = 4 kOe derived from specific heat measurements [68]) is 1.53 K. The temperature at which the isothermal susceptibility at this field has a maximum is 1.52 K, the slope $(\partial\chi_{ad}/\partial T)_H$ is maximal at a temperature of 1.52[5] K. About the same picture describes the susceptibilities observed on the bromide single crystal at H = 8 kOe. T_t resulting from C_H measurements is 1.84 K [75]), χ_T is maximal at 1.83 K but the maximal gradient $(\partial\chi_{ad}/\partial T)_H$ lies somewhat lower in temperature: 1.81 K. Thermodynamical arguments suggested already the equivalence between the maxima in the χ''_{max} and χ_T vs T curves at constant non-zero field and the specific heat anomaly. From the measurements of Giauque et al. [68]) it is known that the maxima of the C_H vs T and $(\partial M/\partial T)_H$ vs T curves coincide within the experimental error (cf. fig. 20). Since eq. (27) determines the relation between χ''_{max} (and therefore also χ_T) and the above-mentioned quantities, it is very likely that the maxima of C_H, χ''_{max} and χ_T observed in non-zero magnetic fields occur at the same critical temperature.

Considering the results given above on the imaginary and real parts of the susceptibility together with eq. (27) it seems plausible that the temperature dependence of χ_{ad} has basically the same form at zero or non-zero applied magnetic fields, whereas χ_T consists of two parts: the just mentioned χ_{ad} and a contribution susceptible to relaxation processes: $\chi_T - \chi_{ad} = (T/C_H)(\partial M/\partial T)_H^2$.

Relaxation times. While the theoretical understanding of spin-lattice relaxation in paramagnetic substances is quite thorough, this can not be said of relaxation mechanisms that occur near a phase transition. Recent theoretical work of Barry and Harrington [81]), based on statistical equilibrium theory and the thermodynamics of irreversible processes leads to a Debye-shape for the frequency dependence of the susceptibility in the case of antiferromagnetic relaxation in the limit of zero external field. At zero external magnetic field a frequency dependent susceptibility was not observed, but at non-zero fields the differential susceptibilities showed a Debye-shape. This was mentioned already in section 3.2.3, where the drawn lines in fig. 21 show the Debye shapes. The distribution of relaxation times as reported in a previous paper [55]), was

detected after a sudden change of the spin temperature T_S. To gain sensitivity $T_S - T_L$ might have been too large, causing a non-exponential recovery of $\overline{\chi}$. The relaxation times predicted by Barry and Harrington [81]) show a maximum at T_N. The relaxation times obtained from our present susceptibility measurements ($H \neq 0$) do exhibit such a maximum at the transition temperature, as was seen in fig. 25. However, our results can not be compared with the expressions given in ref. 81, a phenomenological comparison with specific heat data seems more obvious.

Huber [82]) describes spin-lattice relaxation near the critical point, which he identifies with the decay rate of the energy fluctuations in the spin system due to modulation of the exchange. He derives a relaxation time proportional to the specific heat of the spin system at constant magnetic field C_H. This result agrees with the expression $\tau = C_H/\alpha$ which follows from the thermodynamic model for spin-lattice relaxation of Casimir and Du Pré (section 1.1).

It seems interesting to compare the observed relaxation times with specific heat data. If one assumes that α does not show an anomaly at T_N, one can calculate C_H/α. For $MnCl_2 \cdot 4H_2O$ this is done, taking α proportional to $T^{+0.1}$. The result is inserted in fig. 27 (drawn line) and gives a remarkably good description of the observed τ versus T curve.

For $MnBr_2 \cdot 4H_2O$ a calculation based on α proportional to $T^{+0.8}$, also gives good agreement with the experimental relaxation times.

Detailed information on C_H versus H is not known, so a comparison between τ and C_H/α cannot be made. However, the intensity of the steps in the τ versus H curves agrees with C_H versus H if the value of α is not strongly dependent on external magnetic field.

From this phenomenological approach the conclusion might be that the observed anomalies in the relaxation times are closely connected with the anomalies in the specific heat. The dependences of α used in the calculations are not expected to give information about the spin-lattice interactions occurring.

The numerical values of the relaxation times of the powdered and the single crystal samples of both salts differ by about a decade at the same temperature and field, compare for instance, the relaxation times of the powdered sample of $MnCl_2 \cdot 4H_2O$ at T = 1.38 K (fig. 22) and the times of the single crystal at T = 1.44 K (fig. 25). Knowing the numerical agreement between the relaxation times at strong fields in the powdered sample and the estimated direct process, it is obvious to suppose that phonon-bottleneck effects occurring in the single crystal are the reason for this difference. But the fact that the complex susceptibility of the single crystal fulfils the Casimir-Du Pré relations, makes it

very unlikely that these effects play a similar role as is the case in copper Tutton salts at strong magnetic fields (section 2.4).

3.3 *Relaxation phenomena near the spin-flop phase transition of caesium manganese chloride dihydrate*

3.3.1 *Introduction.* Some magnetic systems not only have a paramagnetic and an antiferromagnetic state, as dealt with in the preceding section, but also a so-called spin-flop phase. According to the molecular field theory [70]) this type of antiferromagnetic ordering, in which the spins tend to align perpendicular to the preferred axis, occurs if the anisotropy energy is not too large. The spin-flop phase occurs in external magnetic fields stronger than the spin-flop transition field H_{SF}.

Among the salts discussed in section 3.2, the spin-flop phase is demonstrated only by $MnCl_2 \cdot 4H_2O$ but this occurs at temperatures below 1.25 K, while the present experiments were performed above that temperature. In order to study the relaxation behaviour near a spin-flop transition, we examined $CsMnCl_3 \cdot 2H_2O$, a salt that orders in this phase at liquid-helium temperatures above $H_{SF} \simeq 20$ kOe.

The crystal structure of $CsMnCl_3 \cdot 2H_2O$ is investigated by Jensen et al. [83]) using X-ray techniques. This study indicated an orthorhombic structure. Each manganese ion is octahedrally surrounded by four chlorine ions and two water molecules. These octahedra are linked to each other, forming chains along the a axis, by sharing a chlorine ion. The magnetic properties of this salt have been studied by various authors. Smith and Friedberg [84]) conclude from susceptibility measurements at zero external field that $CsMnCl_3 \cdot 2H_2O$ behaves above 9 K as a system of weakly interacting linear Heisenberg chains [85]), with an isotropic g-value of 2.00 and an intrachain exchange constant J/k of -3.00 K. The preferred direction for the spins proved to be the b axis. This chain structure is confirmed by susceptibility and neutron scattering experiments by Skalyo et al. [86]), which indicated that the magnetic linear chains are parallel to the a axis and that J/k = -3.6 K. Spence et al. [87]) examined the magnetic structure at liquid-helium temperatures by means of N.M.R. techniques. At these temperatures the interchain interactions, which appear to be about a factor 100 weaker than the intrachain coupling, are capable of establishing three-dimensional antiferromagnetic ordering, consisting of eight sublattices with the sublattice magnetization along the b axis. The magnetic phase diagram of $CsMnCl_3 \cdot 2H_2O$ was determined by Butterworth and Woollam [88]), using magnetothermal methods. These

experiments yield a critical spin-flop field H_{SF} at liquid-helium temperatures which depends only weakly on temperature according to $H_{SF} = 16.10 + 1.02\ T$ (T in Kelvin and H_{SF} in kOe). The magnetic triple point occurs at T = 4.36 K and H = 20.55 kOe; the Néel temperature is found to be 4.88 K.

3.3.2 *Experimental results.* Dispersion-absorption measurements were performed on a single crystal of $CsMnCl_3 \cdot 2H_2O$, oriented with the easy axis, i.e. the crystallographic b axis, along the externally applied magnetic field. This single crystal, which was 9 x 10 x 3 mm along the a, b, and c axes respectively, was grown from a slowly evaporated aqueous solution at 25 °C. The data resulting from these measurements, show almost constant dispersions without absorption as a function of the external field within the antiferromagnetic and within the spin-flop phase. The dispersions observed in the spin-flop phase are about 2 times larger than χ_0 at 4.2 K and about 4 times χ_0 at the lowest temperatures. At the boundary between these two regions both the dispersion and the absorption show a sharp maximum for most applied frequencies of the oscillating part of the external magnetic field. The positions of these maxima in the H-T plane agree with the phase diagram as determined by Butterworth and Woollam [88]), as can be seen in fig. 31. Typical values for the halfwidth of the peaks of the susceptibility are about 500 Oe for the dispersion and about 100 Oe for the absorption.

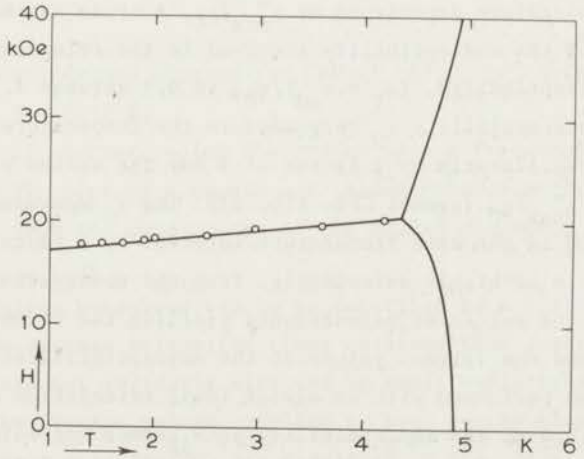

Fig. 31 *The magnetic phase diagram of* $CsMnCl_3 \cdot 2H_2O$, *H//b axis.* O *from susceptibility measurements;* —— *from Butterworth and Woollam* [88]).

Since these peaks are so sharp, the oscillating part of the magnetic field must be sufficiently small to avoid non-linearity effects. In practice the applied amplitude, which is smaller than 5 Oe, fulfilled this requirement.

The magnitude of the susceptibility peaks is very easily affected by variations of the orientation of the crystal with respect to the direction of the external field. Variations of only a few degrees change the susceptibility maxima by a factor of ten. With the present equipment it is not possible to change the orientation of the crystal in situ, in order to maximize these peaks. Due to this effect the numerical values of the susceptibility peaks are not reliable, but their dependences on frequency and temperature do not seem to be affected. Some scatter in the measurements (e.g. fig. 32) is probably caused by small changes of the orientation of the sample with respect to the external field brought about by the frequent displacements of the sample within the measuring coils (see description of the measuring procedure, section 1.3.1).

Fig. 33 shows the maximal absorption χ''_{max}/χ_0 as a function of temperature for two slightly different orientations. Both series of measurements show the same considerable rise of χ''_{max}/χ_0 at decreasing temperature ($\propto T^{-5.5}$), while this temperature dependence becomes weaker at the lowest temperatures. The scatter in the susceptibility measurements, as mentioned above, together with the fact that the frequency dependences of the dispersion and absorption do not show the Debye form (fig. 32), make it impossible to determine accurate values for χ_T/χ_0 and χ_{ad}/χ_0 at H_{SF}. The experiments suggest that these quantities have about the same temperature dependence as χ''_{max}/χ_0. A crude estimate for the ratio between the part of the susceptibility involved in the relaxation process and the isothermal susceptibility, $(\chi_T - \chi_{ad})/\chi_T$, is 0.3 between 1.3 and 4.2 K.

The initial susceptibility χ_0 decreases in the temperature interval between 4.2 and 1.3 K almost linearly by a factor of 5 for the series yielding the largest values of χ''_{max}/χ_0 (symbol □ in fig. 33). The χ_0 measured by Smith and Friedberg [84]) drops in the same temperature interval by a factor of 4. These authors report χ_0 to be highly anisotropic. From the observations of χ_0, one may conclude that the series of measurements yielding the strongest temperature dependence of χ_0 and the largest values of the susceptibilities at the phase transition has been performed with an almost ideal orientation of the crystal.

As mentioned above, the susceptibility at H_{SF} does not fulfil the Casimir-Du Pré relations (eqs. (1) and (2)). The results, obtained at T = 2.05 K deviate least from these relations. Fig. 32 shows the Argand diagram and the corresponding plot of the absorption vs angular frequency of these measurements. At other temperatures the Argand diagrams show more flattened curves, which means

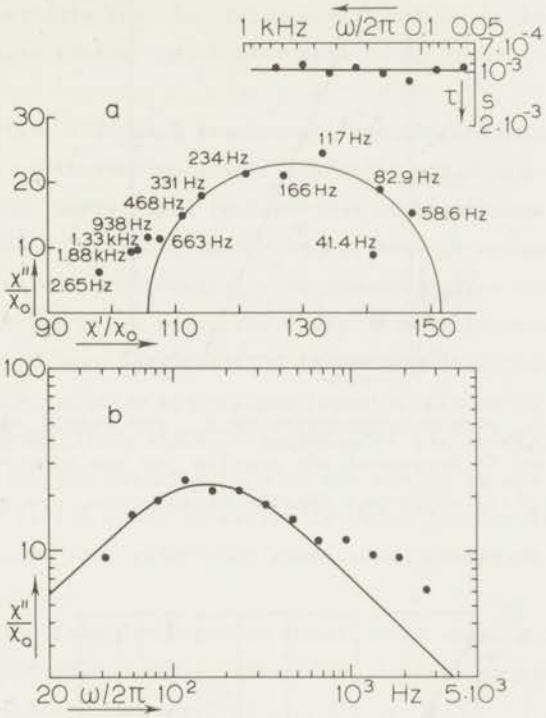

Fig. 32 *a) Argand diagram for $CsMnCl_3 \cdot 2H_2O$, H//b axis at H_{SF} and T = 2.05 K.*
b) corresponding absorption versus frequency curve.
The plot of τ versus ω/2π shows relaxation times as obtained from the data points of the Argand diagram.

that the relaxation behaviour has to be described by a distribution of relaxation times. The average relaxation times obtained from absorption versus frequency curves are not seriously affected by small variations of the crystal orientation. The average values, yielded by both series of measurements with slightly different orientation, are displayed in fig. 34 as a function of temperature. Their temperature dependence can be described by $\tau \propto T^{-4}$.

The determination of relaxation times at magnetic fields differing from H_{SF} is restricted to a small range of field values, since the halfwidth of the

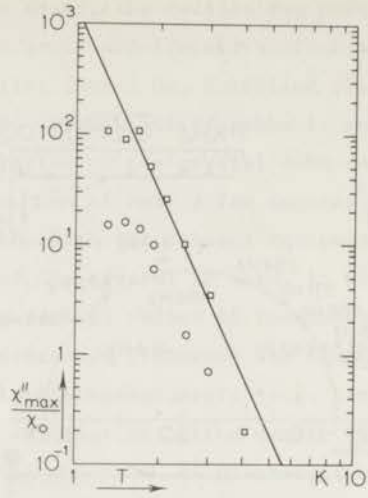

Fig. 33 χ''_{max}/χ_0 *versus temperature at* H_{SF} *for* $CsMnCl_3 \cdot 2H_2O$, *H//b axis.* □ *and* ○ *represent the results for two measuring series with a slightly different crystal orientation.* —— $\chi''_{max}/\chi_0 \propto T^{-5.5}$.

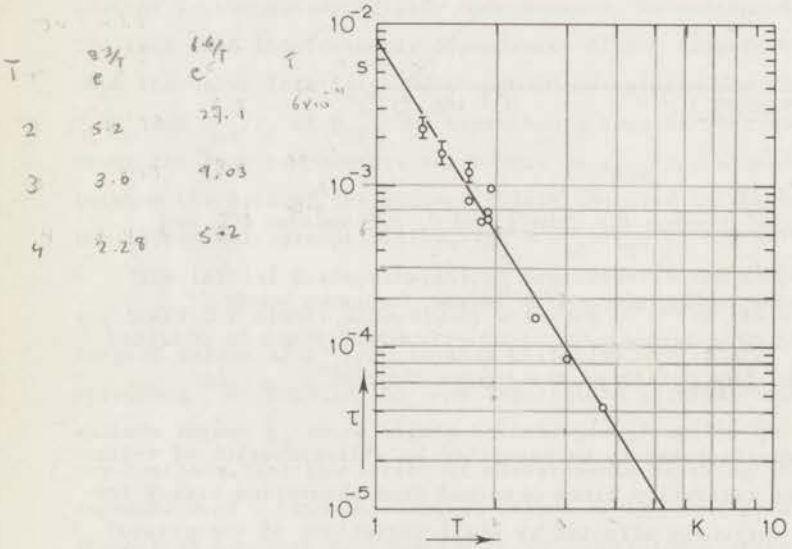

Fig. 34 *Relaxation time as a function of temperature at* H_{SF} *for* $CsMnCl_3 \cdot 2H_2O$, *H//b axis.* —— $\tau \propto T^{-4}$.

absorption peaks is only 100 Oe. Because of this fact the accuracy of these relaxation times is not large. A proper τ versus H curve, as realized for $MnCl_2 \cdot 4H_2O$ and $MnBr_2 \cdot 4H_2O$ (fig. 25), could not be obtained. From results at 1.90 K, one can estimate that the relaxation times at fields that differ 50 Oe from H_{SF} are about a factor two shorter than at H_{SF}.

3.3.3 *Discussion.* The phase transition from the antiferromagnetic to the spin-flop phase is a thermodynamical first order phase transition according to the molecular field theory. This implies that at this phase transition the specific heat becomes infinite, that a latent heat is present and also that the magnetization shows a discontinuity, corresponding to an infinite differential susceptibility. As far as we know, there are no specific-heat or magnetization data of $CsMnCl_3 \cdot 2H_2O$ near the spin-flop transition available.

The first order character of the phase transition seems to be confirmed experimentally by the magnitude and the sharpness of the susceptibility at H_{SF} (χ'/χ_0 up to 200, halfwidth 500 Oe). The form of the sample is not ellipsoidal, so the demagnetizing field, which is maximally about 100 Oe, is not uniform at all sites in the crystal. This effect may cause some broadening of the susceptibility peaks.

The well-known Clausius-Clapeyron equation is usually applied to the (first order) liquid-vapour phase transition. Applied to a first order magnetic transition this equation becomes [89]):

$$dH/dT = - Q_1/(T\Delta M) \qquad (28)$$

where dH/dT denotes the slope of the transition line in the H-T diagram, Q_1 the latent heat and ΔM the change of the magnetization per unit mass, across the transition. The slope of the spin-flop transition line of $CsMnCl_3 \cdot 2H_2O$ is constant within experimental accuracy (fig. 31). This means that the latent heat Q_1 is proportional to $T\Delta M$. The change of the magnetization ΔM is equal to $\int_{peak} \chi_T dH$. The width of the peak in the susceptibility is almost constant as a function of temperature, yielding $\Delta M \propto \chi_T(H_{SF})$. The absolute values of $\chi_T(H_{SF})$ are not known, but as mentioned above the measurements suggest that the temperature dependences of χ_T and χ''_{max} are similar. The temperature dependence of χ''_{max}/χ_0 can be derived from the $T^{-5.5}$ dependence of χ''_{max}/χ_0 for $1.8\ K < T < 4.2\ K$ and the temperature dependence of χ_0, which is proportional to $T^{0.5}$ if written as a power law. So one obtains $\chi_T \propto T^{-5}$ and consequently approximately a T^{-4} dependence for the latent heat in the above-mentioned

temperature range. It is remarkable that the latent heat and the relaxation time, along the transition line, show the same T^{-4} dependence. This suggests that there is some relation between these quantities.

Crossing the spin-flop phase line at increasing temperature and constant magnetic field, the latent heat appears as a specific heat which becomes infinite at the transition point, according to a δ-function. The latent heat is the energy involved if the magnetic state is changed independently, whether this happens at constant magnetic field or at constant temperature. The thermodynamical Casimir-Du Pré theory relates the relaxation time to the specific heat by $\tau = C_H/\alpha$ (section 1.1). If one assumes that the thermal conductivity coefficient α does not show a discontinuity at the phase transition field, one may expect that the relaxation time exhibits, just as C_H does, a sharp maximum at H_{SF}. Although the field dependence of τ at constant temperature could not be measured accurately, the experiments suggest such a maximum at H_{SF}, as sharp as the peaks of the χ'' versus H plots.

The dependences discussed above of the relaxation time near the spin-flop transition line, suggest that these relaxation times are closely connected with the specific and latent heats, thus supporting the applicability of the Casimir-Du Pré theory to the relaxation phenomena near this spin-flop transition.

The non-Debye form of the susceptibility may have several reasons. Of course one can expect that phonon-bottleneck effects are present in the large single crystal. However, these effects cannot be very strong because the observed relaxation time depends strongly on temperature. The inhomogeneity of the demagnetizing field may also contribute to the deviation of the Debye-form, since the relaxation time depends on the magnetic field.

Since the magnetization exhibits a steep rise at the spin-flop field, one can expect the occurrence of domains, analogously to the ferromagnetic behaviour at zero field. If domains are formed, hysteresis effects in the observed susceptibilities are likely to occur, but these effects are not found. However, their existence, which cannot be excluded, may be related to the observed relaxation behaviour.

3.4 *Relaxation behaviour at the phase transitions in cobalt chloride dihydrate*

3.4.1 *Introduction.* In this section some experimental results are described on relaxation phenomena associated with the magnetic phase transitions in $CoCl_2 \cdot 2H_2O$. This salt has a monoclinic crystal structure [90]). Chlorine bridged chains of Co^{2+} ions are formed along the c axis; these chains are held together

by relatively weak hydrogen bonds. Measurements at zero external magnetic field of the specific heat [91]) and the susceptibility [92,93]) indicate that $CoCl_2 \cdot 2H_2O$ orders antiferromagnetically below T_N = 17.2 K with the sublattice magnetizations parallel to the crystal b axis. If an external magnetic field is applied along the b axis, magnetization measurements [92,94]), susceptibility and N.M.R. measurements [95]) and neutron diffraction experiments [96]) demonstrated the existence of three magnetic regions at T = 4.2 K. The exchange interaction within a chain (i.e. along the c axis) is ferromagnetic ($J_0 > 0$) and much stronger than the inner-chain interactions [97]). Therefore, it is accepted that the spin structure may be represented as a set of ferromagnetic Ising chains. At weak external magnetic fields these chains are ordered antiferromagnetically as indicated in fig. 35. At H_{c1} (= 32 kOe) this ordering changes into a 6-sublattice

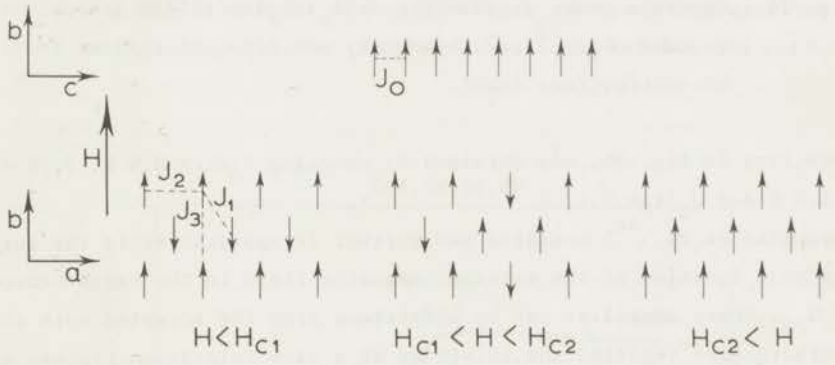

Fig. 35 *Spin structure of $CoCl_2 \cdot 2H_2O$, H//b axis. $H < H_{c1}$ antiferromagnetic state; $H_{c1} < H < H_{c2}$ 6-sublattice ferrimagnetic state; $H_{c2} < H$ ferromagnetic state. (From Kuramitsu et al. [56]).)*

ferrimagnetic arrangement, consisting of layers of parallel spins in a ++-++- sequence along the a axis [96]). At H_{c2} (= 46 kOe) a ferromagnetic state with fully saturated magnetization along the b axis is reached. Fig. 35 displays the various spin arrangements, while the various exchange interactions are also indicated.

Lowe et al. [98]) investigated the temperature dependence of the phase transitions by detection of the strain occurring in the $CoCl_2 \cdot 2H_2O$ crystal. Their results are displayed in the H-T diagram of fig. 36. The magnetic triple point is found to be at 8.8 K and 38.4 kOe. These authors calculated phase boundaries, based on the molecular field model [99]). The best fit, indicated by

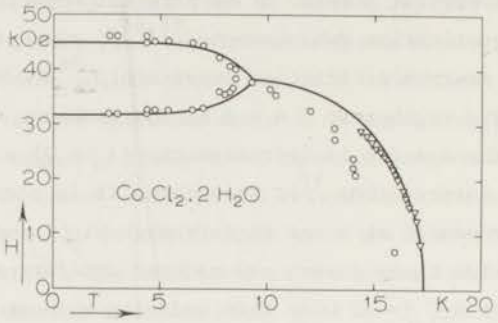

Fig. 36 *Magnetic phase diagram for $CoCl_2 \cdot 2H_2O$ with H//b axis. o Lowe et al.[98], ∇ this work, —— calculated phase boundaries (see text).*

the drawn line in fig. 36, was obtained by choosing J_0/k = 8.6 K, J_1/k = 4.5 K, J_2/k = 1.0 K and J_3/k = 0.12 K [95,96,97,100]).

Kuramitsu et al. [56]) measured two further irregularities in the susceptibility as a function of the external magnetic field in the range between H_{c1} and H_{c2}. These anomalies can be understood from the accepted spin structures. These authors also reported the existence of a slow relaxation process at the transition field H_{c1}; they estimated the corresponding relaxation time at 4.2 K to be longer than 2×10^{-3} s.

The variety of magnetic phase transitions in $CoCl_2 \cdot 2H_2O$ makes this salt very suitable for study with our experimental equipment at liquid-helium as well as at liquid-hydrogen temperatures.

3.4.2 *Experimental results and discussion.* The crystals were grown from a slowly evaporated aqueous solution at 70 °C. At this temperature $CoCl_2 \cdot 2H_2O$ forms long needles along the c axis with dominant (110)-type crystal surfaces; the crystals are easily cleaved in any plane containing the c axis. In order to mount the crystal with the b axis along the external magnetic field, its dimension in the c direction had to be reduced. To avoid damage of the crystal this was done by means of a wet-wire saw, which dissolves the material rather than cutting it mechanically. Most measurements were performed on a crystal with dimensions 3 x 3 x 5 mm along the a, b and c axes, respectively, oriented with

the easy axis (b axis) along the external field.

a) *Phase diagram.* At temperatures below T_N = 17.2 K, the registered measuring plots of the dispersion versus the external magnetic field show sharp peaks. At liquid-hydrogen temperatures the field values of these peaks depend on the temperature and are denoted by the symbol ▽ in fig. 36. These points agree much better with the phase boundary calculated by Lowe et al. [98]) on the basis of the molecular field model than the results of their own strain measurements, that are inaccurate at these temperatures. In the liquid-helium temperature range two large susceptibility peaks, which do not depend on temperature, are observed at field values H_{c1} = 32.0 kOe and H_{c2} = 45.6 kOe. These values are about the same as those reported by Lowe et al. (H_{c1} = 32 kOe, H_{c2} = 45 kOe) and those found by Kuramitsu et al. [56]) (H_{c1} = 31.8 kOe, H_{c2} = 46.0 kOe).

Measurements of the initial susceptibility χ_0 versus temperature around T_N displayed in fig. 37 yield the same result as found by Kobayashi and Haseda [92]):

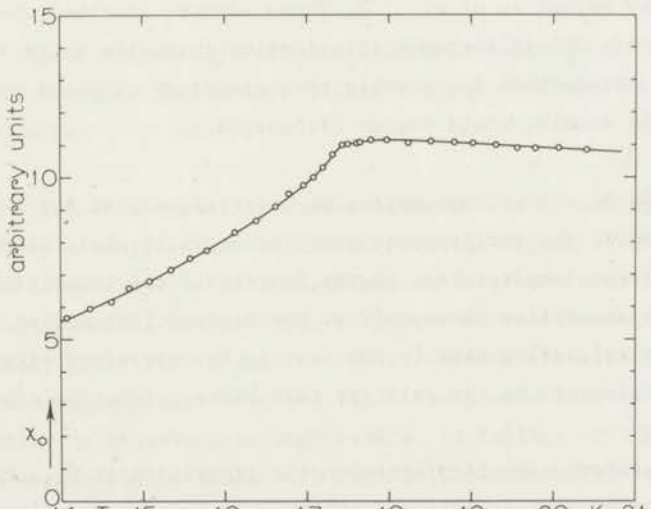

Fig. 37 *The initial susceptibility χ_0 as a function of temperature for $CoCl_2 \cdot 2H_2O$, H//b axis. Drawn line for visual aid only.*

a flat maximum near 18 K and a maximal value of the derivative $d\chi_0/dT$ at 17.3 K. This value is close to T_N = 17.2 K as derived from the specific heat anomaly [91]. Thus the behaviour of χ_0 near the Néel temperature is similar to that observed in $MnCl_2 \cdot 2H_2O$ and $MnBr_2 \cdot 2H_2O$ (section 3.2).

The magnitude of the susceptibility peaks at H_{c1} and H_{c2} depend on the applied frequency of the oscillating part of the external magnetic field; these dependences will be described later. As an example, we mention values obtained at 117 Hz: χ'/χ_0 = 6.1 and χ''/χ_0 = 4.2 at H_{c1}, and χ'/χ_0 = 110 and χ''/χ_0 = 20 at H_{c2}. The halfwidth values, which are equal for χ' and χ'', amount to approximately 600 Oe at H_{c1} and 900 Oe at H_{c2}. The peaks observed at H_{c1} and H_{c2} are both somewhat asymmetrical, as one can notice from the drawn line in fig. 40. No hysteresis is observed in the position of the peaks, but the magnitude of the peak at H_{c1} is a few percent larger if measured with increasing magnetic field than with decreasing field. Between the large peaks at H_{c1} and H_{c2}, two small peaks are observed at 36.1 kOe and 40.5 kOe. These peaks can only be observed in a continuously increasing external field starting from an initial field below H_{c1}. These small peaks do not occur at decreasing field. Approximately the same field values (36.8 kOe and 41.1 kOe) and hysteresis character are reported by Kuramitsu et al. [56]. These authors ascribed these small peaks to the occurrence of antiferromagnetic domains in fields up to 36.8 kOe, where these domains change into the 4-sublattice structure proposed by Oguchi [97]. At 41.1 kOe the domains would become ferromagnetic.

b) *Relaxation behaviour*. Absorption is observed only at the phase transitions H_{c1} and H_{c2} and at the antiferromagnetic-paramagnetic phase transition observed at liquid-hydrogen temperatures. At the last-mentioned transition non-zero values for the absorption occur only at the highest frequencies ($\gtrsim$ 1 MHz). This means that the relaxation time is too fast to be determined accurately with the present equipment. We can only say that these relaxation times are shorter than 10^{-7} s.

At the antiferromagnetic-ferrimagnetic transition at H_{c1}, however, the opposite situation occurs. Here one observes at 4.2 K increasing absorptions at decreasing frequencies, indicating that the relaxation time is too long to be measured. Fig. 38 shows the Argand diagram at H_{c1} and T = 4.2 K. No influence is found resulting from the amplitude of the oscillating part of the external field. The data points of fig. 38 seem to lie on a semicircle, but the positions of these points, corresponding to the indicated frequencies, are too close to each other to fulfil the Casimir-Du Pré relations eqs. (1) and (2). This

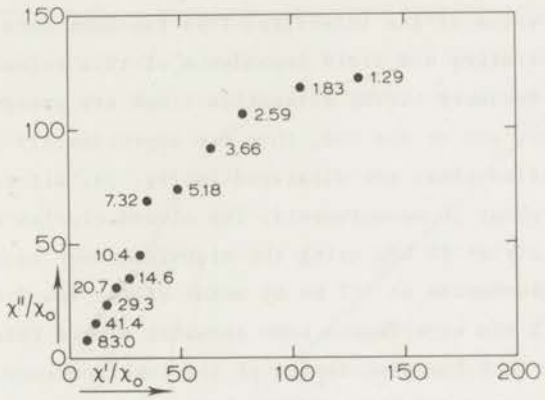

Fig. 38 *Argand diagram of $CoCl_2 \cdot 2H_2O$, H//b axis at H_{c1} = 32.0 kOe and T = 4.2 K. The numbers in the diagram indicate the frequency in Hz.*

means that the relaxation behaviour cannot be described by a single relaxation time but rather by a distribution of times. From the Argand diagram one can estimate that the lower-limit of this distribution is of the order of 0.1 s. Since these relaxation phenomena are so slow, they were further investigated by the field-step method, described in section 1.3.2. Because the susceptibility peak is sharp, it is very important that the final field at which the recovery of the susceptibility is observed, be very stable. Variations in the final field are registered accurately by means of a circuit, which compensates the major part of the shunt voltage produced by the current flowing through the superconducting magnet. The variation of the magnetic field during the registration of the recovery curve does not exceed 20 Oe.

The recovery of the susceptibility after the field step was not an exponential function. This means that the relaxation behaviour has to be described by a distribution of times, just as was concluded from the non-Debye form of the frequency dependence of $\bar{\chi}$.

The observed time dependence of the susceptibility was not influenced by the magnitude and/or the sign of the applied field step. From the plots of log χ versus time, which show a straight line if the recovery is exponential, we determined an average relaxation time representative of the susceptibility at half the initial value of the intensity. This has been done to allow an analysis of the temperature and field dependence of this relaxation behaviour. At the start of the recovery curves relaxation times are present which are about a factor of 2 shorter, and at the end, they are approximately 3 times longer. The resulting relaxation times are displayed in fig. 39. All fully drawn symbols are the averages of about 20 measurements. The closed circles were determined from the susceptibility at 15 kHz using the high-frequency equipment; the open symbols refer to measurements at 117 Hz by means of the low-frequency equipment. The times from the 15 kHz experiments seem somewhat slower than those from 117 Hz. It must be noted that the electronics of the low-frequency system are rather slow, so this system can not follow time variations faster than 1.4 s. The longest relaxation times, observed at the lowest temperatures, are of the order of 10^4 s, where the stability of the complete measuring system becomes a bottlenecking feature.

The relaxation times in fig. 39 are displayed as a function of the reciprocal temperature, because the experimental results are best described by an exponential temperature dependence. The drawn line represents $\tau^{-1} \propto \exp(-\Delta/kT)$ with $\Delta/k = 90$ K.

The temperature dependence of τ at H_{c1} was also investigated for a smaller crystal with dimensions 1 x 1 x 5 mm along the a, b and c axes, respectively. This crystal was obtained from the same solution as the larger crystal. The resulting relaxation times, indicated by the symbol Δ in fig. 39 are somewhat shorter than those of the other crystal. The temperature dependence of τ can also be described by $\tau^{-1} \propto \exp(-\Delta/kT)$, buth with $\Delta/k = 70$ K (- - - line in fig. 39). There may be several reasons for the difference between the results of the two crystals. Since a distribution of relaxation times is observed, it is possible that phonon-bottleneck effects which would be more severe in the larger crystal play a role. Another reason may be a small difference in the orientation of the crystals with respect to the external field. Also magnetic domains whose structure can depend on the shape and size of the crystal, are likely to occur. Hence they can also be responsible for the observed difference between the two crystals.

The relaxation behaviour has also been studied at a constant temperature (T = 3.67 K) as a function of the external magnetic field. Since the width of

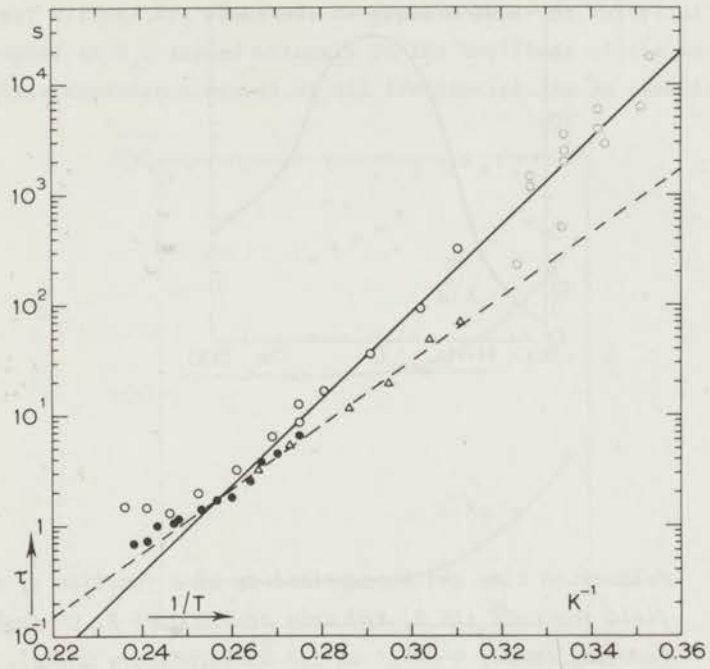

Fig. 39 *Relaxation time as a function of 1/T at H_{c1} for $CoCl_2 \cdot 2H_2O$, H//b axis. ● from recovery curves of χ' at 15 kHz (large crystal); ○ , ◌ from recovery curves of χ' at 117 Hz (large crystal); Δ from recovery curves of χ' at 117 Hz (small crystal); fully drawn symbols are averages of about 20 measurements; dotted symbols refer to one measurement; —— $\tau^{-1} \propto e^{-\Delta/kT}$, $\Delta/k = 90$ K; - - - idem $\Delta/k = 70$ K.*

the susceptibility peak is small and the intensity of the observed relaxation process is closely related to the value of χ, relaxation measurements can only be performed successfully in the vicinity of H_{c1}. Fig. 40 shows the field dependence of the relaxation time of the large crystal at 3.67 K. The data points of this figure are averaged values from at least ten measurements. No influence from the sign of the field step on the observed relaxation behaviour is found in this series of measurements. In fig. 40 the field dependence of χ' at 117 Hz,

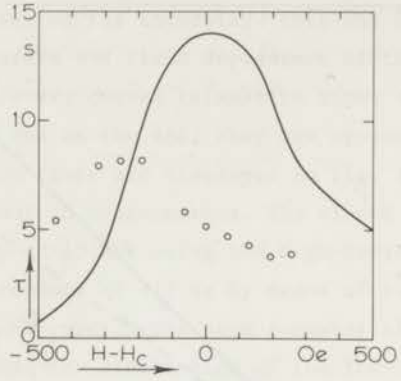

Fig. 40 *Relaxation time and susceptibility as a function of magnetic field for $CoCl_2 \cdot 2H_2O$, H//b axis at T = 3.67 K. ○ from the recovery curve; —— χ' at 117 Hz (arbitrary units).*

the frequency at which these relaxation measurements were performed, is also shown. It is remarkable that the maximum of the τ versus H curve does not coincide with the maximum of the susceptibility, but occurs at a field value 250 Oe below H_{c1}.

The origin of the observed relaxation process is not clear. One might think of a mechanism in which the magnetic domains play an important role. These domains can be the reason for the observed distribution of relaxation times. The exponential temperature dependence of the relaxation time suggests changes in the domain structure which have to surpass an energy barrier by thermal activation, yielding a temperature dependence of the inverse relaxation time proportional to Boltzmann's factor. In this context, one might also turn to the model proposed by Néel [101]) of an assembly of fine ferromagnetic particles, whose magnetizations undergo a sort of Brownian rotation due to the thermal

fluctuations [102]). This model yields an exponential temperature dependence for the relaxation rate τ^{-1}.

The relaxation behaviour at the ferrimagnetic-ferromagnetic phase transition at H_{c2} = 45.6 kOe differs completely from that at H_{c1}. While at H_{c1} no non-linear effects are observed, it appears that the values of χ'/χ_0 and χ''/χ_0, measured at H_{c2} depend strongly on the amplitude of the oscillating field, h. This dependence occurs at all frequencies. As an example, fig. 41

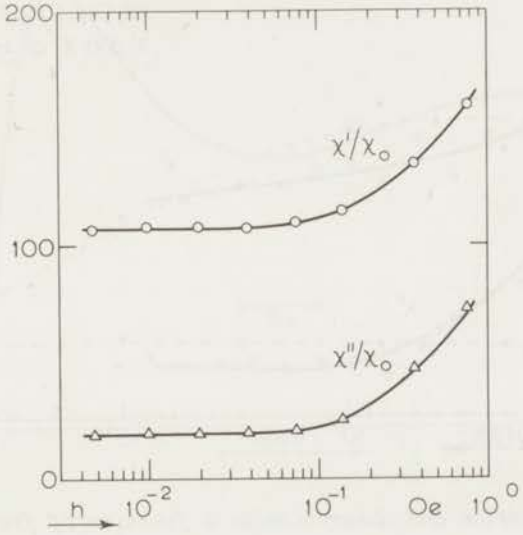

Fig. 41 *χ'/χ_0 and χ''/χ_0 for $CoCl_2 \cdot 2H_2O$ (H//b axis at H_{c2} = 45.6 kOe, T = 4.2 K) as a function of the amplitude of the oscillating part of the external magnetic field ($\omega/2\pi$ = 117 Hz).*

shows this dependence observed at 4.2 K and a frequency of 117 Hz. As this figure shows, non-linearity occurs for values of the amplitude larger than 0.1 Oe; at smaller values $CoCl_2 \cdot 2H_2O$ behaves linearly. It is remarkable that this value of 0.1 Oe at which non-linearity starts is much smaller than the width of the susceptibility peak and that the values of χ' and χ'' increase as a function of h. One could expect a decrease if the amplitude would be of the order of the width of the susceptibility peak. A reason for the increase above 0.1 Oe may be the occurrence of domains at this phase transition, whose walls are displaced by the oscillating field, if its amplitude surpasses a certain limit and gives rise to an extra contribution to the susceptibility.

To determine relaxation times, the dispersion-absorption technique can only be used successfully if both χ' and χ'' are independent of the value of h.

Hence the frequency dependence of the absorption and dispersion is studied at an amplitude of 0.08 Oe instead of the usual applied values of the order of a few Oersted. Fig. 42 shows this frequency dependence; in this figure results

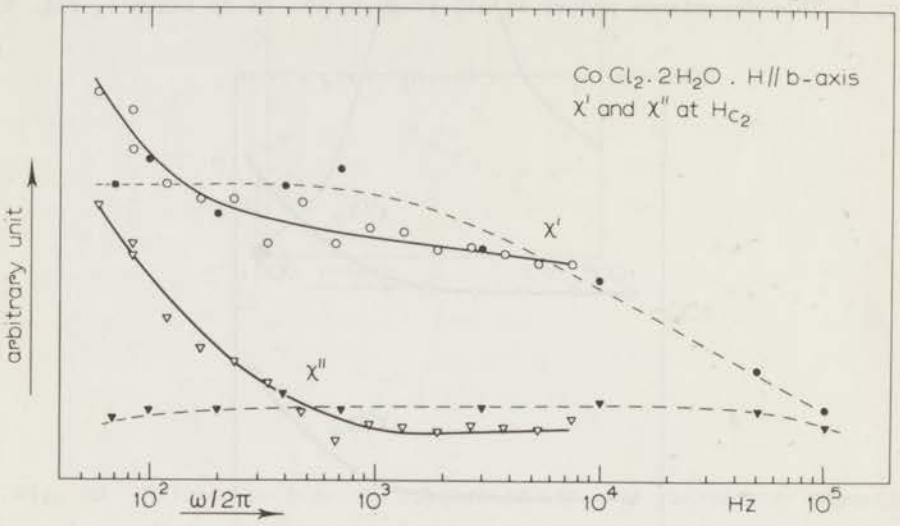

Fig. 42 *Dispersion and absorption as a function of frequency for $CoCl_2 \cdot 2H_2O$, H//b axis, at H_{c2} = 45.6 kOe and T = 4.2 K. Open symbols denote results from the present work; closed symbols denote results by Kuramitsu et al. [56]; lines for visual aid only.*

by Kuramitsu et al. [56]) are also inserted. The arbitrary scale for the susceptibility is chosen in such a way that both measurements give the same value for χ' at 3 kHz. There is a large discrepancy between the results of the two sets of measurements. This discrepancy occurs because the measurements by Kuramitsu are performed with amplitudes of the oscillating field between 10 and 40 Oe, thus the system cannot be considered to be linear. From fig. 42 one may conclude that the relaxation time of 2×10^{-5} s, as reported by Kuramitsu is not correct.

The increase of χ' and χ'' at decreasing frequencies down to 70 Hz (fig. 42) suggests long relaxation times, which may be measured with the field-step arrangement. Also at these field-step measurements the influence of the amplitude

of the oscillating field was observed. At amplitudes larger than 0.1 Oe hardly any intensity of a relaxation mechanism was found. At smaller amplitudes ($h < 0.1$ Oe) a complicated relaxation behaviour was observed, as is indicated in fig. 43. The intensity of this periodic relaxation phenomenon did not depend

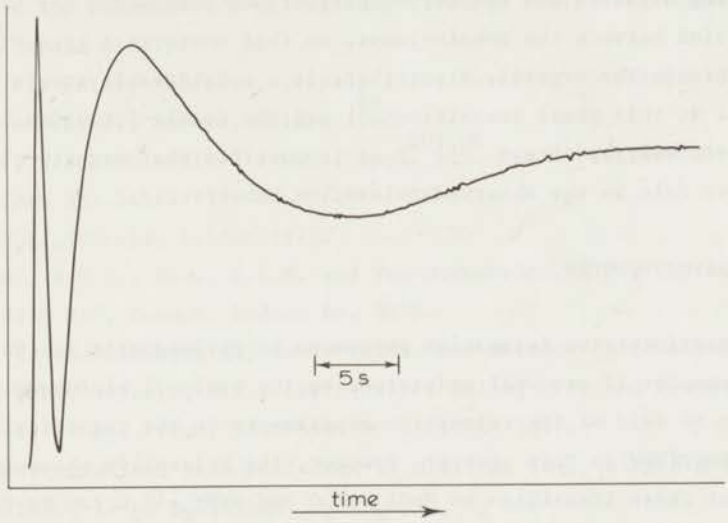

Fig. 43 *Time dependence of the voltage induced in the measuring coils after a field step to H_{c2} = 45.6 kOe for $CoCl_2 \cdot 2H_2O$, H//b axis.*

on the amplitude h. The same recovery curve was also observed at h = 0. This means that at H_{c2} the $CoCl_2 \cdot 2H_2O$ crystal transmits an electro-magnetic signal for some time after a field step, when the external magnetic field is completely constant. The frequencies present in this relaxation process were studied by synchronous detection of this signal at frequencies between 100 Hz and 100 kHz. In this frequency range similar recovery curves were found; at lower frequencies the noise present in the signal inhibited the observation of the recovery curve. No dependence on the temperature was found for temperatures between 4.2 K and 1.3 K. These recovery curves show five areas, each with their own time constant. The last three areas of fig. 43 show time constants of approximately 10, 5 and 1 s.

This remarkable relaxation effect is probably caused by domain formation

at the ferrimagnetic-ferromagnetic transition. One might think of a mechanism in which domains are formed or domain walls are moved with shocks (cf. the Barkhausen effect occurring in ferromagnetic domains), so that the magnetization instantaneously changes locally in the crystal [70]. Such jumps of the magnetization as a function of time are accompanied by emission of an electromagnetic signal, in which all frequencies are present.

The long duration and the periodicity of the phenomenon may be caused by an interaction between the domain-jumps, so that there is a kind of propagation of jumps through the crystal. Since there is a considerable strain present in the crystal at this phase transition [98] and the domain-formation is generally affected seriously by strain [70,102] it is possible that magneto-elastic effects play a major role in the observed relaxation behaviour.

3.5 *Concluding remarks*

The experiments on relaxation phenomena in paramagnetic solids as described in chapter II are well understood on the basis of microscopic theories. This cannot be said of the relaxation experiments on the magnetically ordered crystals described in this chapter. However, the relaxation phenomena at the second order phase transition in $MnCl_2 \cdot 4H_2O$ and $MnBr_2 \cdot 4H_2O$ can be reasonably understood on the basis of thermodynamics. Notably the relaxation time observed at these phase transitions agrees with the relation $\tau = C_H/\alpha$ as results from the Casimir-Du Pré formalism. There is experimental evidence that the relaxation behaviour near the spin-flop transition in $CsMnCl_3 \cdot 2H_2O$ is also related to thermodynamic quantities. The complicated relaxation behaviour, as observed in $CoCl_2 \cdot 2H_2O$ at liquid-helium temperatures, might be dominated by the presence of magnetic domains.

The understanding of these interesting phenomena can be increased by the availability of specific-heat data in external magnetic fields near these phase transitions. Also the extension of complex susceptibility measurements to other solids with magnetic ordering may be of great help. Since many of the described results depend strongly on the crystal orientation, it would be desirable to have the facility to rotate the crystal investigated during the measurements.

The utilization of ^3He equipment to perform complex susceptibility measurements down to 0.3 K may be even more important for the experimental understanding, since many crystals which are easily studied with the present equipment become magnetically ordered below 1.3 K.

REFERENCES

1) Casimir, H.B.G. and Du Pré, F.K., Physica 5 (1938) 507; Commun. Kamerlingh Onnes Lab. Leiden Suppl. No. 85a.

2) Cole, K.S. and Cole, R.H., J. Chem. Phys. 9 (1941) 341.

3) Gorter, C.J., Paramagnetic Relaxation, Elsevier publishing Company, Amsterdam (1947).

4) Debije, P., Polare Moleküle, Leipzig 1929; Phys. Z. 35 (1934) 101.

5) Van den Broek, J., thesis, Leiden 1960.

6) De Vries, A.J. and Livius, J.W.M., Appl. sci. Res. 17 (1967) 31; Commun. Leiden No. 349a.

7) Roest, J.A., thesis, Leiden 1972.

8) Eijkelhof, H.M.C., Pouw, C.L.M. and Van Duyneveldt, A.J., Physica 62 (1972) 257; Commun. Leiden No. 395b.

9) Girard, B. and Sauzade, M., Nucl. instr. and methods 25 (1964) 269.

10) Wilson, M.N., Wolters, C.R., Lewin, J.D., Smith, P.F. and Spurway, A.H., Brit. J. App. Phys. (J. Phys. D) 3 (1970) 1517.

11) These determinations were performed by M.W. van Tol, using N.M.R. techniques.

12) Pouw, C.L.M., to be published.

13) Orbach, R., Proc. Roy. Soc. A264 (1961) 458.

14) Verstelle, J.C. and Curtis, D.A., Handbuch der Physik (1968) Bd. 18/1.

15) Kronig, R. de L., Physica 6 (1939) 33.
Van Vleck, J.H., Phys. Rev. 57 (1940) 426.

16) Hebel, L.C. and Slichter, C.P., Phys. Rev. 113 (1959) 1504.

17) Ziman, J.M., Proc. Roy. Soc. A226 (1954) 436.
Rogers, W.M. and Powell, R.L., Tabels of Transport Integrals. Nat. Bureau of Standards, Circular No. 595, Washington D.C. (1958).

18) Kramers, H.A., Proc. Kon. Ned. Akad. Wetenschap. 33 (1930) 959.

19) Van Duyneveldt, A.J., Pouw, C.L.M. and Breur, W., Phys. stat. sol. (b) 55 (1973) k63.
Van Duyneveldt, A.J. and Pouw, C.L.M., Proc. XVIIth Colloque AMPERE, Turku (1972) 404.

20) Orbach, R. and Blume, M., Phys. Rev. Letters 8 (1962) 478.

21) Brons, F., thesis, Groningen 1938.
Van Vleck, J.H., Phys. Rev. 57 (1940) 426.

22) Orbach, R., Proc. Roy. Soc. A264 (1961) 485.

23) Stoneham, A.M., Proc. Phys. Soc. 86 (1965) 1163.

24) Van Vleck, J.H., Phys. Rev. 59 (1941) 724.

25) Scott, P.L. and Jeffries, C.D., Phys. Rev. 127 (1962) 32.
26) Roest, J.A., Van Duyneveldt, A.J., Van der Bilt, A. and Gorter, C.J., Physica 64 (1973) 306; Commun. Leiden No. 400a.
27) Gorter, C.J., Van der Marel, L.C. and Bölger, B., Physica 21 (1955) 103; Commun. Leiden Suppl. 109c.
28) Tutton, A.E.H., Phil. Trans. Roy. Soc. A216 (1916) 1.
29) Stoneham, A.M., Proc. Phys. Soc. 85 (1965) 107.
30) Cox, S.F.J., Gill, J.C. and Wharmby, D.O., J. Phys. C. Solid State Phys. 4 (1971) 371.
31) Lijphart, E.E., De Vroomen, A.C. and Poulis, N.J., Proc. XVIIth Colloque AMPERE, Turku (1972) 397.
32) Gill, J.C., Proc. Phys. Soc. 85 (1965) 119.
33) De Vroomen, A.C., Lijphart, E.E., Prins, D.Y.H., Marks, J. and Poulis, N.J., Physica 61 (1972) 241; Commun. Leiden No. 393b.
34) De Vries, A.J., Curtis, D.A., Livius, J.W.M., Van Duyneveldt, A.J. and Gorter, C.J., Physica 36 (1967) 91; Commun. Leiden No. 356b.
35) Roeland, L.W., Muller, F.A. and Gersdorf, R., Proc. Conf. Champs magnétiques intenses, Grenoble (1966) 175.
36) Gersdorf, R., Muller, F.A. and Roeland, L.W., Proc. Conf. Champs magnétiques intenses, Grenoble (1966) 185.
37) Van Duyneveldt, A.J., Soeteman, J. and Gorter, C.J., Physica 47 (1970) 1; Commun. Leiden No. 377a.
38) Roest, J.A., Van Duyneveldt, A.J., Van der Bilt, A. and Gorter, C.J., Physica 64 (1973) 324; Commun. Leiden No. 400b.
39) De Vroomen, A.C., Lijphart, E.E. and Poulis, N.J., Physica 47 (1970) 458; Commun. Leiden No. 377b.
40) De Vries, A.J., Livius, J.W.M., Curtis, D.A., Van Duyneveldt, A.J. and Gorter, C.J., Physica 36 (1967) 65; Commun. Leiden No. 356a.
41) Van Dijk, C., thesis, Leiden 1970.
42) Van Duyneveldt, A.J., Tromp, H.R.C. and Gorter, C.J., Physica 45 (1969) 272; Commun. Leiden No. 374b.
43) Orton, J.W., Electron paramagnetic resonance, Iliffe books, London 1968.
44) Brom, H.B. and Huiskamp, W.J., Physica 63 (1973); Commun. Leiden No. 398a.
45) Stöhr, J., Olsen, D.N. and Gruber, J.B., J. Chem. Phys. 55 (1971) 4463.
46) Kalvius, G.M., Shenoy, G.K., Dunlap, B.D., Proc. XVIth Colloque AMPERE (1970) 584.
47) Hillaert, J.G.A., private communication.
48) Hillaert, J.G.A., thesis, Leiden 1973.

49) Benzie, R.J., Cooke, A.H. and Whitley, S., Proc. Roy. Soc. 232 (1955) 277.
50) Locher, P.R. and Gorter, C.J., Physica 27 (1961) 997; Commun. Leiden No. 329a.
51) Verstelle, J.C., thesis, Leiden 1962.
52) Brom, H.B., Soeteman, J. and Van Duyneveldt, A.J., Proc. XVIIth Colloque AMPERE (1972) 401.
53) Pfeffer, W., Z. Physik 164 (1961) 295.
54) Lasheen, M.A., Van den Broek, J. and Gorter, C.J., Physica 24 (1958) 1076; Commun. Leiden No. 312c.
55) Soeteman, J., Van Duyneveldt, A.J. and Gorter, C.J., Physica 45 (1969) 435; Commun. Leiden No. 375a.
56) Kuramitsu, Y., Amaya, K. and Haseda, T., J. Phys. Soc. Japan 33 (1972) 83.
57) Groth, P., "Chemische Krystallographie" Vol. I, Wilhelm Engelmann, Leipzig (1908).
58) Zalkin, A., Forrester, J.D. and Templeton, D.H., Inorg. Chem. 3 (1964) 529.
59) Friedberg, S.A. and Wasscher, J.D., Physica 19 (1953) 1072; Commun. Leiden No. 293c.
60) Henry, W.E., Phys. Rev. 91 (1953) 435; ibid. 92 (1953) 844; ibid. 94 (1954) 1146.
61) White, J.J. and Rives, J.E., Phys. Rev. B6 (1972) 4352.
62) Hempstead, R.D. and Mochel, J.M., Phys. Rev. B7 (1973) 287.
63) Gijsman, H.M., Poulis, N.J. and Van den Handel, J., Physica 25 (1959) 954; Commun. Leiden No. 317b.
64) Gorter, C.J. and Van Peski-Tinbergen, Tineke, Physica 22 (1956) 273; Commun. Leiden Suppl. No. 110b.
65) Spence, R.D. and Nagarajan, V., Phys. Rev. 149 (1966) 191.
66) De Vries, A.J., thesis, Leiden 1965.
67) Reichert, T.A. and Giauque, W.F., J. Chem. Phys. 50 (1969) 4205.
68) Giauque, W.F., Fisher, R.A., Hornung, E.W. and Brodale, G.E., J. Chem. Phys. 53 (1970) 1474.
69) Schmidt, V.A. and Friedberg, S.A., J. Appl. Phys. 38 (1967) 5319.
70) Morrish, A.H., The Physical Principles of Magnetism, Wiley (1965).
71) Bowers, K.D. and Owen, J., Rep. Prog. Phys. XVIII (1955) 304.
72) Van Duyneveldt, A.J., Pouw, C.L.M. and Breur, W., Physica 57 (1972) 205; Commun. Leiden No. 387b.
73) Gorter, C.J. and Van Duyneveldt, A.J., Proc. XIIIth Conf. Low Temperature Physics, Boulder (1972) 621.

74) De Vries, A.J., Livius, J.W.M., Curtis, D.A., Van Duyneveldt, A.J. and Gorter, C.J., Physica 36 (1967) 65; Commun. Leiden No. 356a.
75) Schelleng, J.H. and Friedberg, S.A., Phys. Rev. 185 (1969) 728.
76) Fisher, M.E. and Sykes, M.F., Physica 28 (1962) 939.
77) Turrell, B.G. and Yue, C.L., Can. J. of Phys. 49 (1971) 2520.
78) Cerdonio, M. and Paroli, P., Phys. Letters 38A (1972) 533.
79) Fisher, M.E., Proc. Roy. Soc. A254 (1960) 66.
80) Fisher, M.E., Phil. Mag. 7 (1962) 1731.
81) Barry, J.H. and Harrington, D.A., Phys. Rev. B4 (1971) 3068.
82) Huber, D.L., Phys. Rev. B3 (1971) 836.
83) Jensen, S.J., Andersen, P. and Rasmussen, S.E., Acta Chem. Scand. 16 (1962) 1890.
84) Smith, T. and Friedberg, S.A., Phys. Rev. 176 (1968) 660; ibid. B2 (1970) 781.
85) Bonner, J.C. and Fisher, M.E., Phys. Rev. 135 (1964) A640.
86) Skalyo, J., Shirane, G., Friedberg, S.A. and Kobayashi, H., Phys. Rev. B2 (1970) 1310.
87) Spence, R.D., De Jonge, W.J.M. and Rama Rao, K.V.S., J. Chem. Phys. 51 (1969) 4694.
88) Butterworth, G.J. and Woollam, J.A., Phys. Letters 29A (1969) 259.
89) Rives, J.E., Phys. Rev. 162 (1967) 491.
De Jongh, L.J., Sol. State Commun. 10 (1972) 537.
90) Morosin, B. and Graeber, E.J., Acta Cryst. 16 (1963) 1176.
91) Shinoda, T., Chihara, H. and Seki, S., J. Phys. Soc. Japan 19 (1964) 1088.
92) Kobayashi, H. and Haseda, T., J. Phys. Soc. Japan 19 (1964) 765.
93) Narath, A. and Barham, D.C., Bull. Am. Phys. Soc. 9 (1964) 112.
94) Narath, A., J. Phys. Soc. Japan 19 (1964) 2244.
95) Narath, A., Phys. Rev. 136A (1964) 766; ibid. 140A (1965) 552.
96) Cox, D.E., Shirane, G., Frazer, B.C. and Narath, A., J. Appl. Phys. 37 (1966) 1126.
97) Oguchi, T., J. Phys. Soc. Japan 20 (1965) 2236.
98) Lowe, M.A., Abeledo, C.R. and Misetich, A.A., Phys. Letters 37A (1971) 274.
99) Garrett, C.G.B., J. Chem. Phys. 19 (1951) 1154.
100) Torrance, J.B. and Tinkham, M., Phys. Rev. 187 (1969) 595.
101) Néel, L., Compt. Rend. Acad. Sci. 228 (1949) 664; Ann. Géophys. 5 (1949) 99.
102) Magnetism, Rado, G.T. and Suhl, H., editors, Volume III, Academic Press (1963).

SAMENVATTING

Dit proefschrift behandelt magnetische relaxatieverschijnselen in enige paramagnetische en antiferromagnetische vaste stoffen. Hiertoe is voornamelijk gebruik gemaakt van de complexe susceptibiliteitsmethode, waarmee de dispersie en absorptie als functie van de frequentie worden gemeten. Indien de optredende relaxatietijden te lang worden ($\tau > 0{,}5$ s) is gebruik gemaakt van de veld-stap methode, waarmee men het gedrag van de susceptibiliteit na een plotselinge veldverandering als functie van de tijd waarneemt. Beide methodes worden in hoofdstuk I besproken, tezamen met de verschillende opstellingen, waarmee de experimenten zijn verricht. Een opstelling, welke een supergeleidende magneet bevat (H tot 35 kOe) in een bad van vloeibare helium met binnen de magneetspoel een aparte cryostaat voor de meetspoelen en het preparaat, wordt uitvoerig behandeld. Het voordeel van een dergelijke opstelling is, dat, indien het gewenst is het preparaat bij hoge uitwendige velden te onderzoeken, men niet gebonden is aan de temperatuur van het heliumbad van de supergeleidende magneet.

Het tweede hoofdstuk bevat, na een overzicht van de microscopische paramagnetische spin-rooster relaxatietheorie, metingen aan koper Tutton zouten en ytterbium chloride hexahydraat. In $CuCs_2(SO_4)_2 \cdot 6H_2O$ wordt het directe relaxatieproces ($\tau^{-1} = AH^4T$) waargenomen zowel bij temperaturen van vloeibare helium als van vloeibare waterstof. De numerieke waarde van de coëfficiënt A is bepaald en stemt goed overeen met theoretische berekeningen. De veldonafhankelijke relaxatietijd bij 1,4 K, gevonden door Cox, werd bij onze experimenten niet waargenomen. De oorzaak van dit verschil is het feit, dat het onderhavige relaxatieproces niet met één tijdconstante beschreven kan worden, zoals onze metingen aantoonden. In een reeks koper Tutton zouten is bij zwakke magneetvelden (ca. 1 kOe) het Raman-relaxatieproces onderzocht. Dit relaxatieproces is reeds het onderwerp geweest van talrijke onderzoekingen, welke leidden tot verschillende waarden van de Debije-temperatuur (deze kan bepaald worden uit de temperatuurafhankelijkheid van de Raman-relaxatietijd ($\tau^{-1} = BT^9 J_8(\Theta_D/T)$). Onze metingen resulteren in een Θ_D, welke afhankelijk is van het temperatuurgebied waarin Θ_D bepaald wordt. Deze temperatuurafhankelijkheid verklaart grotendeels de verschillende waarden zoals door anderen vermeld.

Van $YbCl_3 \cdot 6H_2O$ zijn het hoekafhankelijke directe proces en het Raman-proces onderzocht. De gevonden resultaten van het hoekafhankelijke directe proces

zijn (ook numeriek) in goede overeenstemming met metingen van Brom. De relaxatietijden gevonden in lage uitwendige velden stemmen goed overeen met de $T^9 J_8(\Theta_D/T)$ temperatuur afhankelijkheid van het Raman-proces en niet met die van het Orbach-proces zoals voorgesteld door Kalvius.

In hoofdstuk III worden relaxatieverschijnselen behandeld die optreden in magnetisch geordende stoffen. In $MnCl_2 \cdot 4H_2O$ en $MnBr_2 \cdot 4H_2O$ zijn relaxatieverschijnselen onderzocht, welke optreden bij de overgang tussen de antiferromagnetische en paramagnetische toestand. Bij deze faseovergang worden relaxatietijden waargenomen welke een duidelijk maximum vertonen. Dit gedrag kan beschreven worden met de relatie $\tau = C_H/\alpha$, welke volgt uit de thermodynamische Casimir-Du Pré theorie. De intensiteiten van deze relaxatieverschijnselen (χ''_{max}/χ_0) zijn in goede overeenstemming met waarden, die via thermodynamische relaties uit metingen van M en C_H volgen. De intensiteit van het relaxatieproces vertoont bij de faseovergang in uitwendige velden een scherp maximum, net als de isotherme susceptibiliteit (χ_T), terwijl de adiabatische susceptibiliteit (χ_{ad}) een veel minder geprononceerd maximum heeft. De piek in de χ_T welke feitelijk dezelfde is als die in χ''_{max} ($\chi_T = \chi_{ad} + 2\chi''_{max}$), is in overeenstemming met de berekeningen van Fisher aan het 'decorated' Ising rooster. Ook worden resultaten van de nulveld susceptibiliteit besproken.

Metingen van de relaxatietijden in de paramagnetische toestand in $MnCl_2 \cdot 4H_2O$ en $MnBr_2 \cdot 4H_2O$ stemmen onderling minder goed overeen. In hoge velden wordt een H^{-2} veldafhankelijkheid voor τ gevonden, welke karakteristiek is voor het directe proces van S-toestand ionen zoals Mn^{2+} ($\tau^{-1} = AH^2T$). De numerieke waarden van de coefficiënt A verschillen aanzienlijk tussen beide zouten, terwijl deze waarden ook flink afwijken van de resultaten gevonden in andere Mn^{2+} zouten. Mogelijk is de sterke exchange in beide mangaan halogeniden hiervan de oorzaak.

Relaxatieverschijnselen bij de antiferromagnetische spinflop overgang zijn onderzocht in $CsMnCl_3 \cdot 2H_2O$. De relaxatieverschijnselen welke optreden op deze eerste orde faseovergang kunnen beschreven worden met een relaxatietijd die sterk toeneemt bij dalende temperatuur. Ook bij deze magnetische overgang lijkt het relaxatiegedrag zinvol te kunnen worden beschreven met de thermodynamische relatie $\tau = C_H/\alpha$.

Tenslotte wordt in hoofstuk III het gecompliceerde relaxatiegedrag van $CoCl_2 \cdot 2H_2O$ besproken. Zeer snelle relaxatieverschijnselen zijn waargenomen bij vloeibare waterstof temperaturen en zeer langzame bij vloeibare helium temperaturen. Bij de overgang tussen de antiferromagnetische en ferrimagnetische toestand (H_{c1} = 32 kOe) worden relaxatietijden gevonden tot 10^4 s, welke van de

temperatuur afhangen volgens $\tau^{-1} = e^{-\Delta/kT}$, met Δ/k = 90 en 70 K, afhankelijk van de kristalgrootte. Het gedrag bij de ferrimagnetische-ferromagnetische toestandsovergang (H_{c2} = 46 kOe) is niet lineair voor amplitudes van het wisselveld groter dan 0,1 Oe. Het blijkt, dat na een veldstap naar H_{c2}, het $CoCl_2 \cdot 2H_2O$ kristal enige tijd (ongeveer 30 s) een electromagnetisch signaal uitzendt, dat periodiek fluctueert in de tijd. Deze verschijnselen moeten waarschijnlijk toegeschreven worden aan het optreden van magnetische domeinen.

Op verzoek van de faculteit der Wiskunde en Natuurwetenschappen volgt hier een overzicht van mijn studie.

Nadat ik in 1961 het diploma Gymnasium-B behaald had aan het Libanon Lyceum te Rotterdam, begon ik mijn studie aan de Rijksuniversiteit te Leiden. Het candidaatsexamen met de hoofdvakken natuurkunde en wiskunde en bijvak scheikunde werd in 1965 afgelegd. In dat jaar trad ik toe tot de werkgroep paramagnetische relaxatie van het Kamerlingh Onnes Laboratorium onder leiding van prof. dr. C.J. Gorter, waar ik dr. D.A. Curtis en dr. A.J. Van Duyneveldt bij hun onderzoekingen assisteerde. Sinds 1967 was ik tevens werkzaam bij het natuurkundig practicum. In januari 1969 legde ik het doctoraalexamen in de experimentele natuurkunde af. In de hierop volgende periode tot eind 1970 was ik grotendeels werkzaam als reserve officier der Koninklijke Marine, gedetacheerd bij het Physisch Laboratorium R.V.O.-T.N.O. te Den Haag. Hier verrichtte ik onderzoek betreffende "phased-array" radar.

Dit proefschrift is tot stand gekomen dankzij de medewerking van vele anderen.

De nauwe en plezierige samenwerking met dr. A.J. van Duyneveldt heeft zeer veel bijgedragen tot de uiteindelijke vorm en inhoud ervan. De belangstelling getoond door prof. dr. C.J. Gorter heb ik zeer op prijs gesteld. Ook de vriendschappelijke samenwerking met drs. C.L.M. Pouw en dr. J.A. Roest was zeer waardevol.

Bij de uitvoering der experimenten werd ik gedurende langere of kortere tijd geholpen door de heren L. Bevaart, H.A. Groenendijk, drs. A. van der Bilt en J.P.C. Vreugdenhil. De metingen verricht met de pulsmagneet-opstelling van het Natuurkundig Laboratorium te Amsterdam werden uitgevoerd in samenwerking met en dankzij bemiddeling van dr. W. Breur. Het onderzoek aan het ytterbium chloride hexahydraat werd gedaan in samenwerking met dr. H.B. Brom en dr. J.G.A. Hillaert. Overleg met prof. dr. T. Haseda en dr. J.L. de Jongh betreffende het onderzoek vermeld in hoofdstuk III, was eveneens waardevol.

Bij de bouw en onderhoud van de diverse opstellingen werd veel hulp ondervonden van de technische staf van het laboratorium. De heren W.F. Elbers en J. Bij verzorgden grotendeels het cryogene gedeelte. De heer C.J. van Klink vervaardigde het glazen gedeelte, o.a. de asymmetrische staart-cryostaten.

De meeste preparaten werden gemaakt door Mevr. M.A. Otten-Scholten, de heer W.F. Tegelaar verzorgde de tekeningen. Dr. D.A. Curtis corrigeerde het Engels van het eerste en grootste gedeelte van het proefschrift; waarna

prof. dr. R.L. Carlin het laatste gedeelte nakeek. Het manuscript werd op vaardige wijze getypt door Mevr. E. de Haas-Walraven.